Biofunctionalized polymer interfaces for capture, isolation, and characterization of bacteria

by

Mohammadali Masigol

B.S., Isfahan University of Technology, 2009
M.S., Isfahan University of Technology, 2012

AN ABSTRACT OF A DISSERTATION

submitted in partial fulfillment of the requirements for the degree

DOCTOR OF PHILOSOPHY

Tim Taylor Department of Chemical Engineering
Carl R. Ice College of Engineering

KANSAS STATE UNIVERSITY
Manhattan, Kansas

2020

Abstract

The goal of this research is to develop bio-functional interfaces, designed using polymeric materials, for improved separation and isolation of bacteria for detection and characterization. Microbes impact many aspects of our society, from health to environment to industrial processes. In most cases, microbes exist in complex environments, where thousands of other organisms may also be present. Thus, detecting and characterizing specific microbial targets often necessitates that they are first isolated. Polymeric materials hold several advantages for this type of separation. They can be modified with biomolecules to capture specific microorganisms and can be designed to release captured organisms on-demand using an environmental stimulus. This thesis will explore each of these concepts, beginning with (1) the design of patterned polymer interfaces to tailor the surface reactivity towards biomolecules, (2) bio-functionalization of surface polymers with lectin molecules for bacteria capture, and (3) bio-functional, photodegradable hydrogels for dissection of microbes from membrane surfaces during early-stage biofouling events.

The first portion of this thesis aims at fabricating micro/nano-structured patterns of the novel block co-polymer, poly(glycidyl methacrylate)–*block*–poly(vinyl dimethyl azlactone) ($PGMA_{56}$-*b*-$PVDMA_{175}$) onto silicon slides. These polymers use azlactone-based reactions to covalently couple biomolecules to the surface. Bottom-up and top-down chemical co-patterning methods, including microcontact printing, parylene lift-off, and interface directed assembly are investigated for formation of reproducible, brush-like and crosslinked polymers on the substrates.

The second portion of this thesis uses these polymer interfaces to capture microbial contaminants from solution using lectin-based binding. Lectin-functionalized interfaces are promising for affinity-based microorganism capture and isolation of bacteria from samples such as blood, urine, and wastewater. However, the equilibrium dissociation constants (K_D) of lectin-

carbohydrate interactions, 2-3 orders of magnitude higher than antibody-antigen binding constants, results in poor cell capture efficiency. To address this limitation, surfaces are designed to combine reactive polymer coatings that generate high lectin surface densities with nanoscale surface structures, ultimately improving cell capture. Both detection sensitivity and bactericidal impact of these optimized surfaces are characterized. Finally, the competing effects on capture due to lectin surface density and due to exopolysaccharide expression levels on the bacteria cell surface is compared.

The final portion of this thesis focuses on the use of lectin-functionalized, photodegradable hydrogels to separate and isolate microbes that attach to membrane surfaces during early-stage biofouling, an approach termed polymer surface dissection (PSD). Photo-responsive, biofunctional polyethylene glycol (PEG)-based hydrogels are developed to detach targeted biofilm flocs or cells adhered onto PVDF membranes. A patterned illumination tool then delivers light to the hydrogel in a spatiotemporally controlled manner to release an extracted floc without damage. Microbes can then be sequenced to identify the composition of biofilm flocs at different stages of aggregation. The PSD approach can be used to characterize biofouling in many membrane-based bioseparation processes, here it has been developed to investigate membrane biofouling in anaerobic membrane bioreactors. Understanding the initial stages of biofouling from a mechanistic standpoint could help understand the critical microorganisms in wastewater communities that initiate the biofouling process, information that can inform novel techniques to mitigate biofilm formation.

Biofunctionalized polymer interfaces for capture, isolation, and characterization of bacteria

by

Mohammadali Masigol

B.S., Isfahan University of Technology, 2009
M.S., Isfahan University of Technology, 2012

A DISSERTATION

submitted in partial fulfillment of the requirements for the degree

DOCTOR OF PHILOSOPHY

Tim Taylor Department of Chemical Engineering
Carl R. Ice College of Engineering

KANSAS STATE UNIVERSITY
Manhattan, Kansas

2020

Approved by:

Major Professor
Dr. Ryan R. Hansen

Copyright

© Mohammadali Masigol 2020.

Abstract

The goal of this research is to develop bio-functional interfaces, designed using polymeric materials, for improved separation and isolation of bacteria for detection and characterization. Microbes impact many aspects of our society, from health to environment to industrial processes. In most cases, microbes exist in complex environments, where thousands of other organisms may also be present. Thus, detecting and characterizing specific microbial targets often necessitates that they are first isolated. Polymeric materials hold several advantages for this type of separation. They can be modified with biomolecules to capture specific microorganisms and can be designed to release captured organisms on-demand using an environmental stimulus. This thesis will explore each of these concepts, beginning with (1) the design of patterned polymer interfaces to tailor the surface reactivity towards biomolecules, (2) bio-functionalization of surface polymers with lectin molecules for bacteria capture, and (3) bio-functional, photodegradable hydrogels for dissection of microbes from membrane surfaces during early-stage biofouling events.

The first portion of this thesis aims at fabricating micro/nano-structured patterns of the novel block co-polymer, poly(glycidyl methacrylate)–*block*–poly(vinyl dimethyl azlactone) ($PGMA_{56}$-*b*-$PVDMA_{175}$) onto silicon slides. These polymers use azlactone-based reactions to covalently couple biomolecules to the surface. Bottom-up and top-down chemical co-patterning methods, including microcontact printing, parylene lift-off, and interface directed assembly are investigated for formation of reproducible, brush-like and crosslinked polymers on the substrates.

The second portion of this thesis uses these polymer interfaces to capture microbial contaminants from solution using lectin-based binding. Lectin-functionalized interfaces are promising for affinity-based microorganism capture and isolation of bacteria from samples such as blood, urine, and wastewater. However, the equilibrium dissociation constants (K_D) of lectin-

carbohydrate interactions, 2-3 orders of magnitude higher than antibody-antigen binding constants, results in poor cell capture efficiency. To address this limitation, surfaces are designed to combine reactive polymer coatings that generate high lectin surface densities with nanoscale surface structures, ultimately improving cell capture. Both detection sensitivity and bactericidal impact of these optimized surfaces are characterized. Finally, the competing effects on capture due to lectin surface density and due to exopolysaccharide expression levels on the bacteria cell surface is compared.

The final portion of this thesis focuses on the use of lectin-functionalized, photodegradable hydrogels to separate and isolate microbes that attach to membrane surfaces during early-stage biofouling, an approach termed polymer surface dissection (PSD). Photo-responsive, biofunctional polyethylene glycol (PEG)-based hydrogels are developed to detach targeted biofilm flocs or cells adhered onto PVDF membranes. A patterned illumination tool then delivers light to the hydrogel in a spatiotemporally controlled manner to release an extracted floc without damage. Microbes can then be sequenced to identify the composition of biofilm flocs at different stages of aggregation. The PSD approach can be used to characterize biofouling in many membrane-based bioseparation processes, here it has been developed to investigate membrane biofouling in anaerobic membrane bioreactors. Understanding the initial stages of biofouling from a mechanistic standpoint could help understand the critical microorganisms in wastewater communities that initiate the biofouling process, information that can inform novel techniques to mitigate biofilm formation.

Table of Contents

List of Figures xii
List of Tables xviii
Acknowledgements xix
Dedication xx
Chapter 1 - Introduction 1
1.1 The Need for Capture of Bacterial Contaminants from Environmental Samples 1
1.2 Conventional Methods for Microbial Detection and Characterization 3
1.2.1 Molecular Based Methods 4
1.2.2 Immunological Assays 6
1.2.3 Biosensor Based Assays 7
1.3 Nanomaterial-based Pathogen Capture and Detection 8
1.4 Biofunctional Interfaces for Capture and Isolation of Target Bacteria 10
1.4.1 Biorecognition Molecules Used for Affinity-Based Bacteria Capture 10
1.4.2 Lectins-Carbohydrates Interactions for Bacteria Capture 12
1.4.3 Surface Chemistry of Interfaces Designed to Capture Bacteria 15
1.4.4 Nano/Micro Patterned Interfaces for Bacteria Capture 17
1.5 Biofunctional Polymer Interfaces for Capture and Characterization of Microbes 19
1.5.1 Polymeric Interfaces as Template Support for Bioaffinity Molecules 19
1.5.2 Azlactone-based Polymers for Tunable Interfaces 21
1.6 Biofouling in Industrial Systems 23
1.6.1 Fouling Mitigation Strategies 24
1.6.2 Understanding Biofilm Assembly on Surfaces from a Mechanistic Standpoint 25
1.7 Methods of Dissecting Biofilms 26
1.7.1 Laser Capture Microdissection for Characterization of Biofilms 26
1.7.2 Light Responsive Polymers for Cell Manipulation 27
1.8 References 28
Chapter 2 - Thesis Approaches and Objectives 60
Chapter 3 - Chemical Co-Patterning Strategies Using Azlactone-Based Block Co-Polymers 62
3.1 Overview 62

3.2 Introduction 63
3.3 Experimental Section 65
3.3.1 Materials 65
3.3.2 Fabrication of polymer interfaces 65
3.3.3 Instrumentation 70
3.4 Results and Discussion 71
3.4.1 Formation of Two-dimensional, Brush-like Patterns of PGMA-b-PVDMA 71
3.4.2 Formation of Three-dimensional Patterns of PGMA-b-PVDMA 74
3.5 Conclusion 77
3.6 Acknowledgements 77
3.7 References 78
Chapter 4 - Fabricating Reactive Surfaces with Brush-like and Crosslinked Films of Azlactone-Functionalized Block Co-Polymers 81
4.1 Overview 81
4.2 Introduction 82
4.3 Experimental Section and Protocols 83
4.3.1 PGMA-b-PVDMA Synthesis 83
4.3.2 Generation of Parylene Stencil Patterns Over Silicon Substrates 86
4.3.3 Parylene Lift-off Procedure 88
4.3.4 PGMA-b-PVDMA Interface-Directed Assembly Procedure 90
4.3.5 Custom PGMA-b-PVDMA Micro-Contact Printing (μCP) 92
4.4 Representative Results 95
4.5 Discussion 99
4.6 Acknowledgments 102
4.7 References 102
Chapter 5 - Identification of Critical Surface Parameters Driving Lectin-Mediated Capture of Bacteria from Solution 109
5.1 Overview 109
5.2 Introduction 111
5.3 Experimental Section 114
5.3.1 Materials 114

5.3.2 Polymer Cross-linking Over Flat Si Substrates and Lectin Functionalization 115
5.3.3 Fabrication of Nanopillar Array Surfaces 116
5.3.4 Preparation of Bacterial Samples and Capture Conditions 117
5.3.5 Lectin Binding Assay 118
5.3.6 EDC-NHS Coupling 119
5.3.7 Limit of Detection (LOD) Determination 119
5.3.8 Live/Dead Assay 120
5.3.9 Instrumentation 120
5.3.10 Image Analysis 121
5.3.11 Statistical Analysis of Data 121
5.4 Results and Discussion 122
5.4.1 Investigation of Lectin - Polymer Interactions on Flat Substrates 122
5.4.2 Investigation of a Lectin Panel for PVDMA Coupling and Microbe Capture 126
5.4.3 Characterization of PVDMA-coated Nanopillar Array Surfaces 129
5.4.4 Sensitivity and Quantitative Detection of *E. coli* 132
5.4.5 Bacteria Viability After Capture on Functional Nanopillar Array Surfaces 138
5.4.6 Importance of Bacteria UPP Expression vs Lectin Density on Capture 140
5.5 Conclusion 143
5.6 Acknowledgements 144
5.7 References 144
Chapter 6 - Polymer Surface Dissection for Investigation of the Early Stage Biofilm Formation on AnMBR Membranes 155
6.1 Overview 155
6.2 Introduction 156
6.3 Experimental Section 158
6.3.1 Materials 158
6.3.2 Thiol SAM formation 159
6.3.3 Flocs Transfer from Membrane to Hydrogel 159
6.3.4 Hydrogel Preparation 160
6.3.5 Hydrogel Functionalization with Bioaffinity Ligands 160
6.3.6 Use of Second Hydrogel for Clean Extraction and Hydrogel Degradation 161

6.3.7 Live-Dead Assay 161
6.4 Results and Discussion 162
6.4.1 Hydrogel Characterization 162
6.4.2 Flocs Size Distribution and Transfer Efficiency 165
6.4.3 Hydrogel Photopatterning, Degradation, and Extraction 167
6.4.4 DNA Quantification and Analysis of Quantity of Extracted Samples 169
6.5 Conclusion 171
6.6 Acknowledgements 172
6.7 References 172
Chapter 7 - Conclusions and Recommendations 176
7.1 Design of patterned polymer interfaces to tailor the surface reactivity towards biomolecules 176
7.1.1 Ideas for Future Investigation 177
7.2 Bio-functionalization of surface polymers with lectin molecules for bacteria capture 179
7.2.1 Ideas for Future Investigations 180
7.3 Bio-functional, photodegradable hydrogels for dissection of microbes from surfaces during early-stage biofouling events 183

List of Figures

Figure 3.1 Strategies for generating 2-D and 3-D patterns of PGMA-*b*-PVDMA. (a) Parylene lift-off procedure for patterning 2-D brush-like polymer onto silicon substrates. (b) Interface directed assembly procedure for patterning 2-D brush-like polymer onto biological/chemical (PEG/TPS) inert substrates. (c) Generation of 3-D polymer structures onto silicon by using μCP method. 68

Figure 3.2 Parylene stencil thickness influences the PGMA-b-PVDMA film morphology. (a) Brightfield image and cross-sectional height profile of polymer generated from 80 nm thick parylene stencils shows patterns with uniform, brushlike thickness. (b) 1 μm thick parylene generated patterned films with non-uniform thickness. 72

Figure 3.3 Interface directed assembly methods generate 2-D films of PGMA-*b*-PVDMA in chemically and biologically inert backgrounds. (a) Brightfield and SEM images of PGMA-*b*-PVDMA patterns on the chemically inert (TPS) and biologically inert (PEG) substrates. (b) AFM images of PGMA-*b*-PVDMA patterns on the patterned TPS surfaces and cross-sectional polymer height. 73

Figure 3.4 μCP can be used to generate 3-D PGMA-*b*-PVDMA structures. (A) Cross-sectional height profile of PGMA-*b*-PVDMA patterns (inset: brightfield images of PGMA-*b*-PVDMA patterned on silicon substrates (i) without annealing and (ii) with annealing, scale bar = 30 μm). (B) FTIR analysis of bare silicon (line without any significant peak) and PGMA-*b*-PVDMA (line with three significant peaks) transferred to the surface through the μCP method. (C) Average micropillar height for various inking concentrations. 76

Figure 4.1 Contact angle measurements for treated silicon substrates. (A) Bare silicon, (B) Plasma-cleaned silicon, (C) Spin-coated silicon with PGMA-b-PVDMA (after annealing and sonication in chloroform). 90

Figure 4.2 ATR-FTIR measurements for treated PDMS stamps (Relative intensity). (Inset A) Contact angle measurements for bare PDMS stamp. (Inset B) Contact angle measurements for TPS treated PDMS stamp. 94

Figure 4.3 Setup for μCP of PGMA-*b*-PVDMA solutions onto silicon substrates. The procedure includes use of a (A) manual drill press, (B) a TPS-functionalized PDMS stamp coated with

the PGMA-*b*-PVDMA polymer, (C) a plasma cleaned 2×2 cm silicon substrate, and (D) double-sided tape. 94

Figure 4.4 Details of the developed techniques for generating PGMA-*b*-PVDMA into patterned, crosslinked or brush films. This figure has been modified from Masigol *et al.*[24] (A) Schematic representation of the parylene lift-off protocol for patterning polymer brushes onto silicon substrates, 1. silicon wafer (w/native oxide), 2. parylene deposition (1 μm or 80 nm), 3. photoresist spin coating, 4. UV exposure and development, 5. oxygen plasma etching, 6. polymer spin coating, 7. annealing and parylene lift-off. (B) IDA procedure for patterning polymer brushes onto biological/chemical (PEG/TPS) inert substrates, 1. silicon wafer (w/native oxide), 2. PEG/TPS deposition, 3. parylene deposition (1 μm or 80 nm), 4. photoresist spin coating, 5. UV exposure and development, 6. oxygen plasma treatment, 7. parylene lift-off, 8. polymer spin coating, 9. annealing and sonication. (C) Generation of crosslinked polymer structures onto silicon using the μCP method, 1. soft-lithography for making PDMS stamp followed by TPS coating, 2. polymer inking on TPS-functionalized PDMS, 3. stamp/substrate contact, 4. annealing and sonication..... 96

Figure 4.5 Representative results of the parylene lift-off procedure. (A) Brightfield images of PGMA-*b*-PVDMA polymer patterns on silicon with annealing (inset i) and without annealing (inset ii) (Scale bar = 40 μm). (B) Polymer thickness measured after 10 min sonication in chloroform with or without annealing. (C) Cross-sectional polymer height profile for 1 μm thick parylene stencils. (D) Cross-sectional polymer height profile for 80 nm thick parylene stencils..... 97

Figure 5.1 Growth curve of the *A. tumefaciens* JX110 culture solution. The 22-24 hr initial culture was spun down (4000 rpm, 10 min), re-suspended in fresh medium, diluted (10 μL in 2 mL fresh media), and OD_{600} measurements were then started. Culturing conditions: 28 ^{o}C, 22 hr, 215 rpm. 118

Figure 5.2 Film thickness and corresponding areal chain density of the polymer obtained via spin coating of different concentrations of $PGMA_{56}$-b-$PVDMA_{175}$ from chloroform. 123

Figure 5.3 ATR-FTIR analysis of surface coated with different polymer concentrations (0.25-1 wt. %). The orange line shows the IR spectra of 0.75 wt. % polymer films incubated with WGA in 1X PBS. All spectra were background subtracted from bare silicon substrates. 123

Figure 5.4 Surface characterization of lectin functionalized $PGMA_{56}$-*b*-$PVDMA_{175}$ films using ellipsometry, ATR-FTIR, and fluorescent microscopy. (A) Azlactone reaction conversion after WGA coupling at each polymer surface density before and after WGA functionalization. (A Inset) IR spectra of surfaces functionalized with 0.75 wt.% polymer (blue line) and then coupled with WGA (red line). (B) WGA density measured for surfaces pre-coated with different polymer concentrations. (C) Fluorescent intensity of polymer-functionalized surfaces immobilized with 0.1 mg/mL of WGA-FITC or HPA-A488 in 1X PBS. (Control: 1X PBS without lectin incubated over substrates). ** = $P < 0.01$, * = $P < 0.05$, statistical differences apply to both WGA and HPA data sets. n = 3 independent substrates per condition. Values are the average ± standard deviation. 125

Figure 5.5 Results demonstrating the lectin addition and hydrolysis of azlactone groups at various pH. Variation of azlactone reaction conversion with different pH levels calculated by the percentage decrease in the height of IR spectra peak at 1818 cm^{-1} due to (A) WGA immobilization, (B) HPA, and (C) ConA. Contribution of each lectin was measured by subtracting the summation (buffer + lectin) from hydrolysis data (buffer). * = $P < 0.05$, n = 3 independent substrates per condition. Values are the average ± standard deviation. 127

Figure 5.6 (A) Representative fluorescent images of *E. coli*-mCherry captured by the polymer surfaces immobilized with WGA, HPA and ConA at high concentrations (10^8 CFU/mL). As the control, BSA solution (1 wt.%) was incubated on the PVDMA substrates to account for non-specific binding of cells to the surface under these conditions. (B) Calculated number of captured *E. coli* on the surface via using ImageJ. The values were given as the mean of five different surface locations from three independent surfaces. *** = $P < 0.001$, ** = $P < 0.01$. Values are the average ± standard deviation. 129

Figure 5.7 Scanning electron micrographs of NPAs before and after PVDMA spin coating. (A and B) Uncoated LAR-NPA surfaces; (C) PVDMA-coated LAR-NPA surfaces; (D and E) Uncoated HAR-NPA surfaces; (F) PVDMA-coated HAR-NPA surfaces. Spin coating used a 0.75 wt.% PVDMA solution followed by annealing at 110 °C. 131

Figure 5.8 Characterization of flat and nanopillar surfaces with SEM-EDX and auto-fluorescent measurements. (A) Composition analysis and sum spectrum of the bare LAR-NPA by SEM-EDX (B) Composition analysis and sum spectrum of the PVDMA-coated LAR-NPA surface by SEM-EDX (C) Autofluorescence measurements of uncoated and PVDMA-coated

surfaces. (0.75 wt.% PVDMA solution in chloroform). Spin coating conditions: 1500 rpm, 15 sec. A ratio greater than 1 indicates an increase in autofluorescence compared to the uncoated substrate. 132

Figure 5.9 (A) Representative microscopic images of *E. coli* captured by the WGA immobilized on EDC-NHS surfaces, functional flat-PVDMA surfaces, and functional LAR-NPA surfaces after contact with bacteria at different concentrations. Yellow arrows indicate a representative bacteria cell on the surface. (B) Corresponding analysis of the number of captured *E. coli* for different bacteria solution concentrations. The values were given as the mean of five different locations from three independent surfaces. Values are the average ± standard deviation.. 133

Figure 5.10 (A-C) Representative microscopic images of *E. coli* captured by WGA immobilized on $PGMA_{56}$-*b*-$PVDMA_{175}$ surfaces incubated with different bacteria concentration. (A) 10^7 CFU/mL, (B) 10^5 CFU/mL, (C) 10^3 CFU/mL (near the estimated LOD). (D-F) Representative microscopic images of *E. coli* captured by WGA immobilized on EDC-NHS surfaces incubated with different bacteria concentration. (D) 10^7 CFU/mL, (E) 10^5 CFU/mL, (F) 10^3 CFU/mL (One order of magnitude below the estimated LOD) (Inset scale bar: 5 µm). Both methods treated with the same bacteria but the efforts to increase the contrast and quality of images by ImageJ made the bacteria in EDC-NHS darker. Yellow arrows demonstrate the location of representative bacteria cells on the surface..... 134

Figure 5.11 (A) Representative fluorescent images of lectin surfaces treated with EDC-NHS and PGMA-b-PVDMA and functionalized by a labeled lectin (WGA-FITC) (B) Corresponding fluorescent intensity measurements of each surface. 135

Figure 5.12 Comparison of bacteria capture levels on flat functional PVDMA surfaces using 1X PBS and LB media as the capture solution. (A) Representative brightfield images, and (B) surface density of captured bacteria at each solution concentration tested. NS = no statistical difference. 138

Figure 5.13 (A) Scanning electron micrographs and microscopic images of *E. coli* after capture onto functional NPA surfaces. Bacteria or cellular debris were colored pink to distinguish them from the pillars. (B) Representative fluorescent images and % of live cells after capture to each surface. Control: Attached bacteria were exposed to a 2.5% glutaldehyde solution and 70% isopropanol solution to verify that dead cells could be detected with the live/dead assay. Live/dead assay images were adjusted with ImageJ to maximize color contrast. 139

Figure 5.14 (A) Variation of fluorescent intensity of *A. tumefaciens* JX110 cells after culturing at different IPTG concentrations and labeling with FITC-conjugated WGA lectins. ANOVA one-way and Tukey's test were applied to measure overall and pairwise p-values, respectively. Tukey test categorized IPTG concentrations into 3 different groups (a, b, and c). (B) Number of captured *A. tumefaciens* JX110 cells on the surface at different IPTG concentrations. All solutions of JX110 cells were incubated on the surface at OD 0.1 and lectin density was held constant at 0.46 WGA/nm^2. (C) Number of captured *A. tumefaciens* JX110 on the surface at different the lectin densities. All solutions were again incubated over the surface at OD 0.1 and IPTG concentration was kept constant at 200 µM. The values were given as the mean of five different locations from three independent surfaces. ** = P < 0.01, * = P < 0.05, NS = Not Significant. Values are the average ± standard deviation. 142

Figure 6.1 (A) Hydrogel preparation and bioaffinity ligand conjugation. (B) Schematic of the PSD method. (i) PVDF Membranes are contacted with wastewater solutions and cell attachment to the surface is characterized using an optical microscope. (ii) The substrate is then contacted with a pre-formed polymer gel loaded with bacteria affinity ligands for flocs transfer (iii) The hydrogel is removed from the membrane surfaces and a second pre-formed hydrogel is placed on the first hydrogel to trap not-desired flocs and ensure clean extraction. (iv) Cells of interest are sectioned from the base hydrogel using patterned UV light. (v) The sectioned cell(s) are lifted off the base hydrogel for molecular analysis. 158

Figure 6.2 (A) Representative fluorescent images and (B) Percentage of live cells in contact with the hydrogel without affinity ligand (control), and functionalized hydrogels with WGA, and poly lysine. Negative control: Attached bacteria were exposed to a 2.5% glutaraldehyde solution and 70% isopropanol solution to verify that dead cells could be detected with the live/dead assay. The values were given as the mean of five different surface locations from three independent surfaces. 163

Figure 6.3 (A) Representative fluorescent images of stained-*E. coli* JM 109 transferred from membrane to the hydrogels functionalized with poly-$_L$-lysine and WGA at two different bacteria concentrations. Control: Hydrogel without affinity ligand. (B) Calculated number of transferred *E. coli* JM 109 to the hydrogel surfaces using ImageJ. The values were given as the mean of five different surface locations from three independent surfaces. *** = P < 0.001, ** = P < 0.01, * = P < 0.05. Values are the average ± standard deviation. 164

Figure 6.4 Representative (A) fluorescent images of stained-flocs with FM 1-43 lipid dye on the PVDF membrane and (B) upright brightfield and fluorescent images of flocs after transfer to the hydrogel surfaces after 30 min membrane-hydrogel contact. Inset scale bar: 50 μm (C) Flocs size distribution plot on the PVDF membrane surface after 3, 6, 18, and 24 hrs incubation with the wastewater solution. Floc sizes measured by using ImageJ software. (D) Transfer percentage from membrane to affinity-functionalized hydrogels at different floc areas after 24 hrs. Control: Hydrogel without affinity ligand. Dashed lines indicate the average floc transfer percentage for each affinity ligand. The percentage values for each size range were given as the mean of three independent surfaces. Stars demonstrate the statistical analysis of each case compared to control. *** = $P < 0.001$, ** = $P < 0.01$, * = $P < 0.05$. Values are the average ± standard deviation. 167

Figure 6.5 Hydrogel photopatterning, degradation and extraction. (A) (i) A targeted single floc after extraction from the PVDF membrane. (ii) Pattern projected on the flocs and release was observed after 5 s (iii) Complete release of the targeted floc from the hydrogel base occurred after 15 s (B) (i) Two flocs targeted for biofilm extraction (ii) Pattern projected on the flocs and release after light exposure. Dashed circles indicate flocs during their release into solution. (iii) Hydrogel after removal of targeted flocs. (C) (i) Floc selected for biofilm extraction. (ii) Pattern projected on the floc and complete release after light exposure. (iii) Recovered floc on a coverslip. 169

List of Tables

Table 6.1 Minimum requirements, the DNA concentration, and DNA quality measurements of the floc samples extracted from hydrogel base. 170

Acknowledgements

From the formative stages of this thesis, to the final draft, I owe an immense debt of gratitude to my advisor Dr. Ryan R. Hansen. His sound advice and careful guidance was always with me through my entire PhD studies. I could not have imagined having a better advisor and mentor. I consider myself lucky to have had him as a supervisor for my PhD thesis.

I wish to thank my committee members who were more than generous with their expertise and precious time. Thank you Dr. John R. Schlup, Dr. Prathap Parameswaran, Dr. Thomas G. Platt, and Dr. Gregory Finnigan for agreeing to serve on my committee. I express my gratitude to Dr. Andre´ J. van der Vlies, Dr. Bradley S. Lokitz, and Dr. Scott T. Retterer, for kindly helping me with all the proceedings of the thesis.

I would like to thank my family, especially my mother and father for always believing in me, for their continuous love and supporting me spiritually throughout my life.

I cannot begin to express my unfailing gratitude and love to my beloved wife and best friend, Narges who has supported me throughout this process and has constantly encouraged me when the tasks seemed arduous and insurmountable.

Above all, from the depth of my heart, I thank God Almighty, for having made everything possible by giving me strength and courage to do this work and keep me going on…..

Dedication

To my dearest, Narges,
and land of Ahuramazda, my country, which is presently experiencing hardship

Chapter 1 - Introduction

1.1 The Need for Capture of Bacterial Contaminants from Environmental Samples

Microbial pathogens have a prevalent influence on public health and are responsible for millions of infections around the world. *Escherichia coli* O157:H7, *Bacillus subtilis, Salmonella, Pseudomonas aeruginosa, Staphylococcus aureus, Listeria monocytogenes, Legionella parisiensis* and *Campylobacter* are major cause of illness through air, food, or water-borne contaminations[1,2,3,4]. According to worldwide statistics reported by Centers for Disease Control (CDC), an estimated one-third of human fatalities are caused by infectious bacterial diseases[5]. This includes an estimated annual 5.9 million illnesses by waterborne bacteria such as *P. aeruginosa* and *Salmonella*, and 3000 casualties by foodborne bacteria such as *Escherichia coli* O157:H7, *Campylobacter* spp, and *Listeria* just in the US[6]. Foodborne diseases cost 15.6 billion dollars in the US annually and have become an issue in the international food industry worth 578 billion dollars[7]. Among the identified pathogens, *Escherichia coli* (*E. coli*) has gotten increasing attention[8], with an infective dose of ~100 cells.[9] Transmission of *E. coli* to human body can occur through the consumption of contaminated food products such as under-cooked meet, polluted water, cheese, yogurt, and vegetables[9]. Oral exposure to ~500 cells of *Campylobacter* can cause illness within 2-5 days that can damage the intestinal epithelium of humans[10,11]. A conventional method for bacterial detection is the plate count method which requires biochemical confirmation, large sample volume, long incubation time, and significant technician labor[5]. Using these culture-

based methods, it can take 3-7 days to confirm the presence of these pathogens through a process which includes isolation, biochemical testing of colonies, DNA sequencing, and serological confirmation.

Many researchers have developed alternative methods to provide rapid results within minutes or hours with improved detection sensitivity[12]. In addition, assays are designed to have simple procedures with reduced analysis time such that the operating personnel do not need microbiological expertise[13]. Well-known, molecular-based techniques including enzyme-linked immunosorbent assay (ELISA), polymerase chain reaction (PCR), and loop mediated isothermal amplification (LAMP) are examples of molecular based methods that significantly decrease analysis time. Some tests can identify genus and species. However, the chemical reagents and instruments can be expensive, and contamination can occur due to the complicated preparation. Some reagents have a short shelf life and must be kept below 0°C[5], a factor that may limit the utility of these methods in developing countries and resource-limited environments. Another critical challenge is detection of bacteria in food samples that normally include a complex food matrix containing a variety of components, including carbohydrates, sugars, proteins, fats, and other biochemical ingredients[14,15]. Fats can interfere with antibody-binding interactions, while carbohydrates are able to interfere with nucleic acid amplification methods[16,17]. Sodium chloride, sucrose, and lysine existing in food matrices also make bonds to the nucleic acids causing interference to DNA polymerase, ultimately inhibiting the accuracy of PCR and reduces its sensitivity[18]. It was shown that interference of lipids and proteins in broiler meat could decrease the surface plasmon resonance (SPR)-based sensing and detection of *Campylobacter jejuni* (*C. jejuni*)[19]. Sugars and fats in milk have also reported to

decrease the sensor resonance frequency of piezoelectric cantilever devices designed to detect the *L. monocytogenes*[20].

These limitations motivate culture free detection after direct isolation and identification of bacteria from an environmental sample[17,21]. Many new innovations of rapid methods for capture and detection of microbial pathogens use nanomaterials. Nanomaterials have offered significant improvements in capture efficiency, detection sensitivity, and practicality compared to traditional assays[22]. They can be used to develop synthetic, biofunction interfaces for sensitive and rapid isolation for culture-free detection of bacteria.

Chapter 1 of this thesis is divided by the following sections which review the current knowledge and highlighted research on detection and capture of microbes from contaminated matrices. Sections 1.2) Conventional methods for microbial detection and characterization; 1.3) Nanomaterial-based pathogen capture and detection; 1.4) Biofunctional interfaces for capture and isolation of target bacteria; 1.5) Biofunctional polymer interfaces for capture and characterization of microbes; and 1.6) Lectins-carbohydrates interactions for bacteria capture.

1.2 Conventional Methods for Microbial Detection and Characterization

Conventional or "gold standard" techniques for bacteria detection are based on culture–based methods with basic steps including pre-enrichment, plating, culturing, standard biochemical detection/counting of bacteria, and serological validations[23]. Culture-based procedures provide quantitative information in a cost-effective and simple process. Unfortunately, these techniques are insensitive, labor intensive, and time-consuming. Culturing takes 2–3 days to obtain preliminary results and more than 7 days for confirmation[24,25], which is insufficient for practical

application. For example it was reported that chromogenic and fluorogenic growth media such as SM-ID agar and Rambach agar could be successfully use for detection, enumeration, and identification of *Salmonella*, but these selective medias were determined to be too slow for use in an outbreak or product recall[26]. Over the past two decades, various rapid detection methods with high reliability, sensitivity and clinical or field feasibility have been introduced to address the limitations of culture-based approaches[27,28,29,30]. These rapid methods should provide interfaces to detect the existence of bacterial pathogens in various medias such as water and raw/processed foods with certain level of accuracy and reliability. The sensitivity of the interface should approach a point that makes detection possible even at low concentrations. Rapid detection techniques are categorized into nucleic acid-based, immunological-based, and biosensor-based methods, all with their own limitations and advantages[6,31]. Sections 1.3.1, 1.3.2, and 1.3.3 focus on these detection methods and their applications in bacteria cell capture and detection, along with their advantages and limitations, and highlight the need for synthetic materials and interfaces to improve the way bacteria are isolated and detected.

1.2.1 Molecular Based Methods

Compared to the conventional techniques, molecular-based methods are more sensitive, fast, and less laborious. Nucleic acid methods apply oligonucleotides complementary to the DNA/RNA sequences of targeted microbes to obtain accurate results[32,33]. As the platform for biosensors, nucleic acid-based methods are able to identify the genetic makeup of the pathogen[34]. Recent reports in the literature demonstrate use of nucleic acid-based methods for pathogen detection. For example simple polymerase chain reaction (PCR) has been applied to identify *C.*

jejuni in chickens[35] and *E. coli* O157:H7 in water[36]. Multiplex polymerase chain reaction (mPCR) has been employed to simultaneous detection of *Salmonella*, *E. coli* O157:H7, and *S. aureus* in milk and duck hatcheries[37,38]. Quantitative polymerase chain reaction (qPCR) was also used for enumeration and simultaneous detection of *C. jejuni* and *Salmonella* in broiler breast meat[39].

Single PCR and multiplex PCR use one or more primers to detect pathogens. PCR provides high detection sensitivities, down to one cell in different media. This method plays a critical role in the identification and detection of microbial strains that exist in water and food samples. Real time PCR is able to detect the pathogens by determining the fluorescent signal as a continuous condition and is considered as the most common technique due to its high sensitivity and specificity[25]. For instance, TaqMan real-time PCR assay for the detection of 12 pathogens at the same time has been reported[25]. Limit of detection (LOD) of the assay for cultured bacteria were 296, 495, 500, and 875 CFU/mL (*E. coli O157:H7*, *C. jejuni*, *S. aureus*, and *L. monocytogenes*). LOD in meat samples measured as 10^4 for 11 strains, while for *V. parahaemolyticus* it was 10^3 CFU/g. It was shown that TaqMan real-time PCR assay could be considered as a fast and efficient alternative option for the high-throughput screening of multiple microbes simultaneously[25]. PCR also has been reported to be used for recognition and detection of bacteria strains that are viable but not culturable[40]. However, there are some limitations associated with each PCR technique. PCR might not be able to distinguish the viable and dead bacterial pathogens without using expensive chemical reagents and protocols and because the method is destructive to the cells, isolates cannot be further characterized. This results in inaccurate interpretation of cell viability[41,42,43]. In multiplex PCR, the interference of primers could occur resulting in some bacteria to go undetected[44].

1.2.2 Immunological Assays

In immunological based methods, a specific antibody interacts with a targeted antigen. Sensitivity and specificity of the method are directly affected by the strength of this specific binding. Polyclonal and monoclonal antibodies are particularly generated to detect microbe-specific epitopes to be used in immunological based techniques. Most widely applied immunological assays for the screening of microbes are enzyme linked immunosorbent assays (ELISA)[45,46,47], flow cytometry[48,49], and quantitative immunofluorescence[50]. ELISA identifies the protein, peptides, polysaccharide, and bacterial pathogens in a precise and sensitive way[51]. Double-antibody sandwich ELISA has been used for the sensitive and fast detection of *Bacillus Cereus* in meat. The detection range of this assay reported in the range of 1.0×10^4–2.8×10^6 cells/mL with the estimated LOD of 0.9×10^3 cells/mL in phosphate buffer silane. The assay could provide selective detection and 94.9-98.4% recovery of *B. cereus* in a meat sample possessing similar pathogens such *as B. thuringiensis, B. subtilis, B. licheniformis* and *B. perfringens*[52]. Paper-based ELISA (p-ELISA) for detection of *E. coli* O157:H7 from Chinese cabbage, providing an operation time of 3 hrs and detection sensitivity of 10^4 CFU/mL was also reported[53]. Literature reports the ability of using nanoparticles in conjunction with ELISA to improve the detection sensitivity of this technique. As an example, functional nanoparticle (FNP)-ELISA technique has been demonstrated to enhance the detection sensitivity of *E. coli* O157:H7 by nearly four orders of magnitude compared to conventional ELISA[54]. Here LODs were reported as 68 CFU/ml in the phosphate buffer solution and had a range of 6.8×10^2 - 6.8×10^3 CFU/ml in milk, vegetable and ground beef. Applying gold nanoparticles (AuNP) to the ELISA assay also improved the detection sensitivity of *E. coli* O157:H7 in whole milk by a factor of 185 compared to a conventional

ELISA[55]. Cross-interaction among the similar species in ELISA could lead to lower sensitivity and specificity in mixed cultures.

Flow cytometry can perform single cell analysis and bacteria detection with high specificity and sensitivity[56]. A hybridization chain reaction (HCR)-based flow cytometric bead assay designed for the specific and sensitive fluorescent detection of emetic *B. cereus* from milk demonstrated the LOD of 9.2×10^2 and 7.6×10^0 CFU/mL in spiked milk and pure culture. Fluorescent signal readout demonstrated the high specificity of the designed primer towards emetic *B. cereus* detection in a mixture of non-targeted bacteria[48].

1.2.3 Biosensor Based Assays

Biosensors have been introduced to address the conventional limitations associated with immunological and nucleic acid-based techniques such as need of expensive chemical and biological reagents, trained staff, and complex laboratory settings. There is also the possibility of inaccurate results due to interference between similar antigens and inaccurate detection of dead cells[6]. A biosensor is an integrated receptor-transducer tool that converts a biorecognition or complementary biological binding event into electrical signal[57]. Biosensors are categorized based on the types of recognition element (enzymatic, nucleic-acid, aptamer, antibody, and whole cell) or transducer (optical, electrochemical, and piezoelectric)[58]. Biosensors could be connected to equipment such as microfluidic devices to expand their detection capabilities. For instance, an impedance based microfluidic biosensor including two pre-functionalized microchannels with anti-*Salmonella* antibodies and electrode arrays for the impedance measurements has been reported with detection sensitivity of 300 cells/ml after 1 hour. The biosensor was also able to differentiate live and dead *Salmonella* cells by observing very low detection signals when dead

bacteria solution was pumped into the sensor[59]. SPR is one of the most sensitive optical biosensor techniques that provides a real-time monitoring of the interactions between the target analytes and bioreceptors[60]. There are reports of direct bacteria capture on the SPR biosensor surfaces by using antibody-antigen interactions[61]. Antibodies are used extensively as an effective recognition element in SPR biosensors to address limitations regarding loss of sensitivity and specificity due to cross-reactivity in complex matrixes[62]. A SPR biosensor functionalized with monoclonal antibodies to detect the *Salmonella typhimurium* with high specificity in romaine lettuce provided high detection sensitivity as low as 0.9 log CFU/gr[63].

Compared to the optical techniques, electrochemical-based biosensors offer lower cost and can handle many samples at once but are less specific[6]. The critical step here is to generate a sensitive recognition electrode surface as the platform for bacteria or cell attachment[64]. Similar to antibodies, aptamers are promising biorecognition elements in electrochemical biosensors because of their high stability and strong affinity. An electrochemical biosensor functionalized with a biotin-modified aptamer allowed for fast and efficient detection of *E. coli* in Licorice extract has been reported with enhance detection sensitivity of 80 CFU/mL in bacterial solution with buffer and 9.02×10^4 CFU/mL in Licorice extract samples[65].

1.3 Nanomaterial-based Pathogen Capture and Detection

Microbial pathogens with low infectious dose and harmful effects to the human body make the creation of sensitive, selective, fast, and reliable isolation and detection methods necessary to control infection. As mentioned in section 1.3, current approaches are slow, show limited sensitivity, cannot detect the pathogens in real time, and require days to obtain correct information.

A novel approach to address these challenges is use of nanotechnology and development of nanomaterial-based detection techniques that are able to achieve the required criteria of this field. Nano-biotechnology proposes nanomaterials and nanostructured devices that first; because of their unique sizes, are able to provide high surface-to-volume ratio, and demonstrate physical strength, chemical functionality, and excellent electrical/optical characteristics, and second; their physical properties and chemical functionality can be manipulated. Tuning the physicochemical behavior of nanointerfaces is done by engineering size, composition, shape, and chemical functionalization with different functional groups[66,67,68]. Recent developments in high-resolution synthesis and characterization of nanostructured surfaces such as nanoparticles, nanotubes, quantum dots, and nanowires have motivated researchers to apply nanotechnology for bio-detection, drug delivery, and synthesis of functional devices[69]. Nanomaterials used for capture and detection of microbial pathogens offer unique identifying and detection approaches specific to the target and create differentiating signals from the analyte. The signal can be produced by nanostructure itself or from immobilized biomolecules existing on the surface[70]. These nanostructures can be functionalized with a variety of nanomaterials and targeting groups such as antibodies, aptamers, peptides, and ligands which enhance capture efficiency and detection sensitivity[71,72]. Nanomaterial-based detection techniques have shown a reduction in detection time and capability for performing high throughput, multiplexed screening[73,74]. Improved surface nanopatterning techniques, such as nanolithography and electron beam lithography, have led the generation of nanoscale arrays and nanopatterned interfaces for cellular receptors that can greatly enhance the accuracy of techniques designed for pathogen isolation and detection[5]. Nanopatterned and nanoarray interfaces provide the capability of spatial control and high throughput screening of targeted cells within a small capture region[66].

1.4 Biofunctional Interfaces for Capture and Isolation of Target Bacteria

1.4.1 Biorecognition Molecules Used for Affinity-Based Bacteria Capture

Application of interfaces conjugated with affinity ligands can lead to enhanced cell capture efficiency and detection sensitivity[75]. Among various types of interfaces, nanostructured interfaces are able further enhance the attachment of capture since they provide a high surface area. This increases the interaction between the bacteria cell and conjugated ligands, which drives bacteria attachment to the surface and correspondingly improves detection sensitivity[22]. Bio-recognition elements used for capture include antibody/antigen[76,77], nucleic acids[78], enzymes/ligands[79], aptamers[65], peptides[80], carbohydrates[81], or synthetic bioreceptors designed with strong affinity and specificity toward epitopes on bacteria surface structures[82,83].

Monoclonal, polyclonal, and recombinants antibodies conjugated on nanoparticles, quantum dots, and nanotubes are widely used as probe for highly selective and sensitive capture of bacteria. Literature reports use of antibody-conjugated nanointerfaces for antigen interaction-based detection of *E. coli* O157:H7 and *Salmonella* sp. in food complexes such as hamburger and cucumber[84], *S. typhimurium* in ground beef and chicken rinse water[85], *S. aureus* in apple juice/lettuce[86], *C. jejuni* in poultry samples[87], *L. monocytogenes* in sausage and pork[88], and *E. coli* O157:H7 in drinking water[89]. Antibodies are selective, sensitive, available for wide variety of pathogens, and are able to enhance the capture efficiency when conjugated to a nanointerface. For instance, Maurer et al. reported that use of anti-*E. coli* coated gold nanoparticles could enhance the *E. coli* capture by a factor of 1.89 compared to uncoated particles[90]. However, antibodies are expensive, have nonspecific interactions, and normally cannot differentiate between live and dead pathogens[91,92].

Carbohydrates (oligosaccharides or polysaccharides) are another affinity probe for bacteria capture. Compared to antibodies and nucleic acids, carbohydrates show more resistance against the denaturation. In addition, higher local surface density of carbohydrates is achievable because of their lower molecular weight, which provides multivalent interactions with bacteria surfaces, resulting in improve of the binding affinity[93,94]. Carbohydrate-mediated recognition occurs through the interaction with molecules present on the cell surface such as lipopolysaccharides and lectins[95]. Carbohydrates can be considered as a potential option when antibodies and nucleic acids don't have specific affinity to recognize mutants that differ slightly from the original target[78,96]. It has been shown that silica-coated magnetite nanoparticles functionalized with galactose (Gal) and D-mannose (Man) have the capability of determining the identity of three *E. coli* strains including *E. coli* ORN178 (Man strong, Gal weak), *E. coli* ORN208 (Man weak, Gal weak), and *E. coli* ES (Man strong, Gal strong)[97]. Similar to carbohydrates, peptides and proteins demonstrate binding capability to multiple targets including fungi and virus through interaction with surface components of the cells[98,99,100]. The use of peptide-functionalized interfaces provides the opportunity to differentiate between live and dead pathogens in detection-based approaches[101]. Under equal conditions (considering same number of recognition molecules), peptide-based assays are able to detect larger number of target pathogens compared to antibodies since the binding event is semi-selective. Additionally, peptides can attach to different pathogens with different affinities[102,103,104].

1.4.2 Lectins-Carbohydrates Interactions for Bacteria Capture

Carbohydrates, including oligosaccharides or polysaccharides, glycolipids, and glycoproteins are important extracellular elements present on almost all bacterial cell structures. One capture approach is to use biomolecules and ligands as the biomarkers with the capability of recognizing and binding with specific carbohydrates present on the bacteria surface[94,92]. This lectin-carbohydrate interactions can be used for capture and identification of targeted bacterial pathogens[105,106]. Lectins, as a group of carbohydrate binding proteins, specifically interact with carbohydrates in a highly reversible, non-covalent manner[107]. Interaction can occur through van der Waals forces, hydrophobic interactions, hydrogen bindings, and metal coordination[108]. Capture approaches based on lectin-carbohydrates interactions have several advantages in comparison with antibody and nucleic acid methods. Lectins are less expensive and their agglutination with bacteria occurs quickly[109,110]. They show higher resistance in extreme conditions such as basic and acidic environments[111]. Their molecular size is smaller than antibodies, which allows them to be functionalized on the interfaces with higher densities per unit area leading to an increase of multivalent interactions with bacterial cell constituents. This achieves higher detection sensitivities in capture approaches[112]. Considering carbohydrate binding specificity and affinity, lectins are mainly classified in five categories including N-acetylglucosamine (GlcNAc), mannose, galactose/N-acetylgalactosamine (GalNAc), sialic acid, and fucose [113,114]. Due to the high affinity, they are able to attach and detect broad range of microbes. *Wheat Germ Agglutinin* (WGA), *Concanavalin A* (Con A), *Peanut Agglutinin* (PNA), *Maackia Amurensis* (MAL), *Elex Europaeus Agglutinin* (UEA), and *Lens Culinaris Agglutinin* (LCA) are the most common lectins used in capture and isolation of microbes from environmental samples, each with their level of specificity

and affinity through bacterial EPS content[106,115]. Literature reports functionalization of WGA (GalNAc, GlcNAc, and Sialic acid-binding lectin) and LCA (fucose, mannose, and GlcNAc-binding lectin) on anisotropic silver nanoparticles (AgNPs) for capture and quantitative detection of *S. aureus* 5233 and *E. coli* M 17. The detection sensitivity data obtained from WGA-functionalized nanoparticles was one order of magnitude less than LCA-functionalized nanoparticles demonstrating that WGA is more specific to these bacteria[116]. In another work the specificity of WGA and LCA for capture of *Pseudomonas fluorescens* has been compared. Results demonstrated that both WGA and LCA can bind with microbes, but WGA showed more capture efficiency[117]. Con A is one of the most famous mannose binding lectins that binds with wide range of microbes such as *E. coli* O157:H7, *Bacillus subtilis*, and *Saccharomyces cerevisiae*[118,119]. A novel Con A-functionalized microtubular engine has been reported for fast, real-time, and selective capture of *E. coli* from drinking water and apple juice[120]. Hsu et al. reported that WGA lectin has higher binding affinity for *E. coli* than ConA[121]. Five different types of lectins including WGA, Con A, UEA, PNA, and MAL have been reported in the work of Wang et al., to be used for direct capture of *E. coli* O157:H7 on the surface of a SPR biosensor. The most significant binding response came from WGA confirming the highest binding ability for *E. coli* O157:H7[122]. These are all examples indicating that the capture efficiency and bacteria attachment to the lectin-functional interfaces are directly affected by lectin-sugar specificity and bacteria membrane composition. In a very recent report, Kaushal et al., developed a novel platform for capture, detection and photothermal ablation of *E. coli* and *P. aeruginosa* in water and coconut by using gold nanorods (AuNRS) functionalized with Con A and PNA. Compared to Con A, PNA-functionalized AuNRS demonstrated stronger aggregation around the *P. aeruginosa* cell surface.

These observations revealed higher sugar specificity of PNA through the carbohydrate molecules existing in *P. aeruginosa* wall [123].

Lectin-carbohydrate interactions can also be applied to differentiate different isolates and strains of a specific bacterial species. This is an advantage compared to antibody and nucleic acids-based detection systems that need prior knowledge regarding target bacteria. The specific affinity of Con A with *E. coli* DH5α has been reported while it does not bind to *E. coli* HB101[94]. Series of lectins including ConA and LCA (specific to-mannose and-glucose), MAL (β-N-acetylglucosamine) , WGA (sialic acid), and UEA (specific fucose) have been studied in a quartz crystal microbalance (QCM) biosensor to identify and differentiate seven strains of *C. jejuni*, three strains of *Helicobacter pylor*, and *E. coli*. Con A was shown to be specific to wide range of the pathogens examined, especially strains of *C. jejuni.* UEA demonstrated limited specificity, could distinguish different strains of *H. pylori* and *C. jejuni*, binding to just one strain of *H. pylori* and *C. jejuni*[124]. Lectins can also be applied to amplify the bacteria detection signal. WGA has been used as a signal amplifier in an electrochemical impedance sensor for the detection of *E. coli* O157:H7. Bacteria solutions were incubated on the electrode surface and then WGA solution was used to amplify the signal. Impedance measurements were performed before and after WGA incubation. The impedance value determined for WGA-incubated detection improved compared to the detection based on just antibody. Here, high number of lectin-binding locations present on the surface *E. coli* O157:H7 enhanced impedance signals[125].

Although lectin-carbohydrate based detection techniques offer several advantages, there are still some critical limitations that need to be addressed to fully utilize the benefits of lectin-based capture. Compared to antibody−antigen interaction, equilibrium dissociation constant (K_D) for the binding of an individual lectin to a monosaccharide is usually higher by 2-3 orders of

magnitude[24]. Functionalized interfaces with improved lectin density could overcome this limit by providing maximized multivalent lectin-carbohydrate interactions, leading to binding through enhanced avidity[126]. This is based on the theory of "glycoside cluster effect" introduced by Lee et al., describing the effect of presenting multiple binding sites specific to the receptor to increase binding avidity[127,128]. Interfaces should also be able to tune spatial arrangement and orientation, and to prevent denaturation of lectins, each factor which is critical for optimizing lectin-carbohydrate binding events[129,130,131]. Considering these factors, bio-functional polymers have attracted attention as a template for lectin-based detection approaches because of their excellent ability to tune the physico-chemical properties of interfaces[117,132].

1.4.3 Surface Chemistry of Interfaces Designed to Capture Bacteria

There are several methods for immobilization of affinity biomolecules onto surfaces, including electrostatic interaction, direct covalent attachment, and non-covalent interaction[133]. Electrostatic interaction is based on the charge difference between the surface and side chain of the biomolecules. Some biomolecules such as peptides can interact with the surface directly. Functional biomolecules can also attach to surface ligands using covalent bonds[134,135].

Although many biorecognition elements can adhere to the surfaces physically, covalent immobilization is often favored[136]. Covalent attachment provides stronger bonds and inhibits desorption and can be used to control the number and orientation of biomolecules. Modifying surface chemistry with the desired chemical functional group(s) for covalent immobilization of bioreceptors is a critical step before surface functionalization with the biomolecule[137]. The type of the functional group is normally designated based on the physico-chemical characteristics of the

surface, bioreceptor, and target cell[138]. Carboxyl[139], amine[140,141], epoxy[142], aldehyde[143,144], thiol[145], and succinimidyl esters[146] are commonly used as chemical groups functionalized on variety of substrates including glass, silicon, and gold which are then covalently reacted with bioreceptor molecules[147]. For instance, surfaces functionalized with carboxyl could be covalently coupled with amine-containing biomolecules such as proteins. Amine-modified surfaces are good candidates for reaction with a broad range of biomolecules containing iso(thio)cyanates and succinimidyl esters [137,148]. In addition, oligonucleotides can be immobilized on thiol-functionalized substrates through disulfide-coupling chemistry.

Functional groups can also affect other surface properties such as stability and dispersity in different medias. This emphasizes the importance of optimizing surface chemistry to generate high-efficient detection interfaces. As an example, multiwall carbon nanotubes (MWCNTs) have been reported to be functionalized with carboxylic groups in order to inhibit formation of aggregates and to obtain better dispersion[149]. Polyallylamine then was functionalized on carboxylic acid functionalized MWCNT followed by antibody immobilization. These physiochemically stable surfaces then were applied to an electrochemical immunosensor designed for multiplexed detection of *E. coli* O157:H7, *Campylobacter* and *Salmonella* from spiked milk samples[149]. In another example, Santra et al. functionalized nanoparticles with a negatively charged organosilane possessing phosphonate (3-(trihydroxysilyl) propyl methyl phosphonate (THPMP)) to raise the repulsive forces among the nanoparticles and enhancing their colloidal stability in buffer[150]. These examples highlight the dual-role of surface chemistry to control the both the biological reactivity and physical properties of interfaces. In a reverse direction to bacteria capture approaches, chemical groups could also inhibit the attachment of bacteria targets and other analytes to the surface and create anti-adhesive properties. For instance, polyethylene glycol (PEG) linkers could

be functionalized on the surface to perform as hydrophilic spacer and reduce the nonspecific binding and attachment of non-desired bacteria and biomolecules[151,105].

1.4.4 Nano/Micro Patterned Interfaces for Bacteria Capture

Generating surfaces with micro/nanoscale patterns of specific biomolecule receptors has been possible with improvements in nano/microfabrication techniques, including photolithography, dip-pen nanolithography (DPN), microcontact printing (μCP), inject printing, and surface coupling chemistry methods[152]. When functionalized with different bioreceptors, these patterned interfaces motivate capture within pre-determined areas on the surface while show strong attachment resistivity by surrounding regions[153]. This allows spatial control and the capability of placing bacteria in designated working areas separated from other capture sites[154]. Preparation of surfaces patterned with bacteria microarrays is performed by using surface patterning methods followed by chemical functionalization to provide surfaces patterned with bioaffinity molecules or chemicals surrounded by passive or blocked areas. Bacteria then attach to those specific patterns by using different mechanisms[155]. There are reports in the literature that demonstrate the use of μCP technique to covalently immobilize anti-*E. coli* antibody patterns onto the gold electrodes functionalized with self-assembled monolayer of mercaptohexadecanoic acid (MHDA). Here PEG3-thiol was also applied to minimize non-specific interactions in non-patterned areas. Gold electrodes were used in an electrochemical impedance spectroscopy (EIS)-base sensor for detection of *E. coli* O157:H7 with very high sensitivity (2 CFU/mL)[105]. Application of μCP to pattern anti-*E.coli* O157:H7 antibodies on indium tin oxide (ITO) with detection sensitivity of 1

CFU/ml and ability of selective detection of *E.coli* in the mixture containing ratio of 500:1 *S. typhimurium* to *E. coli* O157:H7 was also reported[156].

The excellent capability of patterned surfaces to provide dense antibody spots in a very small capture area allows for improved detection sensitivity at several orders of magnitude. Demers et al. created covalently bonded nanopatterns of proteins and oligonucleotides on gold and silicon oxide by using direct-write DPN. Low-resolution DPN provided spot sizes of 200×200 μm^2 consisting of 50,000 proteins with diameter of ~250 nm, while high-resolution DPN provided 13,000,000 spots in the same area. This is a great ability of DPN to create the reactive patterns with required chemical reactivity and high density of biomolecules with excellent control over size of the structure[157]. In addition to capture and detection, interfaces able to provide properly-tuned patterns of bacteria offer other applications in disease diagnostics and microbe-microbe interaction studies[158]. The use of μCP to immobilize one or more bacteria on the nanoscale pillars of adhesive polydopamine (PD) generated on glass surfaces has been reported by Arnfinnsdottir et al.[155] Here, the structures were used to study bacteria interactions on a single cell scale. Patterns of the generated pillars were surrounded by passive sites functionalized with PEG. As a positively charged polymer, PD can bind to the negatively charged bacteria through electrostatic interactions. After incubating these surfaces with a solution of *Psaudomonas putida*[155].

Chapters 3 and 4 of this thesis provide more background and information on polymer patterning techniques for capture and detection, and is primarily focused on developing fabrication techniques that include top-down and bottom-up patterning using parylene lift-off, interface-directed assembly, and a customized μCP method to generate microscale patterns of a functional azlactone-based block copolymer poly(glycidyl methacrylate)-block-poly(vinyl dimethyl

azlactone) (PGMA-*b*-PVDMA). This biofunctional polymer can be modified with different bioreceptors to introduce new chemical and biological features to the surface[159].

1.5 Biofunctional Polymer Interfaces for Capture and Characterization of Microbes

1.5.1 Polymeric Interfaces as Template Support for Bioaffinity Molecules

Polymers containing active functional groups such as azlactone, methacrylate, ethylene glycol, and ethyleneimine have obtained broad potential applications in biotechnology, biodiagnostics, and biomedical fields[160,146]. They can tune physical and chemical properties of surfaces such as cross-linking density, extend of chemical reactivity, and wetting behavior[161]. Synthetic polymeric materials and polymer brushes have been considered an advantageous support template for lectin covalent immobilization since they can manipulate the concentration of lectin while retaining its biological functionality, and improve the lectin orientation and accessibility[162,128]. For example, a surface-initiated atom transfer radical polymerization (SI-ATRP) of a methacrylate functionalized polymer (2-methyl-acrylic acid 3-(2,4,5-trihydroxy-6-hydroxymethyl-tetrahydro-pyran-3-ylamino)-propyl ester) (GMA-G) on silica microparticle was applied to synthesize a core–shell microparticle structure. Aldehyde groups formed by oxidation of GMA-G vicinal diols followed by immobilization by Con A, WGA, and ricinuscommunis agglutinin (RCA120) lectins. The use of polymer brushes increased the Con A, WGA, and RCA120 loading density on microparticles by a factor of 4.8, 4.2, and 4.8, respectively[162]. This is mainly because of the fact that polymer brushes provide 3D structure supports including huge number of binding locations ready for lectin immobilization. There are reports in the literature that showed poly(amidoamine) (PAMAM) dendrimer polymers can provide multiple reactive sites

available for lectin functionalization and modulating lectin desnity[163]. A thiourea linkage to functionalize sixth generation PAMAM dendrimer polymers with mannose demonstrated an improvement in Con A binding compared to methyl mannose. Degree of Con A clustering and the strength of Con A binding interactions could be tuned by controlling; (1) the number of mannose present on the surface of PAMAM dendrimer polymers, and (2) dendrimer polymer diameter[128].

Controlling the density of other types of biomolecules such as peptides and enzymes has also been achieved using bio-functional polymers. For example, epoxy-based polymer supports can generate stable chemical bonds with amine, thiol, and phenolic groups of proteins and peptides in mild reaction environments[164]. Bayramoğlu et al., showed that film supports of poly (2-hydroxyethyl methacrylate-co-glycidyl methacrylate) (poly (HEMA–GMA)) could be covalently immobilized with invertase enzymes by using the strong epoxy-amine interactions. Here substrates demonstrated 230% increase in immobilized enzyme density by increasing GMA density in polymer films from 0.58 to 2.33 mmol/gr[164]. This clearly confirms the capability of poly (HEMA–GMA) films to modulate enzyme density since GMA density can be simply tuned to a desired value via manipulating the ratio of monomer to co-monomer in polymerization step. In another work, GMA as an anchor for covalent protein immobilization was shown. Poly (GMA)-grafted PET (PGMA-PET) surfaces were used to immobilize high density of Immunoglobulin G (IgG) and anti-rat IgG proteins microarrays with protein detection sensitivity of 10 pg/mL. The reported LOD and detection dynamic range were better or comparable compared to other commercialized protein microarrays[165].

In addition to controlling lectin and protein density to prepare a template for bacteria detection and isolation approaches, synthesized biofunctional glycopolymers containing carbohydrate moieties can also be directly used as bacteria probe[166,167]. Raft-based glycopolymers,

polymethacrylamide/acrylamide, 2-Melibionamidoethyl, methacrylamide (PMA-MAEMA) possessing α-galactose residues, and poly(methacrylamide/acrylamide), 2-allolactobionamidoethyl, and methacrylamide (PMA-ALAEMA) possessing β-galactose as the pendant sugar have been employed to bind with *P. aeruginosa* and *S. aureus*. The results for glycopolymers containing corresponding pendant sugars showed a dramatic increase in number of attached bacteria to the polymers compared to controls (~10 times more for *P. aeruginosa* and ~ 8 times more for *S. aureus*)[81].

1.5.2 Azlactone-based Polymers for Tunable Interfaces

Among various classes of biofunctional polymers, use of azlactone-based polymers to generate reactive platforms for biological applications such as bacteria detection and capture has received attention. Azlactone-functional interfaces have been recently explored in a variety of different applications, including chemical capture where carbon sequestration and removal of toxic compounds is extremely important, and biofunctional interfaces for cell culture and enzyme immobilization. Azlactone polymer can also be used to introduce anti-fouling and anti-adhesive characteristics to a variety of substrates[132,147]. They have been employed for cell and biomolecules capture. In many biological applications, patterning azlactone polymer films at nano to micrometer length scales is desirable to facilitate spatial control of biomolecule presentation, cellular interactions, or to modulate surface interactions[168,169]. Azlactones have byproduct-free ring opening nucleophilic reactions with a broad range of nucleophiles such as amines, thiols, and alcohols to make strong covalent amide/amide, amide/thioester, and amide/ester crosslinks, respectively[170]. These reactive polymers can be functionalized with different chemicals to

introduce new chemical functionality, surface interfacial characteristics, and to modulation of biomolecules density[161]. Azlactone-functionalized interfaces are considered excellent platforms for post-fabrication immobilization with a variety of biomolecules such as lectins[132], proteins[171,147], peptides[172], and nucleotides through fast binding with amine or thiol groups[173]. An azlactone-based block copolymer poly (glycidyl methacrylate)-block-poly (vinyl dimethyl azlactone) (PGMA-*b*-PVDMA) has been reported as the template create 3D structures of WGA for capture of *P. fluorescens* from solutions. Here the capability of polymer to couple high density of lectins resulted in significant improvement in bacteria capture compared to surfaces containing physisorbed lectins[117]. One-step and hydrolytically stable reactions of azlactone-based polymers with other biomolecules have also been reported in the works of Kratochvil et al.[174] and Cullen et al.[175]. Interface properties of azlactone polymer films could be adjusted through post-fabrication with molecules that can promote or inhibit bacterial cells attachment. Buck et al., functionalized glass surfaces with poly(ethylene imine) and poly(2-vinyl-4,4′-dimethylazlactone) (PEI/PVDMA) and then coupled these films by amine-functionalized small molecules such as decylamine and D-glucamine to tune the interface properties. A *P. aeruginosa* solution was then incubated over the functionalized surfaces. The results demonstrated that D-glucamine-treated polymers inhibit *P. aeruginosa* cells adhesion and growth while decylamine-functionalized polymers promoted adhesion and growth[176]. Due to their versatile functionality, azlactone-containing polymers have been used in various environmental, biomedical, and biological approaches such as design of anti-fouling/anti-adhesive interfaces[177] and cell adhesion and growth in tissue engineering[172,178].

1.6 Biofouling in Industrial Systems

The latter portion of this thesis transitions from capture and isolation of bacteria from solution to isolation of microbes attached to membrane surfaces during biofouling for follow-up characterization. Thus, a brief review on biofouling is provided here. Biofouling and biofilm formation are the dynamic process of irreversible attachment and growth of microbial organisms on a substrate. Biofilms mainly consist of microbes and their extracellular components such as polysaccharides, lipids, and proteins[179]. Biofilm formation on a surface is a defensive mechanism against harsh environmental conditions such as pH, temperature, and nutrients or oxygen availability. It provides microbes with a protected environment to increase their chance of survival and growth[180]. Microorganisms in biofilm communities demonstrate higher antibacterial resistance and metabolic activities. Cohesion (binding microbes and other materials together) and adhesion (binding microbes to the substrates) are facilitated by bacteria extracellular polymeric substances (EPS). EPS secreted by microbes could also help for better capture of nutrients and facilitate feeding the underneath cells that do not have direct access to food[181]. Biofilms cause significant issues in food and dairy industry, industrial water systems, hip implants, and medical devices[181,182,183,184]. Specific to industrial equipment, microorganisms are able to form thick biofilms and prompt metal corrosion in heat exchangers and industrial pipelines resulting in decrease of equipment efficiency[179]. Biofilm formation and microbial contamination on medical instruments and implants result in device malfunction, persistent infection, and high rate of human casualties in hospitals[183]. In fact, more than 2 million hospital-borne nosocomial infections with 90,000 casualties were reported in the US in 2000[184]. The emergence of the negative effects of biofouling on industrial systems and public health clearly demonstrates that novel approaches are

required to control, prevent, and eliminate biofilms. Here, it is critically important is obtain an in-depth understanding of the mechanisms involved in biofilm formation and growth.

1.6.1 Fouling Mitigation Strategies

Biofouling mitigation techniques are categorized by three main approaches. The first method is disinfecting and sterilizing substrates before microbes attach to the surface tightly or use biofilm detectors to screen the attachment of early colonizing microbes on the surface[179]. Often this is not applicable for industrial systems such as heat exchangers, pipelines or membranes in water treatment processes such as reverse osmosis, ultra/nanofiltration, and electrodialysis, where there is need for continuous operation of equipment for several hours or days[185]. There are reports in the literature demonstrating the use of mechatronic surface sensors (MSS) and optical fiber sensors to monitor surface bacterial contaminations and characterize the fouling properties of early colonizers[186,187].

The second approach focuses on materials chemistry to develop surfaces unfavorable for microbial organisms to adhere to, and that are capable of demonstrating long-term resistance against biofouling. Hydrophobic-hydrophilic chemical interactions and physical structures of the surfaces determine the biofouling rate and bacteria attachment mechanisms in industrials system effluents[188]. As one of the pioneers, Rogers et al. studied the effect of eight different materials including as glass, stainless steel, polyethylene, ethylene-propylene, and latex on the biofilm formation and growth in water systems and revealed that glass and polyethylene have the most inhibitory effect against bacteria colonization while the latex and ethylene-propylene support larger number of attached bacteria[189]. Surface coatings with hydrophilic polymers including

polyethylene glycol and oligo ethylene glycol, or antimicrobial products have been reported to enhance the fouling resistance and decrease the microbial attachment[190,191,192]. Zwitterionic polymers have also been recognized as the promising candidates because of their antifouling behavior especially against *P. aeruginosa* and *E. coli*.[193] Zwitterionic polymer brushes use ionic solvation with water molecules to generate a hydration layer that serves as a steric obstacle opposing the attachment of microbial organisms[194]. Considering these materials chemistries, it is still extremely difficult to find the materials with highest repressive characteristics against the attachment of microorganisms and formation of biofilm[195].

The third approach concentrates on environmental conditions that affect the microorganisms' ability to attach to the surface and form a biofilm. Temperature, pH, nutrient availability, and presence of certain components such as sodium chloride, dextrose, glucose, and ethanol could favor the planktonic behavior of cells instead of sessile biofilms and vice versa[196,197]. There are reports in the literature showing that adding1% of dextrose or 5% sodium chloride to the tryptic soy broth (TSB) media results in stronger biofouling activity of *S. aureus* while adding these materials to the media does not affect the growth phases of *S. aureus*[197].

1.6.2 Understanding Biofilm Assembly on Surfaces from a Mechanistic Standpoint

The fundamental knowledge in the literature describes the basic stages of biofilm formation on the surface as; (1) transfer of planktonic cells in media to the surface and irreversible/reversible adhesion, (2) cell growth to create concentrated microcolonies, (3) inter-species interactions and expression of EPS, and (4) biofilm maturation and detachment[198]. Although there is some fundamental knowledge of these mechanisms, prevention and effective control of biofilm requires

an in-depth, mechanistic understanding of spatiotemporal dynamics of interspecies interactions and communication. These interactions manage the interplay among resource availability, growth rate, and nutrient diffusion inside a biofilm community[199,200]. Second, critical role of early colonizers to trigger biofilm formation and community assembly by production of EPS and recruiting other microorganisms to the surface should be considered. As an example, *Streptocooci* and *Actinomyces* have been shown as the early-stage organizers of biofilm formation on tooth surfaces by release of EPS and control of co-aggregation and co-adhesion pathways[200]. Finally because of the fact that species in the biofilm communicate via EPS expression, studying the initial stage of EPS spatial organization in the systems could provide detailed insights regarding adhesion mechanisms and bacterial community dynamics, and help to design novel physico-chemical protocols to prevent biofilm formation[201].

1.7 Methods of Dissecting Biofilms

1.7.1 Laser Capture Microdissection for Characterization of Biofilms

To obtain an understanding of the spatial heterogeneities of biofilms, it is often favorable to dissect specific areas to characterize the composition and microbes present. Laser capture microdissection (LCM) is the most standard procedure of isolating and harvesting cells of interest from tissues for proteomic analysis. Retrieval of desired cells occurs by using an optical microscope coupled with a laser beam. Microscopic observation determines the desired cells, a solid-state near-infrared laser beam then is applied to adhere an adhesive transfer film to the selected cells[202]. Cells are finally lifted free of the underlying support for follow-up molecular and genomic characterizations such as DNA/RNA sequencing, gene expression, and mass

spectrometry proteomics[203]. Use of LCM for spatiotemporal characterization and understanding of the physiological features of biofilms have been reported[204,205], although LCM has not been widely used in this application. Literature also demonstrates application of LCM for cell-surface interaction studies particularly in animal and plant systems[206,207]. Kerk et al. applied LCM to plant tissues embedded in paraffin and showed that DNA/RNA sequencing and protein analysis was feasible and amplification of LCM-dissected tissues allowed to genotyping plant cells[206]. Although LCM is a rapid and easy procedure to isolate the targeted cell from substrates, destruction of the retrieved cells as well as the surface during the process restricts its functionality since there are limited characterization tools for down-stream analysis of destructed cells. One alternative to LCM is a method called "nondestructive molecular extraction" (NDME) that applies ultrasound and microwave to retrieve cells form the substrates [208]. Chapters 6 of this thesis focuses on polymer surface dissection (PSD) as an improved approach for nondestructive removal of cells from underlying membrane surfaces for their characterization.

1.7.2 Light Responsive Polymers for Cell Manipulation

Light responsive polymers have received interest several applications that require the cell manipulation. In contrast to polymers that respond to changes in temperature, pH, and ionic strength, light offers control of wavelength, intensity, and irradiation time, parameters that be externally controlled[209]. This enables the capability of controlling both spatial and temporal characteristics of materials, a key advantage leading to extensive use of light-responsive polymeric interfaces for tissue engineering, regenerative medicine, and drug delivery applications[210]. Hydrogels consisting of crosslinked hydrophilic polymer structures demonstrate special properties

such as biocompatibility, biodegradability, elasticity, non-toxicity to cells, and high-water content. These features along with capability of nutrients to diffuse through the network, make hydrogels excellent scaffolds for cell attachment, encapsulation, and proliferation approaches[211]. Light-responsive hydrogels for the first time were synthesized by incorporation of a photo-cleavable moieties such as *ortho*-nitrobenzyl (*o*-NB) within hydrogel network [212]. Chapter 6 of this thesis explains the use of a polyethylene glycol (PEG)-based photo-responsive hydrogel altered with *o*-NB chromophores for non-destructive removal and detachment of microbes from AnMBR membrane surfaces. The retrieved cells then be molecularly characterized using 'Omic' technologies such as 16S rRNA sequencing and PCR.

1.8 References

(1) Adell, A. D.; Rivera, D.; Díaz, C.; Serrano, M. J.; Toledo, V.; Moreno Switt, A. I. Research on Major Water and Foodborne Pathogens in South America: Advancements and Gaps. *Curr. Opin. Food Sci.* **2018**, *20*, 38–43. https://doi.org/10.1016/j.cofs.2018.03.001.

(2) Velusamy, V.; Arshak, K.; Korostynska, O.; Oliwa, K.; Adley, C. An Overview of Foodborne Pathogen Detection: In the Perspective of Biosensors. *Biotechnol. Adv.* **2010**, *28* (2), 232–254. https://doi.org/10.1016/j.biotechadv.2009.12.004.

(3) Ramírez-Castillo, F. Y.; Loera-Muro, A.; Jacques, M.; Garneau, P.; Avelar-González, F. J.; Harel, J.; Guerrero-Barrera, A. L. Waterborne Pathogens: Detection Methods and Challenges. *Pathogens* **2015**, *4* (2), 307–334. https://doi.org/10.3390/pathogens4020307.

(4) Dowling, H. F. *Airborne Infections-the Past and the Futurel*; 1966.

(5) Stephen Inbaraj, B.; Chen, B. H. Nanomaterial-Based Sensors for Detection of Foodborne

Bacterial Pathogens and Toxins as Well as Pork Adulteration in Meat Products. *J. Food Drug Anal.* **2016**, *24* (1), 15–28. https://doi.org/10.1016/j.jfda.2015.05.001.

(6) Law, J. W. F.; Mutalib, N. S. A.; Chan, K. G.; Lee, L. H. Rapid Metho Ds for the Detection of Foodborne Bacterial Pathogens: Principles, Applications, Advantages and Limitations. *Front. Microbiol.* **2014**, *5* (DEC). https://doi.org/10.3389/fmicb.2014.00770.

(7) CDC and Food Safety | Food Safety | CDC https://www.cdc.gov/foodsafety/cdc-and-food-safety.html (accessed Feb 18, 2020).

(8) Kumar, S.; Nehra, M.; Mehta, J.; Dilbaghi, N.; Marrazza, G.; Kaushik, A. Point-of-Care Strategies for Detection of Waterborne Pathogens. *Sensors* **2019**, *19* (20), 4476. https://doi.org/10.3390/s19204476.

(9) Sonawane, S. Use of Nanomaterials in the Detection of Food Contaminants. *Eur. J. Nutr. Food Saf.* **2014**, *4* (4), 301–317. https://doi.org/10.9734/ejnfs/2014/6218.

(10) Black, R. E.; Levine, M. M.; Clements, M. L.; Hughes, T. P.; Blaser, M. J. Experimental Campylobacter Jejuni Infection in Humans. *J. Infect. Dis.* **1988**, *157* (3), 472–479. https://doi.org/10.1093/infdis/157.3.472.

(11) Watson, R. O.; Galán, J. E. Campylobacter Jejuni Survives within Epithelial Cells by Avoiding Delivery to Lysosomes. *PLoS Pathog.* **2008**, *4* (1), e14. https://doi.org/10.1371/journal.ppat.0040014.

(12) Augustine, R.; Abraham, A. R.; Kalarikkal, N.; Thomas, S. Monitoring and Separation of Food-Borne Pathogens Using Magnetic Nanoparticles. In *Novel Approaches of Nanotechnology in Food*; Elsevier, 2016; pp 271–312. https://doi.org/10.1016/b978-0-12-804308-0.00009-1.

(13) Mandal, P. K.; Biswas, A. K.; Choi, K.; Pal, U. K. Methods for Rapid Detection of

Foodborne Pathogens: An Overview. *Am. J. Food Technol.* **2011**, *6* (2), 87–102. https://doi.org/10.3923/ajft.2011.87.102.

(14) Suh, J. H.; Knabel, S. J. Comparison of Different Enrichment Broths and Background Flora for Detection of Heat-Injured Listeria Monocytogenes in Whole Milk. *J. Food Prot.* **2001**, *64* (1), 30–36. https://doi.org/10.4315/0362-028x-64.1.30.

(15) Nero, L. A.; de Mattos, M. R.; Barros, M. de A. F.; Beloti, V.; Franco, B. D. G. de M. Interference of Raw Milk Autochthonous Microbiota on the Performance of Conventional Methodologies for Listeria Monocytogenes and Salmonella Spp. Detection. *Microbiol. Res.* **2009**, *164* (5), 529–535. https://doi.org/10.1016/j.micres.2007.04.003.

(16) Dwivedi, H. P.; Jaykus, L. A. Detection of Pathogens in Foods: The Current State-of-the-Art and Future Directions. *Crit. Rev. Microbiol.* **2011**, *37* (1), 40–63. https://doi.org/10.3109/1040841X.2010.506430.

(17) Wang, Y.; Salazar, J. K. Culture-Independent Rapid Detection Methods for Bacterial Pathogens and Toxins in Food Matrices. *Compr. Rev. Food Sci. Food Saf.* **2016**, *15* (1), 183–205. https://doi.org/10.1111/1541-4337.12175.

(18) Vital, P. G.; Van Ha, N. T.; Tuyet, L. T. H.; Widmer, K. W. Application of Quantitative Real-Time PCR Compared to Filtration Methods for the Enumeration of Escherichia Coli in Surface Waters within Vietnam. *J. Water Health* **2017**, *15* (1), 155–162. https://doi.org/10.2166/wh.2016.173.

(19) Wei, D.; Oyarzabal, O. A.; Huang, T. S.; Balasubramanian, S.; Sista, S.; Simonian, A. L. Development of a Surface Plasmon Resonance Biosensor for the Identification of Campylobacter Jejuni. *J. Microbiol. Methods* **2007**, *69* (1), 78–85. https://doi.org/10.1016/j.mimet.2006.12.002.

(20) Sharma, H.; Mutharasan, R. Rapid and Sensitive Immunodetection of Listeria Monocytogenes in Milk Using a Novel Piezoelectric Cantilever Sensor. *Biosens. Bioelectron.* **2013**, *45* (1), 158–162. https://doi.org/10.1016/j.bios.2013.01.068.

(21) Bhardwaj, J.; Devarakonda, S.; Kumar, S.; Jang, J. Development of a Paper-Based Electrochemical Immunosensor Using an Antibody-Single Walled Carbon Nanotubes Bio-Conjugate Modified Electrode for Label-Free Detection of Foodborne Pathogens. *Sensors Actuators, B Chem.* **2017**, *253*, 115–123. https://doi.org/10.1016/j.snb.2017.06.108.

(22) Ray, P. C.; Khan, S. A.; Singh, A. K.; Senapati, D.; Fan, Z. Nanomaterials for Targeted Detection and Photothermal Killing of Bacteria. *Chem. Soc. Rev.* **2012**, *41* (8), 3193–3209. https://doi.org/10.1039/c2cs15340h.

(23) Tissari, P.; Zumla, A.; Tarkka, E.; Mero, S.; Savolainen, L.; Vaara, M.; Aittakorpi, A.; Laakso, S.; Lindfors, M.; Piiparinen, H.; et al. Accurate and Rapid Identification of Bacterial Species from Positive Blood Cultures with a DNA-Based Microarray Platform: An Observational Study. *Lancet* **2010**, *375* (9710), 224–230. https://doi.org/10.1016/S0140-6736(09)61569-5.

(24) Shen, Z.; Huang, M.; Xiao, C.; Zhang, Y.; Zeng, X.; Wang, P. G. Nonlabeled Quartz Crystal Microbalance Biosensor for Bacterial Detection Using Carbohydrate and Lectin Recognitions. *Anal. Chem.* **2007**, *79* (6), 2312–2319. https://doi.org/10.1021/ac061986j.

(25) Liu, Y.; Cao, Y.; Wang, T.; Dong, Q.; Li, J.; Niu, C. Detection of 12 Common Food-Borne Bacterial Pathogens by Taq Man Real-Time PCR Using a Single Set of Reaction Conditions. *Front. Microbiol.* **2019**, *10* (FEB). https://doi.org/10.3389/fmicb.2019.00222.

(26) Nanomaterial-based sensors for detection of foodborne bacterial pathogens and toxins as well as pork adulteration in meat products. - PubMed - NCBI

https://www.ncbi.nlm.nih.gov/pubmed/28911398 (accessed Feb 3, 2020).

(27) Wang, Y.; Qu, K.; Tang, L.; Li, Z.; Moore, E.; Zeng, X.; Liu, Y.; Li, J. Nanomaterials in Carbohydrate Biosensors. *TrAC - Trends Anal. Chem.* **2014**, *58*, 54–70. https://doi.org/10.1016/j.trac.2014.03.005.

(28) Loesche, W. J.; Lopatin, D. E.; Stoll, J.; Van Poperin, N.; Hujoel, P. P. Comparison of Various Detection Methods for Periodontopathic Bacteria: Can Culture Be Considered the Primary Reference Standard? *J. Clin. Microbiol.* **1992**, *30* (2), 418–426. https://doi.org/10.1128/jcm.30.2.418-426.1992.

(29) Valderrama, W. B.; Dudley, E. G.; Doores, S.; Cutter, C. N. Commercially Available Rapid Methods for Detection of Selected Food-Borne Pathogens. *Crit. Rev. Food Sci. Nutr.* **2016**, *56* (9), 1519–1531. https://doi.org/10.1080/10408398.2013.775567.

(30) Priyanka, B.; Patil, R. K.; Dwarakanath, S. A Review on Detection Methods Used for Foodborne Pathogens. *Indian J. Med. Res.* **2016**, *144* (September), 327–338. https://doi.org/10.4103/0971-5916.198677.

(31) Abbas, A.; Linman, M. J.; Cheng, Q. New Trends in Instrumental Design for Surface Plasmon Resonance-Based Biosensors. *Biosens. Bioelectron.* **2011**, *26* (5), 1815–1824. https://doi.org/10.1016/j.bios.2010.09.030.

(32) Ben Aissa, A.; Jara, J. J.; Sebastián, R. M.; Vallribera, A.; Campoy, S.; Pividori, M. I. Comparing Nucleic Acid Lateral Flow and Electrochemical Genosensing for the Simultaneous Detection of Foodborne Pathogens. *Biosens. Bioelectron.* **2017**, *88*, 265–272. https://doi.org/10.1016/j.bios.2016.08.046.

(33) Adzitey, F.; Rusul, G.; Huda, N.; Cogan, T.; Corry, J. Prevalence, Antibiotic Resistance and RAPD Typing of Campylobacter Species Isolated from Ducks, Their Rearing and

Processing Environments in Penang, Malaysia. *Int. J. Food Microbiol.* **2012**, *154* (3), 197–205. https://doi.org/10.1016/j.ijfoodmicro.2012.01.006.

(34) Chen, Y.; Cheng, N.; Xu, Y.; Huang, K.; Luo, Y.; Xu, W. Point-of-Care and Visual Detection of P. Aeruginosa and Its Toxin Genes by Multiple LAMP and Lateral Flow Nucleic Acid Biosensor. *Biosens. Bioelectron.* **2016**, *81*, 317–323. https://doi.org/10.1016/j.bios.2016.03.006.

(35) Van, T. T. H.; Anwar, A.; Scott, P. C.; Moore, R. J. Rapid and Specific Methods to Differentiate Foodborne Pathogens, *Campylobacter Jejuni* , *Campylobacter Coli* , and the New Species Causing Spotty Liver Disease in Chickens, *Campylobacter Hepaticus*. *Foodborne Pathog. Dis.* **2018**, *15* (8), 526–530. https://doi.org/10.1089/fpd.2017.2367.

(36) Lui, C.; Cady, N. C.; Batt, C. A. Nucleic Acid-Based Detection of Bacterial Pathogens Using Integrated Microfluidic Platform Systems. *Sensors* **2009**, *9* (5), 3713–3744. https://doi.org/10.3390/s90503713.

(37) Wei, C.; Zhong, J.; Hu, T.; Zhao, X. Simultaneous Detection of Escherichia Coli O157:H7, Staphylococcus Aureus and Salmonella by Multiplex PCR in Milk. *3 Biotech* **2018**, *8* (1). https://doi.org/10.1007/s13205-018-1086-5.

(38) Su, Y.-C.; Yu, C.; Lin, J.-L.; Lai, J.; Chen, S.-W.; Tu, P.-C.; Chu, C. Emergence of Salmonella Enterica Serovar Potsdam as a Major Serovar in Waterfowl Hatcheries and Chicken Eggs. *Avian Dis.* **2011**, *55* (2), 217–222. https://doi.org/10.1637/9420-060910-Reg.1.

(39) Agrimonti, C.; Sanangelantoni, A. M.; Marmiroli, N. Simultaneous Enumeration of Campylobacter Jejuni and Salmonella Enterica Genome Equivalents by Melting Curve Analysis Following Duplex Real Time PCR in the Presence of SYBR Green. *LWT* **2018**,

93, 542–548. https://doi.org/10.1016/j.lwt.2018.03.077.

(40) Adzitey, F.; Huda, N.; Ali, G. R. R. Molecular Techniques for Detecting and Typing of Bacteria, Advantages and Application to Foodborne Pathogens Isolated from Ducks. *3 Biotech* **2013**, *3* (2), 97–107. https://doi.org/10.1007/s13205-012-0074-4.

(41) Agustí, G.; Fittipaldi, M.; Codony, F. False-Positive Viability PCR Results: An Association with Microtubes. *Curr. Microbiol.* **2017**, *74* (3), 377–380. https://doi.org/10.1007/s00284-016-1189-3.

(42) Wang, L.; Mustapha, A. EMA-Real-Time PCR as a Reliable Method for Detection of Viable *Salmonella* in Chicken and Eggs. *J. Food Sci.* **2010**, *75* (3), M134–M139. https://doi.org/10.1111/j.1750-3841.2010.01525.x.

(43) Abulreesh, H. H.; Paget, T. A.; Goulder, R. *Campylobacter* in Waterfowl and Aquatic Environments: Incidence and Methods of Detection †. *Environ. Sci. Technol.* **2006**, *40* (23), 7122–7131. https://doi.org/10.1021/es060327l.

(44) Shi, X. M.; Long, F.; Suo, B. Molecular Methods for the Detection and Characterization of Foodborne Pathogens. In *Pure and Applied Chemistry*; 2010; Vol. 82, pp 69–79. https://doi.org/10.1351/PAC-CON-09-02-07.

(45) Rodríguez, P.; de, M. M.-B. R. de los másteres; 2019, undefined. Development and Evaluation of a Sandwich-Type ELISA for Multiple and Simultaneous Detection of Five Foodborne Pathogenic Bacteria. *upo.es*.

(46) Demirhan, B.; Demirhan, B. E.; Ertas, N.; Kara, H. E. S. Correction to: Rapid Detection of Acrylamide in Food Using Mn-Doped ZnS Quantum Dots as a Room Temperature Phosphorescent Probe. *Food Anal. Methods* **2018**, *11* (5), 1542–1542. https://doi.org/10.1007/s12161-017-1133-6.

(47) Ahari, H.; Kakoolaki, S.; Anvar, S. A. A. Detection of Salmonella Typhi Using Four Developed Kits of ELISA for Cleaning in Place Purification. *Int. J. Environ. Sci. Technol.* **2017**, *14* (10), 2149–2154. https://doi.org/10.1007/s13762-017-1309-z.

(48) Yu, B.; Li, F.; Zhao, T.; Li, F.; Zhou, B.; Xu, H. Hybridization Chain Reaction-Based Flow Cytometric Bead Sensor for the Detection of Emetic Bacillus Cereus in Milk. *Sensors Actuators, B Chem.* **2018**, *256*, 624–631. https://doi.org/10.1016/j.snb.2017.09.199.

(49) Afari, G. K.; Hung, Y. C. Detection and Verification of the Viable but Nonculturable (VBNC) State of Escherichia Coli O157:H7 and Listeria Monocytogenes Using Flow Cytometry and Standard Plating. *J. Food Sci.* **2018**, *83* (7), 1913–1920. https://doi.org/10.1111/1750-3841.14203.

(50) A., O.; Battie, C. Immunological Methods for the Detection of Campylobacter Spp. - Current Applications and Potential Use in Biosensors. In *Trends in Immunolabelled and Related Techniques*; InTech, 2012. https://doi.org/10.5772/35692.

(51) Sundararaj, N.; Kalagatur, N. K.; Mudili, V.; Krishna, K.; Antonysamy, M. Isolation and Identification of Enterotoxigenic Staphylococcus Aureus Isolates from Indian Food Samples: Evaluation of in-House Developed Aptamer Linked Sandwich ELISA (ALISA) Method. *J. Food Sci. Technol.* **2019**, *56* (2), 1016–1026. https://doi.org/10.1007/s13197-019-03568-1.

(52) Zhu, L.; He, J.; Cao, X.; Huang, K.; Luo, Y.; Xu, W. Development of a Double-Antibody Sandwich ELISA for Rapid Detection of Bacillus Cereus in Food. *Sci. Rep.* **2016**, *6*. https://doi.org/10.1038/srep16092.

(53) Pang, B.; Zhao, C.; Li, L.; Song, X.; Xu, K.; Wang, J.; Liu, Y.; Fu, K.; Bao, H.; Song, D.;

et al. Development of a Low-Cost Paper-Based ELISA Method for Rapid Escherichia Coli O157:H7 Detection. *Anal. Biochem.* **2018**, *542*, 58–62. https://doi.org/10.1016/j.ab.2017.11.010.

(54) Shen, Z.; Hou, N.; Jin, M.; Qiu, Z.; Wang, J.; Zhang, B.; Wang, X.; Wang, J.; Zhou, D.; Li, J. A Novel Enzyme-Linked Immunosorbent Assay for Detection of Escherichia Coli O157:H7 Using Immunomagnetic and Beacon Gold Nanoparticles. *Gut Pathog.* **2014**, *6* (1). https://doi.org/10.1186/1757-4749-6-14.

(55) Guo, Q.; Han, J. J.; Shan, S.; Liu, D. F.; Wu, S. S.; Xiong, Y. H.; Lai, W. H. DNA-Based Hybridization Chain Reaction and Biotin–Streptavidin Signal Amplification for Sensitive Detection of Escherichia Coli O157:H7 through ELISA. *Biosens. Bioelectron.* **2016**, *86*, 990–995. https://doi.org/10.1016/j.bios.2016.07.049.

(56) He, S.; Hong, X.; Huang, T.; Zhang, W.; Zhou, Y.; Wu, L.; Yan, X. Rapid Quantification of Live/Dead Lactic Acid Bacteria in Probiotic Products Using High-Sensitivity Flow Cytometry. *Methods Appl. Fluoresc.* **2017**, *5* (2), 024002. https://doi.org/10.1088/2050-6120/aa64e4.

(57) Picó, Y. *Chemical Analysis of Food: Techniques and Applications*; Elsevier Inc., 2012. https://doi.org/10.1016/C2010-0-64808-5.

(58) Sawant, S. N. Development of Biosensors from Biopolymer Composites. In *Biopolymer Composites in Electronics*; Elsevier Inc., 2017; pp 353–383. https://doi.org/10.1016/B978-0-12-809261-3.00013-9.

(59) Liu, J.; Jasim, I.; Shen, Z.; Zhao, L.; Dweik, M.; Zhang, S.; Almasri, M. A Microfluidic Based Biosensor for Rapid Detection of Salmonella in Food Products. *PLoS One* **2019**, *14* (5), e0216873. https://doi.org/10.1371/journal.pone.0216873.

(60) Homola, J. Present and Future of Surface Plasmon Resonance Biosensors. *Anal. Bioanal. Chem.* **2003**, *377* (3), 528–539. https://doi.org/10.1007/s00216-003-2101-0.

(61) Massad-Ivanir, N.; Shtenberg, G.; Tzur, A.; Krepker, M. A.; Segal, E. Engineering Nanostructured Porous SiO2 Surfaces for Bacteria Detection via "Direct Cell Capture." *Anal. Chem.* **2011**, *83* (9), 3282–3289. https://doi.org/10.1021/ac200407w.

(62) Ricke, S. C.; Feye, K. M.; Chaney, W. E.; Shi, Z.; Pavlidis, H.; Yang, Y. Developments in Rapid Detection Methods for the Detection of Foodborne Campylobacterin the United States. *Front. Microbiol.* **2019**, *10* (JAN). https://doi.org/10.3389/fmicb.2018.03280.

(63) Bhandari, D.; Chen, F.-C.; Bridgman, R. C. Detection of Salmonella Typhimurium in Romaine Lettuce Using a Surface Plasmon Resonance Biosensor. *Biosensors* **2019**, *9* (3), 94. https://doi.org/10.3390/bios9030094.

(64) Xi, F.; Gao, J.; Wang, J.; Wang, Z. Discrimination and Detection of Bacteria with a Label-Free Impedimetric Biosensor Based on Self-Assembled Lectin Monolayer. *J. Electroanal. Chem.* **2011**, *656* (1–2), 252–257. https://doi.org/10.1016/j.jelechem.2010.10.025.

(65) Wang, H.; Zhao, Y.; Bie, S.; Suo, T.; Jia, G.; Liu, B.; Ye, R.; Li, Z. Development of an Electrochemical Biosensor for Rapid and Effective Detection of Pathogenic Escherichia Coli in Licorice Extract. *Appl. Sci.* **2019**, *9* (2), 295. https://doi.org/10.3390/app9020295.

(66) Rosi, N. L.; Mirkin, C. A. Nanostructures in Biodiagnostics. *Chem. Rev.* **2005**, *105* (4), 1547–1562. https://doi.org/10.1021/cr030067f.

(67) Horák, D.; Babič, M.; Macková, H.; Beneš, M. J. Preparation and Properties of Magnetic Nano- and Microsized Particles for Biological and Environmental Separations. *J. Sep. Sci.* **2007**, *30* (11), 1751–1772. https://doi.org/10.1002/jssc.200700088.

(68) Tan, W.; Wang, K.; He, X.; Zhao, X. J.; Drake, T.; Wang, L.; Bagwe, R. P.

Bionanotechnology Based on Silica Nanoparticles. *Med. Res. Rev.* **2004**, *24* (5), 621–638. https://doi.org/10.1002/med.20003.

(69) Yang, H.; Li, H.; Jiang, X. Detection of Foodborne Pathogens Using Bioconjugated Nanomaterials. *Microfluid. Nanofluidics* **2008**, *5* (5), 571–583. https://doi.org/10.1007/s10404-008-0302-8.

(70) Nanotechnology for foodborne pathogen detection https://www.nanowerk.com/nanotechnology-for-foodborne-pathogen-detection.php (accessed Mar 7, 2020).

(71) Hosseinidoust, Z.; Van De Ven, T. G. M.; Tufenkji, N. Bacterial Capture Efficiency and Antimicrobial Activity of Phage-Functionalized Model Surfaces. **2011**, *27*, 5472–5480. https://doi.org/10.1021/la200102z.

(72) Amine-Functionalized Magnetic Nanoparticles for Rapid Capture and Removal of Bacterial Pathogens Y A N-F E N G H U A N G , † , § Y A-F A N W A N G , ‡ A N D X I U-P I N G Y A N *. https://doi.org/10.1021/es102285n.

(73) Jain, K. K. Nanotechnology in Clinical Laboratory Diagnostics. *Clin. Chim. Acta* **2005**, *358* (1–2), 37–54. https://doi.org/10.1016/j.cccn.2005.03.014.

(74) Nath, S.; Kaittanis, C.; Tinkham, A.; Perez, J. M. Dextran-Coated Gold Nanoparticles for the Assessment of Antimicrobial Susceptibility. *Anal. Chem.* **2008**, *80* (4), 1033–1038. https://doi.org/10.1021/ac701969u.

(75) Li, J.; Tan, L.; Liu, X.; Cui, Z.; Yang, X.; Yeung, K. W. K.; Chu, P. K.; Wu, S. Balancing Bacteria-Osteoblast Competition through Selective Physical Puncture and Biofunctionalization of ZnO/Polydopamine/Arginine-Glycine-Aspartic Acid-Cysteine Nanorods. *ACS Nano* **2017**, *11* (11), 11250–11263.

https://doi.org/10.1021/acsnano.7b05620.

(76) Campbell, G. A.; Mutharasan, R. Near Real-Time Detection of Cryptosporidium Parvum Oocyst by IgM-Functionalized Piezoelectric-Excited Millimeter-Sized Cantilever Biosensor. *Biosens. Bioelectron.* **2008**, *23* (7), 1039–1045. https://doi.org/10.1016/j.bios.2007.10.017.

(77) Cui, Y.; Ren, B.; Yao, J. L.; Gu, R. A.; Tian, Z. Q. Synthesis of AgcoreAushell Bimetallic Nanoparticles for Immunoassay Based on Surface-Enhanced Raman Spectroscopy. *J. Phys. Chem. B* **2006**, *110* (9), 4002–4006. https://doi.org/10.1021/jp056203x.

(78) Tombelli, S.; Minunni, M.; Mascini, M. Aptamers-Based Assays for Diagnostics, Environmental and Food Analysis. *Biomol. Eng.* **2007**, *24* (2), 191–200. https://doi.org/10.1016/j.bioeng.2007.03.003.

(79) Miranda, O. R.; Li, X.; Garcia-Gonzalez, L.; Zhu, Z. J.; Yan, B.; Bunz, U. H. F.; Rotello, V. M. Colorimetric Bacteria Sensing Using a Supramolecular Enzyme-Nanoparticle Biosensor. *J. Am. Chem. Soc.* **2011**, *133* (25), 9650–9653. https://doi.org/10.1021/ja2021729.

(80) Ngundi, M. M.; Kulagina, N. V.; Anderson, G. P.; Taitt, C. R. Nonantibody-Based Recognition: Alternative Molecules for Detection of Pathogens. *Expert Rev. Proteomics* **2006**, *3* (5), 511–524. https://doi.org/10.1586/14789450.3.5.511.

(81) Wang, W.; Chance, D. L.; Mossine, V. V.; Mawhinney, T. P. RAFT-Based Tri-Component Fluorescent Glycopolymers: Synthesis, Characterization and Application in Lectin-Mediated Bacterial Binding Study. *Glycoconj. J.* **2014**, *31* (2), 133–143. https://doi.org/10.1007/s10719-013-9508-4.

(82) Li, Y.; Afrasiabi, R.; Fathi, F.; Wang, N.; Xiang, C.; Love, R.; She, Z.; Kraatz, H. B.

Impedance Based Detection of Pathogenic E. Coli O157: H7 Using a Ferrocene-Antimicrobial Peptide Modified Biosensor. *Biosens. Bioelectron.* **2014**, *58*, 193–199. https://doi.org/10.1016/j.bios.2014.02.045.

(83) Wang, Y.; Ye, Z.; Ying, Y. New Trends in Impedimetric Biosensors for the Detection of Foodborne Pathogenic Bacteria. *Sensors* **2012**, *12* (3), 3449–3471. https://doi.org/10.3390/s120303449.

(84) Vaisocherová-Lísalová, H.; Víšová, I.; Ermini, M. L.; Špringer, T.; Song, X. C.; Mrázek, J.; Lamačová, J.; Scott Lynn, N.; Šedivák, P.; Homola, J. Low-Fouling Surface Plasmon Resonance Biosensor for Multi-Step Detection of Foodborne Bacterial Pathogens in Complex Food Samples. *Biosens. Bioelectron.* **2016**, *80*, 84–90. https://doi.org/10.1016/j.bios.2016.01.040.

(85) Xu, M.; Wang, R.; Li, Y. Rapid Detection of Escherichia Coli O157:H7 and Salmonella Typhimurium in Foods Using an Electrochemical Immunosensor Based on Screen-Printed Interdigitated Microelectrode and Immunomagnetic Separation. *Talanta* **2016**, *148*, 200–208. https://doi.org/10.1016/j.talanta.2015.10.082.

(86) Chen, C. T.; Yu, J. W.; Ho, Y. P. Identification of Bacteria in Juice/Lettuce Using Magnetic Nanoparticles and Selected Reaction Monitoring Mass Spectrometry. *J. Food Drug Anal.* **2019**, *27* (2), 575–584. https://doi.org/10.1016/j.jfda.2018.09.006.

(87) Poonlapdecha, W.; Seetang-Nun, Y.; Wonglumsom, W.; Tuitemwong, K.; Erickson, L. E.; Hansen, R. R.; Tuitemwong, P. Antibody-Conjugated Ferromagnetic Nanoparticles with Lateral Flow Test Strip Assay for Rapid Detection of Campylobacter Jejuni in Poultry Samples. *Int. J. Food Microbiol.* **2018**, *286*, 6–14. https://doi.org/10.1016/j.ijfoodmicro.2018.07.009.

(88) Li, Q.; Zhang, S.; Cai, Y.; Yang, Y.; Hu, F.; Liu, X.; He, X. Rapid Detection of *Listeria Monocytogenes* Using Fluorescence Immunochromatographic Assay Combined with Immunomagnetic Separation Technique. *Int. J. Food Sci. Technol.* **2017**, *52* (7), 1559–1566. https://doi.org/10.1111/ijfs.13428.

(89) Ngo, V. K. T.; Nguyen, H. P. U.; Huynh, T. P.; Tran, N. N. P.; Lam, Q. V.; Huynh, T. D. Preparation of Gold Nanoparticles by Microwave Heating and Application of Spectroscopy to Study Conjugate of Gold Nanoparticles with Antibody E. Coli O157:H7. *Adv. Nat. Sci. Nanosci. Nanotechnol.* **2015**, *6* (3), 035015. https://doi.org/10.1088/2043-6262/6/3/035015.

(90) Maurer, E. I.; Comfort, K. K.; Hussain, S. M.; Schlager, J. J.; Mukhopadhyay, S. M. Novel Platform Development Using an Assembly of Carbon Nanotube, Nanogold and Immobilized RNA Capture Element towards Rapid, Selective Sensing of Bacteria. *Sensors (Switzerland)* **2012**, *12* (6), 8135–8144. https://doi.org/10.3390/s120608135.

(91) Jayasena, S. D. Aptamers: An Emerging Class of Molecules That Rival Antibodies in Diagnostics. *Clin. Chem.* **1999**, *45* (9), 1628–1650.

(92) Vikesland, P. J.; Wigginton, K. R. Nanomaterial Enabled Biosensors for Pathogen Monitoring - A Review. *Environ. Sci. Technol.* **2010**, *44* (10), 3656–3669. https://doi.org/10.1021/es903704z.

(93) Houseman, B. T.; Mrksich, M. Model Systems for Studying Polyvalent Carbohydrate Binding Interactions; 2002; pp 1–44. https://doi.org/10.1007/3-540-45010-6_1.

(94) Dechtrirat, D.; Gajovic-Eichelmann, N.; Wojcik, F.; Hartmann, L.; Bier, F. F.; Scheller, F. W. Electrochemical Displacement Sensor Based on Ferrocene Boronic Acid Tracer and Immobilized Glycan for Saccharide Binding Proteins and E. Coli. *Biosens. Bioelectron.*

2014, *58*, 1–8. https://doi.org/10.1016/j.bios.2014.02.028.

(95) Haseley, S. R. Carbohydrate Recognition: A Nascent Technology for the Detection of Bioanalytes. *Anal. Chim. Acta* **2002**, *457* (1), 39–45. https://doi.org/10.1016/S0003-2670(01)01329-0.

(96) Disney, M. D.; Zheng, J.; Swager, T. M.; Seeberger, P. H. Detection of Bacteria with Carbohydrate-Functionalized Fluorescent Polymers. *J. Am. Chem. Soc.* **2004**, *126* (41), 13343–13346. https://doi.org/10.1021/ja047936i.

(97) El-Boubbou, K.; Gruden, C.; Huang, X. Magnetic Glyco-Nanoparticles: A Unique Tool for Rapid Pathogen Detection, Decontamination, and Strain Differentiation. *J. Am. Chem. Soc.* **2007**, *129* (44), 13392–13393. https://doi.org/10.1021/ja076086e.

(98) Caygill, R. L.; Blair, G. E.; Millner, P. A. A Review on Viral Biosensors to Detect Human Pathogens. *Anal. Chim. Acta* **2010**, *681* (1–2), 8–15. https://doi.org/10.1016/j.aca.2010.09.038.

(99) Kulagina, N. V.; Lassman, M. E.; Ligler, F. S.; Taitt, C. R. Antimicrobial Peptides for Detection of Bacteria in Biosensor Assays. *Anal. Chem.* **2005**, *77* (19), 6504–6508. https://doi.org/10.1021/ac050639r.

(100) Alhogail, S.; Suaifan, G. A. R. Y.; Zourob, M. Rapid Colorimetric Sensing Platform for the Detection of Listeria Monocytogenes Foodborne Pathogen. *Biosens. Bioelectron.* **2016**, *86*, 1061–1066. https://doi.org/10.1016/j.bios.2016.07.043.

(101) Liu, X.; Marrakchi, M.; Xu, D.; Dong, H.; Andreescu, S. Biosensors Based on Modularly Designed Synthetic Peptides for Recognition, Detection and Live/Dead Differentiation of Pathogenic Bacteria. *Biosens. Bioelectron.* **2016**, *80*, 9–16. https://doi.org/10.1016/j.bios.2016.01.041.

(102) Kulagina, N. V.; Shaffer, K. M.; Anderson, G. P.; Ligler, F. S.; Taitt, C. R. Antimicrobial Peptide-Based Array for Escherichia Coli and Salmonella Screening. *Anal. Chim. Acta* **2006**, *575* (1), 9–15. https://doi.org/10.1016/j.aca.2006.05.082.

(103) Lillehoj, P. B.; Kaplan, C. W.; He, J.; Shi, W.; Ho, C.-M. Rapid, Electrical Impedance Detection of Bacterial Pathogens Using Immobilized Antimicrobial Peptides. *J. Lab. Autom.* **2014**, *19* (1), 42–49. https://doi.org/10.1177/2211068213495207.

(104) Suaifan, G. A. R. Y.; Alhogail, S.; Zourob, M. Paper-Based Magnetic Nanoparticle-Peptide Probe for Rapid and Quantitative Colorimetric Detection of Escherichia Coli O157:H7. *Biosens. Bioelectron.* **2017**, *92*, 702–708. https://doi.org/10.1016/j.bios.2016.10.023.

(105) Barreiros dos Santos, M.; Agusil, J. P.; Prieto-Simón, B.; Sporer, C.; Teixeira, V.; Samitier, J. Highly Sensitive Detection of Pathogen Escherichia Coli O157: H7 by Electrochemical Impedance Spectroscopy. *Biosens. Bioelectron.* **2013**, *45* (1), 174–180. https://doi.org/10.1016/j.bios.2013.01.009.

(106) Bundy, J. L.; Fenselau, C. Lectin and Carbohydrate Affinity Capture Surfaces for Mass Spectrometric Analysis of Microorganisms. *Anal. Chem.* **2001**, *73* (4), 751–757. https://doi.org/10.1021/ac0011639.

(107) Liener, I. *The Lectins: Properties, Functions, and Applications in Biology and Medicine*; 2012.

(108) Bundle, D. R.; Young, N. M. Carbohydrate-Protein Interactions in Antibodies and Lectins. *Curr. Opin. Struct. Biol.* **1992**, *2* (5), 666–673. https://doi.org/10.1016/0959-440X(92)90199-H.

(109) Bicart-See, A.; Rottman, M.; Cartwright, M.; Seiler, B.; Gamini, N.; Rodas, M.; Penary,

M.; Giordano, G.; Oswald, E.; Super, M.; et al. Rapid Isolation of Staphylococcus Aureus Pathogens from Infected Clinical Samples Using Magnetic Beads Coated with Fc-Mannose Binding Lectin. *PLoS One* **2016**, *11* (6). https://doi.org/10.1371/journal.pone.0156287.

(110) Wang, Y.; Ye, Z.; Ying, Y. New Trends in Impedimetric Biosensors for the Detection of Foodborne Pathogenic Bacteria. *Sensors* **2012**, *12* (3), 3449–3471.

(111) Zeng, X.; Andrade, C. A. S.; Oliveira, M. D. L.; Sun, X.-L. Carbohydrate–Protein Interactions and Their Biosensing Applications. *Anal. Bioanal. Chem.* **2012**, *402* (10), 3161–3176.

(112) Seiler, B. T.; Cartwright, M.; Dinis, A. L. M.; Duffy, S.; Lombardo, P.; Cartwright, D.; Super, E. H.; Lanzaro, J.; Dugas, K.; Super, M.; et al. Broad-Spectrum Capture of Clinical Pathogens Using Engineered Fc-Mannose-Binding Lectin Enhanced by Antibiotic Treatment [Version 1; Peer Review: 2 Approved]. *F1000Research* **2019**, *8*, 108. https://doi.org/10.12688/f1000research.17447.1.

(113) Hu, S.; Wong, D. T. Lectin Microarray. *Proteomics - Clin. Appl.* **2009**, *3* (2), 148–154. https://doi.org/10.1002/prca.200800153.

(114) Pihíková, D.; Kasák, P.; Tkac, J. Glycoprofiling of Cancer Biomarkers: Label-Free Electrochemical Lectin-Based Biosensors. *Open Chem.* **2015**, *13* (1), 636–655. https://doi.org/10.1515/chem-2015-0082.

(115) Safina, G. Application of Surface Plasmon Resonance for the Detection of Carbohydrates, Glycoconjugates, and Measurement of the Carbohydrate-Specific Interactions: A Comparison with Conventional Analytical Techniques. A Critical Review. *Anal. Chim. Acta* **2012**, *712*, 9–29. https://doi.org/10.1016/j.aca.2011.11.016.

(116) Mikaelyan, M. V.; Poghosyan, G. G.; Hendrickson, O. D.; Dzantiev, B. B.; Gasparyan, V. K. Wheat Germ Agglutinin and Lens Culinaris Agglutinin Sensitized Anisotropic Silver Nanoparticles in Detection of Bacteria: A Simple Photometric Assay. *Anal. Chim. Acta* **2017**, *981*, 80–85. https://doi.org/10.1016/j.aca.2017.05.022.

(117) Hansen, R. R.; Hinestrosa, J. P.; Shubert, K. R.; Morrell-Falvey, J. L.; Pelletier, D. A.; Messman, J. M.; Kilbey, S. M.; Lokitz, B. S.; Retterer, S. T. Lectin-Functionalized Poly(Glycidyl Methacrylate)- Block -Poly(Vinyldimethyl Azlactone) Surface Scaffolds for High Avidity Microbial Capture. *Biomacromolecules* **2013**, *14* (10), 3742–3748. https://doi.org/10.1021/bm4011358.

(118) Masárová, J.; Dey, E. S.; Carlsson, J.; Danielsson, B. Novel Peptide Surface for Reversible Immobilization of Concanavalin A. *J. Biochem. Biophys. Methods* **2004**, *60* (2), 163–170. https://doi.org/10.1016/j.jbbm.2004.05.005.

(119) Afonso, C.; Fenselau, C. Use of Bioactive Glass Slides for Matrix-Assisted Laser Desorption/Ionization Analysis: Application to Microorganisms. *Anal. Chem.* **2003**, *75* (3), 694–697. https://doi.org/10.1021/ac025869+.

(120) Campuzano, S.; Orozco, J.; Kagan, D.; Guix, M.; Gao, W.; Sattayasamitsathit, S.; Claussen, J. C.; Merkoç, A.; Wang, J. Bacterial Isolation by Lectin-Modified Microengines. **2011**. https://doi.org/10.1021/nl203717q.

(121) Hsu, K. L.; Mahal, L. K. A Lectin Microarray Approach for the Rapid Analysis of Bacterial Glycans. *Nat. Protoc.* **2006**, *1* (2), 543–549. https://doi.org/10.1038/nprot.2006.76.

(122) Wang, Y.; Ye, Z.; Si, C.; Ying, Y. Monitoring of Escherichia Coli O157:H7 in Food Samples Using Lectin Based Surface Plasmon Resonance Biosensor. *Food Chem.* **2013**,

136 (3–4), 1303–1308. https://doi.org/10.1016/j.foodchem.2012.09.069.

(123) Kaushal, S.; Priyadarshi, N.; Pinnaka, A. K.; Soni, S.; Deep, A.; Singhal, N. K. Glycoconjugates Coated Gold Nanorods Based Novel Biosensor for Optical Detection and Photothermal Ablation of Food Borne Bacteria. *Sensors Actuators, B Chem.* **2019**, *289*, 207–215. https://doi.org/10.1016/j.snb.2019.03.096.

(124) Safina, G.; van Lier, M.; Danielsson, B. Flow-Injection Assay of the Pathogenic Bacteria Using Lectin-Based Quartz Crystal Microbalance Biosensor. *Talanta* **2008**, *77* (2), 468–472. https://doi.org/10.1016/j.talanta.2008.03.033.

(125) Li, Z.; Fu, Y.; Fang, W.; Li, Y. Electrochemical Impedance Immunosensor Based on Self-Assembled Monolayers for Rapid Detection of Escherichia Coli O157:H7 with Signal Amplification Using Lectin. *Sensors (Switzerland)* **2015**, *15* (8), 19212–19224. https://doi.org/10.3390/s150819212.

(126) Cummings, R. D.; Schnaar, R. L.; Esko, J. D.; Drickamer, K.; Taylor, M. E. Principles of Glycan Recognition. **2017**. https://doi.org/10.1101/GLYCOBIOLOGY.3E.029.

(127) Lee, Y. C.; Lee, R. T. Carbohydrate-Protein Interactions: Basis of Glycobiology. *Acc. Chem. Res.* **1995**, *28* (8), 321–327. https://doi.org/10.1021/ar00056a001.

(128) Woller, E. K.; Walter, E. D.; Morgan, J. R.; Singel, D. J.; Cloninger, M. J. Altering the Strength of Lectin Binding Interactions and Controlling the Amount of Lectin Clustering Using Mannose/Hydroxyl-Functionalized Dendrimers. *J. Am. Chem. Soc.* **2003**, *125* (29), 8820–8826. https://doi.org/10.1021/ja0352496.

(129) Guo, Y.; Nehlmeier, I.; Poole, E.; Sakonsinsiri, C.; Hondow, N.; Brown, A.; Li, Q.; Li, S.; Whitworth, J.; Li, Z.; et al. Dissecting Multivalent Lectin-Carbohydrate Recognition Using Polyvalent Multifunctional Glycan-Quantum Dots. *J. Am. Chem. Soc.* **2017**, *139*

(34), 11833–11844. https://doi.org/10.1021/jacs.7b05104.

(130) Templier, V.; Roux, A.; Roupioz, Y.; Livache, T. Ligands for Label-Free Detection of Whole Bacteria on Biosensors: A Review. *TrAC - Trends Anal. Chem.* **2016**, *79*, 71–79. https://doi.org/10.1016/j.trac.2015.10.015.

(131) Belický, Š.; Katrlík, J.; Tkáč, J. Glycan and Lectin Biosensors. *Essays Biochem.* **2016**, *60* (1), 37–47. https://doi.org/10.1042/EBC20150005.

(132) Hansen, R. R.; Shubert, K. R.; Morrell-Falvey, J. L.; Lokitz, B. S.; Doktycz, M. J.; Retterer, S. T. Microstructured Block Copolymer Surfaces for Control of Microbe Adhesion and Aggregation. *Biosensors* **2014**, *4* (1), 63–75. https://doi.org/10.3390/bios4010063.

(133) Moses, J. E.; Moorhouse, A. D. The Growing Applications of Click Chemistry. *Chem. Soc. Rev.* **2007**, *36* (8), 1249–1262. https://doi.org/10.1039/b613014n.

(134) Willner, I.; Willner, B. Biomolecule-Based Nanomaterials and Nanostructures. *Nano Lett.* **2010**, *10* (10), 3805–3815. https://doi.org/10.1021/nl102083j.

(135) Wang, L.; Gong, C.; Yuan, X.; Wei, G. Controlling the Self-Assembly of Biomolecules into Functional Nanomaterials through Internal Interactions and External Stimulations: A Review. *Nanomaterials* **2019**, *9* (2). https://doi.org/10.3390/nano9020285.

(136) Gao, Y.; Kyratzis, I. Covalent Immobilization of Proteins on Carbon Nanotubes Using the Cross-Linker 1-Ethyl-3-(3-Dimethylaminopropyl)Carbodiimide - A Critical Assessment. *Bioconjug. Chem.* **2008**, *19* (10), 1945–1950. https://doi.org/10.1021/bc800051c.

(137) Zhao, W.; Wang, L.; Tan, W. Fluorescent Nanoparticle for Bacteria and DNA Detection. *Adv. Exp. Med. Biol.* **2007**, *620*, 129–135. https://doi.org/10.1007/978-0-387-76713-0_10.

(138) Rusmini, F.; Zhong, Z.; Feijen, J. Protein Immobilization Strategies for Protein Biochips.

Biomacromolecules **2007**, *8* (6), 1775–1789. https://doi.org/10.1021/bm061197b.

(139) Miranda, O. R.; Li, X.; Garcia-Gonzalez, L.; Zhu, Z.-J.; Yan, B.; Bunz, U. H. F.; Rotello, V. M. Colorimetric Bacteria Sensing Using a Supramolecular Enzyme–Nanoparticle Biosensor. *J. Am. Chem. Soc.* **2011**, *133* (25), 9650–9653. https://doi.org/10.1021/ja2021729.

(140) Deng, Y.; Li, J.; Yu, J.; Zhao, J.; Tang, J. Silver Nanoparticles Well-Dispersed in Amine-Functionalized, One-Pot Made Vesicles as an Effective Antibacterial Agent. *Mater. Sci. Eng. C* **2016**, *60*, 92–99. https://doi.org/10.1016/j.msec.2015.11.011.

(141) Huang, Y.-F.; Wang, Y.-F.; Yan, X.-P. Amine-Functionalized Magnetic Nanoparticles for Rapid Capture and Removal of Bacterial Pathogens. *Environ. Sci. Technol.* **2010**, *44* (20), 7908–7913. https://doi.org/10.1021/es102285n.

(142) Ozalp, V. C.; Bayramoglu, G.; Erdem, Z.; Arica, M. Y. Pathogen Detection in Complex Samples by Quartz Crystal Microbalance Sensor Coupled to Aptamer Functionalized Core-Shell Type Magnetic Separation. *Anal. Chim. Acta* **2015**, *853* (1), 533–540. https://doi.org/10.1016/j.aca.2014.10.010.

(143) Chen, Y.-Y.; Tsai, M.-G.; Chi, M.-C.; Wang, T.-F.; Lin, L.-L. Covalent Immobilization of Bacillus Licheniformis γ-Glutamyl Transpeptidase on Aldehyde-Functionalized Magnetic Nanoparticles. *Int. J. Mol. Sci.* **2013**, *14* (3), 4613–4628. https://doi.org/10.3390/ijms14034613.

(144) Massad-Ivanir, N.; Shtenberg, G.; Raz, N.; Gazenbeek, C.; Budding, D.; Bos, M. P.; Segal, E. Porous Silicon-Based Biosensors: Towards Real-Time Optical Detection of Target Bacteria in the Food Industry. *Sci. Rep.* **2016**, *6* (1), 1–12. https://doi.org/10.1038/srep38099.

(145) Spampinato, V.; Parracino, M. A.; La Spina, R.; Rossi, F.; Ceccone, G. Surface Analysis of Gold Nanoparticles Functionalized with Thiol-Modified Glucose SAMs for Biosensor Applications. *Front. Chem.* **2016**, *4* (FEB), 8. https://doi.org/10.3389/fchem.2016.00008.

(146) Szweda, R.; Lipowska, D.; Silberring, J.; Dworak, A.; Trzebicka, B. Polymers for Peptide/Protein Arrays. *Polimery/Polymers* **2015**, *60* (2), 75–86. https://doi.org/10.14314/polimery.2015.075.

(147) Broderick, A. H.; Carter, M. C. D.; Lockett, M. R.; Smith, L. M.; Lynn, D. M. Fabrication of Oligonucleotide and Protein Arrays on Rigid and Flexible Substrates Coated with Reactive Polymer Multilayers. *ACS Appl. Mater. Interfaces* **2013**, *5* (2), 351–359. https://doi.org/10.1021/am302285n.

(148) Wang, L.; Wang, K.; Santra, S.; Zhao, X.; Hilliard, L. R.; Smith, J. E.; Wu, Y.; Tan, W. Watching Silica Nanoparticles Glow in the Biological World. *Anal. Chem.* **2006**, *78* (3), 646–654. https://doi.org/10.1021/ac0693619.

(149) Viswanathan, S.; Rani, C.; Ho, J. A. A. Electrochemical Immunosensor for Multiplexed Detection of Food-Borne Pathogens Using Nanocrystal Bioconjugates and MWCNT Screen-Printed Electrode. *Talanta* **2012**, *94*, 315–319. https://doi.org/10.1016/j.talanta.2012.03.049.

(150) Santra, S.; Yang, H.; Dutta, D.; Stanley, J. T.; Holloway, P. H.; Tan, W.; Moudgil, B. M.; Mericle, R. A. TAT Conjugated, FITC Doped Silica Nanoparticles for Bioimaging Applications. *Chem. Commun.* **2004**, *0* (24), 2810–2811. https://doi.org/10.1039/b411916a.

(151) Wang, L.; Lofton, C.; Popp, M.; Tan, W. Using Luminescent Nanoparticles as Staining Probes for Affymetrix GeneChips. *Bioconjug. Chem.* **2007**, *18* (3), 610–613.

https://doi.org/10.1021/bc060365u.

(152) Shuster, M. J.; Vaish, A.; Cao, H. H.; Guttentag, A. I.; McManigle, J. E.; Gibb, A. L.; Martinez, M. M.; Nezarati, R. M.; Hinds, J. M.; Liao, W. S.; et al. Patterning Small-Molecule Biocapture Surfaces: Microcontact Insertion Printing vs. Photolithography. *Chem. Commun.* **2011**, *47* (38), 10641–10643. https://doi.org/10.1039/c1cc13002a.

(153) Veiseh, M.; Zareie, M. H.; Zhang, M. Highly Selective Protein Patterning on Gold-Silicon Substrates for Biosensor Applications. *Langmuir* **2002**, *18* (17), 6671–6678. https://doi.org/10.1021/la025529j.

(154) Senaratne, W.; Andruzzi, L.; Ober, C. K. Self-Assembled Monolayers and Polymer Brushes in Biotechnology: Current Applications and Future Perspectives. *Biomacromolecules* **2005**, *6* (5), 2427–2448. https://doi.org/10.1021/bm050180a.

(155) Arnfinnsdottir, N. B.; Ottesen, V.; Lale, R.; Sletmoen, M. The Design of Simple Bacterial Microarrays: Development towards Immobilizing Single Living Bacteria on Predefined Micro-Sized Spots on Patterned Surfaces. *PLoS One* **2015**, *10* (6), e0128162. https://doi.org/10.1371/journal.pone.0128162.

(156) Barreiros dos Santos, M.; Azevedo, S.; Agusil, J. P.; Prieto-Simón, B.; Sporer, C.; Torrents, E.; Juárez, A.; Teixeira, V.; Samitier, J. Label-Free ITO-Based Immunosensor for the Detection of Very Low Concentrations of Pathogenic Bacteria. *Bioelectrochemistry* **2015**, *101*, 146–152. https://doi.org/10.1016/j.bioelechem.2014.09.002.

(157) Demers, L. M.; Ginger, D. S.; Park, S. J.; Li, Z.; Chung, S. W.; Mirkin, C. A. Direct Patterning of Modified Oligonucleotides on Metals and Insulators by Dip-Pen Nanolithography. *Science (80-.).* **2002**, *296* (5574), 1836–1838.

https://doi.org/10.1126/science.1071480.

(158) Costello, C. M.; Kreft, J. U.; Thomas, C. M.; Hammes, D. M.; Bao, P.; Evans, S. D.; Mendes, P. M. Exploiting Additive and Subtractive Patterning for Spatially Controlled and Robust Bacterial Co-Cultures. *Soft Matter* **2012**, *8* (35), 9147–9155. https://doi.org/10.1039/c2sm26111a.

(159) Buck, M. E.; Lynn, D. M. Azlactone-Functionalized Polymers as Reactive Platforms for the Design of Advanced Materials: Progress in the Last Ten Years. *Polym. Chem.* **2012**, *3* (1), 66–80.

(160) Lokitz, B. S.; Messman, J. M.; Hinestrosa, J. P.; Alonzo, J.; Verduzco, R.; Brown, R. H.; Osa, M.; Ankner, J. F.; Kilbey, S. M. Dilute Solution Properties and Surface Attachment of RAFT Polymerized 2-Vinyl-4, 4-Dimethyl Azlactone (VDMA). *Macromolecules* **2009**, *42* (22), 9018–9026.

(161) Zayas-Gonzalez, Y. M.; Lynn, D. M. Degradable Amine-Reactive Coatings Fabricated by the Covalent Layer-by-Layer Assembly of Poly(2-Vinyl-4,4-Dimethylazlactone) with Degradable Polyamine Building Blocks. *Biomacromolecules* **2016**, *17* (9), 3067–3075. https://doi.org/10.1021/acs.biomac.6b00975.

(162) Pan, Y.; Bai, H.; Ma, C.; Deng, Y.; Qin, W.; Qian, X. Brush Polymer Modified and Lectin Immobilized Core-Shell Microparticle for Highly Efficient Glycoprotein/Glycopeptide Enrichment. *Talanta* **2013**, *115*, 842–848. https://doi.org/10.1016/j.talanta.2013.06.031.

(163) Woller, E. K.; Cloninger, M. J. Mannose Functionalization of a Sixth Generation Dendrimer. *Biomacromolecules* **2001**, *2* (3), 1052–1054. https://doi.org/10.1021/bm015560k.

(164) Bayramoğlu, G.; Akgöl, S.; Bulut, A.; Denizli, A.; Arica, M. Y. Covalent Immobilisation

of Invertase onto a Reactive Film Composed of 2-Hydroxyethyl Methacrylate and Glycidyl Methacrylate: Properties and Application in a Continuous Flow System. *Biochem. Eng. J.* **2003**, *14* (2), 117–126. https://doi.org/10.1016/S1369-703X(02)00170-5.

(165) Liu, Y.; Li, C. M.; Hu, W.; Lu, Z. High Performance Protein Microarrays Based on Glycidyl Methacrylate-Modified Polyethylene Terephthalate Plastic Substrate. *Talanta* **2009**, *77* (3), 1165–1171. https://doi.org/10.1016/j.talanta.2008.08.024.

(166) Disney, M. D.; Zheng, J.; Swager, T. M.; Seeberger, P. H. Detection of Bacteria with Carbohydrate-Functionalized Fluorescent Polymers. *J. Am. Chem. Soc.* **2004**, *126* (41), 13343–13346. https://doi.org/10.1021/ja047936i.

(167) Pasparakis, G.; Alexander, C. Synthetic Polymers for Capture and Detection of Microorganisms. *Analyst* **2007**, *132* (11), 1075–1082. https://doi.org/10.1039/b705097f.

(168) Masigol, M.; Barua, N.; Retterer, S. T.; Lokitz, B. S.; Hansen, R. R. Chemical Copatterning Strategies Using Azlactone-Based Block Copolymers. *J. Vac. Sci. Technol. B Nanotechnol. Microelectron.* **2017**, *35* (6). https://doi.org/10.1116/1.4991881.

(169) Masigol, M.; Barua, N.; Lokitz, B. S.; Hansen, R. R. Fabricating Reactive Surfaces with Brush-like and Crosslinked Films of Azlactone-Functionalized Block Co-Polymers. *J. Vis. Exp.* **2018**, *2018* (136), e57562. https://doi.org/10.3791/57562.

(170) Carter, M. C. D.; Lynn, D. M. Covalently Crosslinked and Physically Stable Polymer Coatings with Chemically Labile and Dynamic Surface Features Fabricated by Treatment of Azlactone-Containing Multilayers with Alcohol-, Thiol-, and Hydrazine-Based Nucleophiles. *Chem. Mater.* **2016**, *28* (14), 5063–5072. https://doi.org/10.1021/acs.chemmater.6b01897.

(171) Zayas-Gonzalez, Y. M.; Ortiz, B. J.; Lynn, D. M. Layer-by-Layer Assembly of Amine-

Reactive Multilayers Using an Azlactone-Functionalized Polymer and Small-Molecule Diamine Linkers. **2017**. https://doi.org/10.1021/acs.biomac.7b00043.

(172) Schmitt, S. K.; Trebatoski, D. J.; Krutty, J. D.; Xie, A. W.; Rollins, B.; Murphy, W. L.; Gopalan, P. Peptide Conjugation to a Polymer Coating via Native Chemical Ligation of Azlactones for Cell Culture. *Biomacromolecules* **2016**, *17* (3), 1040–1047. https://doi.org/10.1021/acs.biomac.5b01682.

(173) Tocce, E. J.; Broderick, A. H.; Murphy, K. C.; Liliensiek, S. J.; Murphy, C. J.; Lynn, D. M.; Nealey, P. F. Functionalization of Reactive Polymer Multilayers with RGD and an Antifouling Motif: RGD Density Provides Control over Human Corneal Epithelial Cell-Substrate Interactions. *J. Biomed. Mater. Res. Part A* **2012**, *100A* (1), 84–93. https://doi.org/10.1002/jbm.a.33233.

(174) Kratochvil, M. J.; Carter, M. C. D.; Lynn, D. M. Amine-Reactive Azlactone-Containing Nanofibers for the Immobilization and Patterning of New Functionality on Nanofiber-Based Scaffolds. *ACS Appl. Mater. Interfaces* **2017**, *9* (11), 10243–10253. https://doi.org/10.1021/acsami.7b00219.

(175) Cullen, S. P.; Mandel, I. C.; Gopalan, P. Surface-Anchored Poly(2-Vinyl-4,4-Dimethyl Azlactone) Brushes as Templates for Enzyme Immobilization. *Langmuir* **2008**, *24* (23), 13701–13709. https://doi.org/10.1021/la8024952.

(176) Buck, M. E.; Breitbach, A. S.; Belgrade, S. K.; Blackwell, H. E.; Lynn, D. M. Chemical Modification of Reactive Multilayered Films Fabricated from Poly(2-Alkenyl Azlactone)s: Design of Surfaces That Prevent or Promote Mammalian Cell Adhesion and Bacterial Biofilm Growth. *Biomacromolecules* **2009**, *10* (6), 1564–1574. https://doi.org/10.1021/bm9001552.

(177) Yan, S.; Shi, H.; Song, L.; Wang, X.; Liu, L.; Luan, S.; Yang, Y.; Yin, J. Nonleaching Bacteria-Responsive Antibacterial Surface Based on a Unique Hierarchical Architecture. *ACS Appl. Mater. Interfaces* **2016**, *8* (37), 24471–24481. https://doi.org/10.1021/acsami.6b08436.

(178) Schmitt, S. K.; Xie, A. W.; Ghassemi, R. M.; Trebatoski, D. J.; Murphy, W. L.; Gopalan, P. Polyethylene Glycol Coatings on Plastic Substrates for Chemically Defined Stem Cell Culture. *Adv. Healthc. Mater.* **2015**, *4* (10), 1555–1564.

(179) Simões, M.; Simões, L. C.; Vieira, M. J. A Review of Current and Emergent Biofilm Control Strategies. *LWT - Food Sci. Technol.* **2010**, *43* (4), 573–583. https://doi.org/10.1016/j.lwt.2009.12.008.

(180) Tatsaporn, T. Microbial Biofilm in the Industry. *African J. Microbiol. Res.* **2013**, *7* (17), 1625–1634. https://doi.org/10.5897/ajmr12.2146.

(181) Kumar, C. G.; Anand, S. K. Significance of Microbial Biofilms in Food Industry: A Review. *Int. J. Food Microbiol.* **1998**, *42* (1–2), 9–27. https://doi.org/10.1016/S0168-1605(98)00060-9.

(182) Angles, M. L.; Chandy, J. P.; Cox, P. T.; Fisher, I. H.; Warnecke, M. R. Implications of Biofilm-Associated Waterborne Cryptosporidium Oocysts for the Water Industry. *Trends Parasitol.* **2007**, *23* (8), 352–356. https://doi.org/10.1016/j.pt.2007.06.001.

(183) Khatoon, Z.; McTiernan, C. D.; Suuronen, E. J.; Mah, T. F.; Alarcon, E. I. Bacterial Biofilm Formation on Implantable Devices and Approaches to Its Treatment and Prevention. *Heliyon* **2018**, *4* (12), e01067. https://doi.org/10.1016/j.heliyon.2018.e01067.

(184) Darouiche, R. O. Treatment of Infections Associated with Surgical Implants. *N. Engl. J. Med.* **2004**, *350* (14), 1422–1429. https://doi.org/10.1056/NEJMra035415.

(185) Bereschenko, L. A.; Stams, A. J. M.; Euverink, G. J. W.; Van Loosdrecht, M. C. M. Biofilm Formation on Reverse Osmosis Membranes Is Initiated and Dominated by Sphingomonas Spp. *Appl. Environ. Microbiol.* **2010**, *76* (8), 2623–2632. https://doi.org/10.1128/AEM.01998-09.

(186) Pereira, A.; Mendes, J.; Melo, L. F. Using Nanovibrations to Monitor Biofouling. *Biotechnol. Bioeng.* **2008**, *99* (6), 1407–1415. https://doi.org/10.1002/bit.21696.

(187) Philip-Chandy, R.; Scully, P. J.; Eldridge, P.; Kadim, H. J.; Grapin, M. G.; Jonca, M. G.; D'Ambrosio, M. G.; Colin, F. Optical Fiber Sensor for Biofilm Measurement Using Intensity Modulation and Image Analysis. *IEEE J. Sel. Top. Quantum Electron.* **2000**, *6* (5), 764–772. https://doi.org/10.1109/2944.892616.

(188) Santhosh Kumar, S.; Hiremath, S. S.; Ramachandran, B.; Muthuvijayan, V. Effect of Surface Finish on Wettability and Bacterial Adhesion of Micromachined Biomaterials. *Biotribology* **2019**, *18*. https://doi.org/10.1016/j.biotri.2019.100095.

(189) Rogers, J.; Dowsett, A. B.; Dennis, P. J.; Lee, J. V.; Keevil, C. W. Influence of Plumbing Materials on Biofilm Formation and Growth of Legionella Pneumophila in Potable Water Systems. *Appl. Environ. Microbiol.* **1994**, *60* (6), 1842–1851. https://doi.org/10.1128/aem.60.6.1842-1851.1994.

(190) Romero-Vargas Castrillón, S.; Lu, X.; Shaffer, D. L.; Elimelech, M. Amine Enrichment and Poly(Ethylene Glycol) (PEG) Surface Modification of Thin-Film Composite Forward Osmosis Membranes for Organic Fouling Control. *J. Memb. Sci.* **2014**, *450*, 331–339. https://doi.org/10.1016/j.memsci.2013.09.028.

(191) Yeh, C. C.; Venault, A.; Chang, Y. Structural Effect of Poly(Ethylene Glycol) Segmental Length on Biofouling and Hemocompatibility. *Polym. J.* **2016**, *48* (4), 551–558.

https://doi.org/10.1038/pj.2016.5.

(192) Vaishampayan, A.; de Jong, A.; Wight, D. J.; Kok, J.; Grohmann, E. A Novel Antimicrobial Coating Represses Biofilm and Virulence-Related Genes in Methicillin-Resistant Staphylococcus Aureus. *Front. Microbiol.* **2018**, *9* (FEB). https://doi.org/10.3389/fmicb.2018.00221.

(193) Cheng, G.; Li, G.; Xue, H.; Chen, S.; Bryers, J. D.; Jiang, S. Zwitterionic Carboxybetaine Polymer Surfaces and Their Resistance to Long-Term Biofilm Formation. *Biomaterials* **2009**, *30* (28), 5234–5240. https://doi.org/10.1016/j.biomaterials.2009.05.058.

(194) Liu, C.; Faria, A. F.; Ma, J.; Elimelech, M. Mitigation of Biofilm Development on Thin-Film Composite Membranes Functionalized with Zwitterionic Polymers and Silver Nanoparticles. *Environ. Sci. Technol.* **2017**, *51* (1), 182–191. https://doi.org/10.1021/acs.est.6b03795.

(195) Artyushkova, K.; Cornejo, J. A.; Ista, L. K.; Babanova, S.; Santoro, C.; Atanassov, P.; Schuler, A. J. Relationship between Surface Chemistry, Biofilm Structure, and Electron Transfer in Shewanella Anodes . *Biointerphases* **2015**, *10* (1), 019013. https://doi.org/10.1116/1.4913783.

(196) Toyofuku, M.; Inaba, T.; Kiyokawa, T.; Obana, N.; Yawata, Y.; Nomura, N. Environmental Factors That Shape Biofilm Formation. *Biosci. Biotechnol. Biochem.* **2016**, *80* (1), 7–12. https://doi.org/10.1080/09168451.2015.1058701.

(197) Kim, B. R.; Bae, Y. M.; Lee, S. Y. Effect of Environmental Conditions on Biofilm Formation and Related Characteristics of Staphylococcus Aureus. *J. Food Saf.* **2016**, *36* (3), 412–422. https://doi.org/10.1111/jfs.12263.

(198) Thomen, P.; Valentin, J. D. P.; Bitbol, A. F.; Henry, N. Spatiotemporal Pattern Formation

in: E. Coli Biofilms Explained by a Simple Physical Energy Balance. *Soft Matter* **2020**, *16* (2), 494–504. https://doi.org/10.1039/c9sm01375j.

(199) Bocci, F.; Suzuki, Y.; Lu, M.; Onuchic, J. N. Role of Metabolic Spatiotemporal Dynamics in Regulating Biofilm Colony Expansion. *Proc. Natl. Acad. Sci. U. S. A.* **2018**, *115* (16), 4288–4293. https://doi.org/10.1073/pnas.1706920115.

(200) Kolenbrander, P. E.; Palmer, R. J.; Periasamy, S.; Jakubovics, N. S. Oral Multispecies Biofilm Development and the Key Role of Cell-Cell Distance. *Nat. Rev. Microbiol.* **2010**, *8* (7), 471–480. https://doi.org/10.1038/nrmicro2381.

(201) Wingender, J.; Neu, T. R.; Flemming, H.-C. What Are Bacterial Extracellular Polymeric Substances? *Microb. Extracell. Polym. Subst.* **1999**, 1–19. https://doi.org/10.1007/978-3-642-60147-7_1.

(202) Banks, R. E.; Dunn, M. J.; Forbes, M. A.; Stanley, A.; Pappin, D.; Naven, T.; Gough, M.; Harnden, P.; Selby, P. J. The Potential Use of Laser Capture Microdissection to Selectively Obtain Distinct Populations of Cells for Proteomic Analysis - Preliminary Findings. *Electrophoresis* **1999**, *20* (4–5), 689–700. https://doi.org/10.1002/(SICI)1522-2683(19990101)20:4/5<689::AID-ELPS689>3.0.CO;2-J.

(203) Espina, V.; Heiby, M.; Pierobon, M.; Liotta, L. A. Laser Capture Microdissection Technology. *Expert Rev. Mol. Diagn.* **2007**, *7* (5), 647–657. https://doi.org/10.1586/14737159.7.5.647.

(204) Roy, S.; #1, H. E.; Sinha, M.; Ganesh, K.; Chaney, S.; Mann, E.; Miller, C.; Khanna, S.; Bergdall, V. K.; Powell, H. M.; et al. Mixed-Species Biofilm Compromises Wound Healing by Disrupting Epidermal Barrier Function HHS Public Access. *J Pathol* **2014**, *233* (4), 331–343. https://doi.org/10.1002/path.4360.

(205) Williamson, K. S.; Richards, L. A.; Perez-Osorio, A. C.; Pitts, B.; Mcinnerney, K.; Stewart, P. S.; Franklin, M. J. Heterogeneity in Pseudomonas Aeruginosa Biofilms Includes Expression of Ribosome Hibernation Factors in the Antibiotic-Tolerant Subpopulation and Hypoxia-Induced Stress Response in the Metabolically Active Population. **2012**. https://doi.org/10.1128/JB.00022-12.

(206) Kerk, N. M.; Ceserani, T.; Lorraine Tausta, S.; Sussex, I. M.; Nelson, T. M. Laser Capture Microdissection of Cells from Plant Tissues. *Plant Physiol.* **2003**, *132* (1), 27–35. https://doi.org/10.1104/pp.102.018127.

(207) Gautam, V.; Singh, A.; Singh, S.; Sarkar, A. K. An Efficient LCM-Based Method for Tissue Specific Expression Analysis of Genes and MiRNAs. *Sci. Rep.* **2016**, *6*. https://doi.org/10.1038/srep21577.

(208) Laser Capture Microdissection - an overview | ScienceDirect Topics https://www.sciencedirect.com/topics/agricultural-and-biological-sciences/laser-capture-microdissection (accessed Mar 2, 2020).

(209) Bertrand, O.; Gohy, J.-F. Photo-Responsive Polymers: Synthesis and Applications. *Polym. Chem* **2017**, *8*, 52. https://doi.org/10.1039/c6py01082b.

(210) Peppas, N. A.; Hilt, J. Z.; Khademhosseini, A.; Langer, R. Hydrogels in Biology and Medicine: From Molecular Principles to Bionanotechnology. *Adv. Mater.* **2006**, *18* (11), 1345–1360. https://doi.org/10.1002/adma.200501612.

(211) Drury, J. L.; Mooney, D. J. Hydrogels for Tissue Engineering: Scaffold Design Variables and Applications. *Biomaterials* **2003**, *24* (24), 4337–4351. https://doi.org/10.1016/S0142-9612(03)00340-5.

(212) Kloxin, A. M.; Kasko, A. M.; Salinas, C. N.; Anseth, K. S. Photodegradable Hydrogels for

Dynamic Tuning of Physical and Chemical Properties. *Science (80-.).* **2009**, *324* (5923), 59–63. https://doi.org/10.1126/science.1169494.

Chapter 2 - Thesis Approaches and Objectives

The focus of this thesis is on development of biofunctional polymer interfaces for new applications in the separation and isolation of targeted microorganisms. Chapters 3 and 4 focus on fabricating reactive surfaces with brush-like and crosslinked films of azlactone-functionalized block co-polymers. Here, fabrication strategies were developed by using parylene lift-off, interface-directed assembly, and μCP techniques to generate microscale patterns of an azlactone-based block copolymer in chemically or biologically inert backgrounds. The benefits of each approach were identified and it is expected that these polymers and patterning strategies will provide a versatile toolbox for developing synthetic interfaces with tuned chemical and physical features for sensing, cell culture, or material capture applications. The presented methods could control the polymer film thickness correspond to polymer brushes (~90 nm) or to highly crosslinked structures (~1-10 μm). They were also able to deposit PGMA-*b*-PVDMA films in a manner that completely preserves azlactone functionality through each processing step.

Chapter 5 has centers developing biofunctionalized polymer interfaces for capture, and isolation of microbial pathogens from solution. Capture of microbes on the surfaces occurs through the carbohydrate−lectins interactions. Compared to antibody-antigen interactions, equilibrium dissociation constant for the binding of an individual lectins to carbohydrates existing on the bacterial cell surface is higher by a factor of 100-1000. Here, the central hypothesis was that increasing lectin density on the surface could overcome this issue by providing maximized multivalent lectin-carbohydrate interactions, resulting in improved binding avidity and detection sensitivity. PGMA-*b*-PVDMA was used as a support template for lectin immobilization since it is able to couple rapidly with biomolecules to covalently bond lectins and tune their density on the

surface. After optimizing lectin density, the obtained surface chemistry knowledge for polymer coating and protein immobilization was coupled with physical nanostructures on the interface to achieve maximum bacteria capture and detection sensitivity.

Chapter 6 develops a method for studying membrane biofouling processes in wastewater treatment systems, a method termed Polymer Surface Dissection (PSD) approach. Here, a PEG-based photodegradable hydrogel was used to remove desired flocs, cells, or biofilms adhered to AnMBR membranes. Selective and non-destructive removal of cells was performed by using a patterned illumination tool that delivers user-defined pattern of LED light in a spatiotemporally controlled manner. The PSD approach allows follow-up molecular characterization of principal organisms by 16S rRNA sequencing, PCR, and EPS/SMP analysis.

Chapter 3 - Chemical Co-Patterning Strategies Using Azlactone-Based Block Co-Polymers*

3.1 Overview

Interfaces can be modified with azlactone-functional polymers in order to manipulate the chemical surface reactivity. Azlactone groups are highly reactive towards amine, thiol, and alcohol nucleophiles, providing a versatile coupling chemistry for secondary surface modification. Azlactone-based surface polymers have been explored in numerous applications, including chemical and biological capture, sensing, and cell culture. These applications often require that the polymer is co-patterned within a chemically or biologically inert background, however common fabrication methods degrade azlactone groups during processing steps or result in polymer films with poorly controlled thicknesses. Here, we develop fabrication strategies using parylene lift-off and interface-directed assembly methods to generate microscale patterns of azlactone-based block co-polymer in chemically or biologically inert backgrounds. The functionality of azlactone groups was preserved during fabrication, and patterned films appeared as uniform, 80-120 nm brush-like films. We also develop a patterning approach that uses a novel microcontact stamping method to generate cross-linked, three-dimensional structures of azlactone-based polymers with controllable, microscale thicknesses. We identify the benefits of each approach, and expect these polymers and patterning strategies to provide a versatile toolbox for developing synthetic interfaces with tuned chemical and physical features for sensing, cell culture, or material capture applications.

---

* Manuscript appearing in: Masigol, M., Barua, N., Retterer, S.T., Lokitz, B.S., and Hansen, R.R. Chemical Copatterning Strategies Using Azlactone-Based Block Copolymers. *Journal of Vacuum Science & Technology B* 35 (6), 06GJ01 (2017). doi: 10.1116/1.4991881
Reproduced with the permission from the American Vacuum Society.

3.2 Introduction

Developing materials and methods that allow for precise control of physico-chemical surface features is a critical aspect of materials science and engineering.[1] Polymeric materials are useful for manipulating interface properties, using either grafting-to or grafting-from strategies, and allow for control of surface reactivity based on the chemical functionality of the monomer and the molecular weight of the grafted polymer.[2, 3] In recent years, azlactone-based polymer films have increased in their use as a materials for manipulating surface reactivity.[4] Azlactone groups can be modified post-polymerization with primary nucleophiles, including amines, alcohols, thiols and hydrazine groups, allowing for a versatile chemical route for adding secondary surface functionality.[5-7] Coupling occurs in rapid, one-step "click" reactions without formation of byproducts.[8] For these reasons, azlactone-functional interfaces have been recently explored in a variety of different applications, including chemical capture (carbon sequestration and removal of toxic compounds)[9], biofunctional interfaces (cell culture[7, 10], enzyme immobilization[11], anti-fouling/anti-adhesive substrates[12], and cell capture[13, 14]) and nanolithography.[15]

In effort to harness the attractive benefits of azlactone-based surface polymers, Lokitz *et al.* developed the block co-polymer poly (glycidyl methacrylate-*block*-poly (vinyl dimethyl azlactone) (PGMA-*b*-PVDMA) as a versatile molecule for designer surface modifications. The GMA block was designed to provide covalent attachment of the polymer to the silicon surface. Previous film characterizations using neutron reflectivity revealed that spin coating and annealing of the polymer over silicon substrates generated a GMA-rich layer near in the 0-5 nm region of the surface, followed by a PVDMA-rich region further from the surface.[16] Utilizing this block copolymer strategy amplifies the surface reactivity compared to traditional "grafting to" approaches, as PGMA groups can also cause coupling to other polymers, significantly increasing

the density of PVDMA at the air interface.[16, 17] Tuning the molecular weight of the PVDMA block can be used to modulate surface reactivity. Hansen *et al.* used this polymer to develop bio-functional interfaces for capture of microorganisms. Here, it was demonstrated that high densities of VDMA chains enabled high densities of bio-affinity molecules to be immobilized over the films. This characteristic was key for improving affinity-based cell capture.[13, 14]

Application of PGMA-*b*-PVDMA polymers for use in bio-functional interfaces can be advanced by developing patterning approaches that generate well-defined polymer in positive regions of a substrate, and high resistivity the background regions of the substrate.[18] This would allow for spatial control of biomolecule presentation, useful for multiplexed sensing or for controlling of cell proliferation and cell fate in cell culture applications. It would also allow for control of analyte capture levels in biological or chemical capture applications. However, previous patterning efforts with this polymer using top-down photolithography techniques resulted in poorly controlled background regions that contained silicon contaminated with residual resist material, allowing for non-specific chemical and biological interactions in the background. Attempts at modifying these backgrounds with inert molecules caused cross-reaction with azlactone groups, removing the chemical valency of the polymer. Further, the thickness of these films was poorly controlled, containing non-uniform, 1 mm thick films at pattern edges and 80 nm thicknesses at the center of the patterns.[14] The non-uniformity in these films was likely caused by cross-linking of GMA blocks throughout the polymer film during annealing steps.

In this report, we develop customized patterning methods that address these limitations. These methods are designed to generate reactive polymer patterned within chemically or biologically inert backgrounds, and to generate uniform films with controlled, reproducible film thicknesses. Two considerations are made in the development of these customized patterning

techniques: (1) fabrication steps must not compromise azlactone functionality, and (2) GMA crosslinking reactions can be exploited to generate thick, highly cross-linked structures. With these aspects in mind, we report the development of customized, top-down and bottom-up patterning approaches that utilize parylene liftoff, interface-directed assembly, and a customized microcontact printing (μCP) technique to generate two dimensional (2-D) brush-like patterns (~90 nm) or thicker, three-dimensional (3-D) patterns (> 90 nm) of functional PGMA-*b*-PVDMA within well-controlled thicknesses and with controlled background chemistries.

3.3 Experimental Section

3.3.1 Materials

All chemicals were purchased from Sigma. Silicon (Si) wafers were purchased from Silicon Quest. The PGMA-*b*-PVDMA copolymer was synthesized to contain block lengths (monomer units present in each block) of 56 and 175, respectively, using an established synthesis.[16, 19] A Sylgard 184 silicone elastomer kit was purchased from Dow Corning and used for generating polydimethylsiloxane (PDMS) stamps.

3.3.2 Fabrication of polymer interfaces

Parylene Lift-off

Parylene can be used as a lift-off mask to generate chemical surface patterns, as parylene is chemically inert and will preserve background chemistry.[20-22] This approach was used to generate patterns of azlactone-based polymers over silicon substrates. Two different thicknesses of parylene (80 nm and 1 μm) were deposited on silicon using a parylene coater (PDS 2010 Labcoater, Specialty Coating Systems). A standard photolithographic and reactive ion etching method was then employed to pattern and etch features into the parylene. First, parylene-coated wafers were spin coated with positive resist (AZ1512) at 3000 rpm and for 30 s, then baked on hot

plate at 105 ºC for 1 min. Wafers were then exposed to UV light using a photomask (Advance Reproduction Corporation) and a mask alignment system (Qunitel NXQ-8000) for 10 s, developed in MIF 300 solution for 2 min, washed with Deionized (DI) water, then dried. Wafers were etched with oxygen plasma using an Oxford Instruments Plasma Lab System 100 with oxygen flow rate of 50 cm^3/min and a chamber pressure of 20 mTorr. To identify appropriate etching conditions, the etch rate of parylene was characterized. At RF power of 50W and integrated circuit piezoelectric (ICP) power of 500W the parylene etch rate was 1.18 μm/min and at RF power of 50W and ICP power of 200W the parylene etch rate was 570 nm/min. Etch time was calculated according to these etch rates in order to completely remove parylene in the exposed regions.

To generate polymer patterns, PGMA-*b*-PVDMA was spin coated over the parylene stencils, shown in Figure 3.1(a). Prior to spin coating, parylene stencils were treated with a Harrick Plasma Cleaner (PDC-001) operating at an RF power of 30W. Substrates were cleaned for 3 min to provide a native oxide layer in the exposed regions for polymer coupling.[23] To verify that the parylene was not etched during this cleaning step, the thickness of the parylene layer before and after plasma cleaning, parylene showed less than a 3% decrease in film thickness during this procedure. After cleaning, a 100 μL aliquot of a 1 wt % solution of PGMA-*b*-PVDMA in chloroform was then spin-coated over the wafers (Smart Coater 100-B) at 1500 rpm for 15 s. Chloroform was selected as the solvent because of its high solubility for the polymer, and because the polymer exists as single chains in chloroform, allowing for surface deposition of single chains from solution.[16, 17] Spin coating was performed immediately (1-2 sec) after pipetting a 100 μl drop of solution onto the substrates to minimize film non-uniformity due to chloroform evaporation. Annealing of polymer films was then performed at 110 °C under vacuum for 18 hr to allow for microphase segregation and surface attachment.[16] Polymer films processed under these conditions

were previously characterized using neutron reflectometry, which showed films to be PVDMA-rich at the air/film interface and PGMA-rich at the film/silicon interface, where GMA–surface coupling reactions occur.[16]

Substrates were sonicated in acetone or chloroform solvent for 10 min to remove the parylene layer. Alternatively, parylene could be peeled from the substrate by applying a piece of scotch tape at the edge of the substrate then pulling the tape away from the substrate.[24] Patterned substrates were stored under vacuum in a desiccator until characterization.

Interface Directed Assembly

Interface-directed assembly, a bottom-up patterning approach, was developed as an alternative fabrication method to generate chemical copatterns with PGMA-*b*-PVDMA. The method used substrates containing reactive oxides patterned within a biologically inert polyethylene glycol (PEG) background or a chemically inert (trichloro (1H,1H,2H,2H-perfluorooctyl) silane) (TPS) background. The chemical patterns serve as a template to spatially guide the formation of surface-stable PGMA-*b*-PVDMA films. First, substrates were plasma cleaned for 3 min, then functionalized with TPS for 1 hr using chemical vapor deposition (CVD). Silanized silicon wafers were then immersed into a 0.7% wt/v solution of pluronic F-127 in ultrapure water for 18 hr to generate a PEG layer over the surface.[25] Existence of PEG on the silicon substrates was confirmed by Attenuated total reflection- Fourier transform infrared (ATR-FTIR) analysis. To generate the reactive oxide patterns, parylene stencils were fabricated as previously described, then removed prior polymer spin coating, exposing background. A 100 μL aliquot of a 1 wt % solution of PGMA-*b*-PVDMA in chloroform was spin-coated over these templated substrates and annealed at the same conditions as previously described. Samples were

then sonicated for 10 min. in acetone to remove all polymer loosely attached to the surface. This process is shown in Figure 3.1(b).

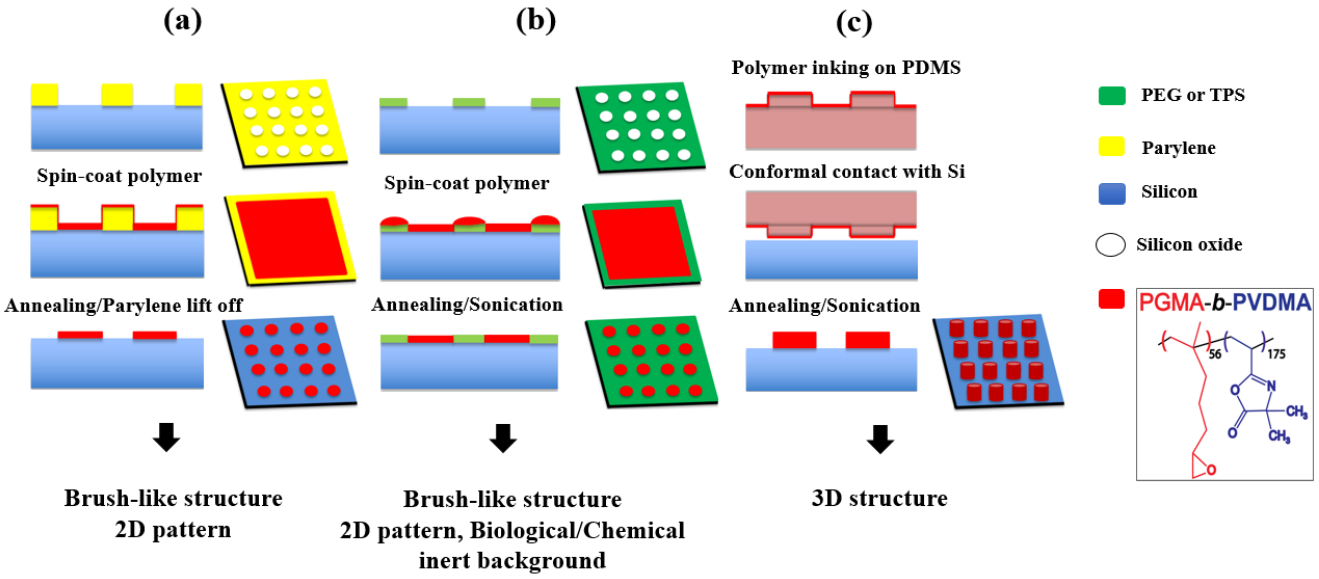

Figure 3.1 Strategies for generating 2-D and 3-D patterns of PGMA-*b*-PVDMA. (a) Parylene lift-off procedure for patterning 2-D brush-like polymer onto silicon substrates. (b) Interface directed assembly procedure for patterning 2-D brush-like polymer onto biological/chemical (PEG/TPS) inert substrates. (c) Generation of 3-D polymer structures onto silicon by using μCP method.

μCP Method

Stamp Fabrication

PDMS mCP printing stamps were generated using standard soft-lithography methods.[26] 10×10 mm microcontact stamps were designed to consist of an array of spots with diameters ranging between 5 to 50 μm with different center to center spacing and with a height of 20 μm. Silicon masters were treated with anti-adhesive TPS, then a PDMS pre-polymer solution (10:1 in base to catalyst ratio) was molded over the silicon masters at 80 ^{o}C for 2 hr.[27] Stamps were removed and cleaned using 1 M HCl, then sonicated for 5 min in acetone, sonicated for 5 min in ethanol,

and finally dried with an air brush. They were further dried in a convection oven at 80°C for 20 min to remove any residual organic solvent.

Stamping Conditions

Prior to μCP, PDMS stamps were conditioned with TPS by CVD, achieved by baking at 80 °C stamp next to a100 μL aliquot of TPS solution for 1 hr. The TPS layer was used to inhibit coupling of the polymer to the stamp surface. Stamps were then submerged into a solution of PGMA-*b*-PVDMA in chloroform for 3 min. In order to investigate the effect of inking concentration, PGMA-*b*-PVDMA concentration was varied between 0.25 and 1 wt%. Silicon substrates (15×15 mm) were treated with oxygen plasma for 3 min using a Harrick plasma cleaner (PDC-001-HP) to provide surface hydroxyl for coupling with epoxy groups present on the PGMA blocks. Inked stamps were then brought in conformal contact with the plasma cleaned silicon substrates using a manual drill press stand (Dremel Rotary Tool Workstation, Model 220). Silicon substrates were placed on polyurethane foam backing (Rogers Corporation, # SF060) to minimize PDMS stamp deformation due to non-uniform or high pressure stamping. Different stamp contact times were tested and 1 min contact time was found as optimum. Printed silicon substrates were immediately annealed in a vacuum oven at 110 ^{o}C for 18 hr to allow for microphase segregation and surface attachment of the patterned polymers. After annealing, samples were sonicated in acetone for 10 min to remove physically adsorbed polymers and then dried with N_2. This process is described in Figure 3.1(c). Patterned substrates were stored under in a vacuum desiccator until characterization.

3.3.3 Instrumentation

Brightfield and Fluorescence Microscopy

All images of substrates containing patterned arrays of PGMA-*b*-PVDMA were taken in brightfield or fluorescence using an upright microscope (BX51, Olympus) with 10×, N.A. 0.30 or 20×, NA 0.50 objectives, an Infinity 3S-1URM camera, and Infinity software.

Surface Profilometer

Profilometer (Dektak 150) was used for characterization of the surfaces and to measure the height of the polymer structures. Scan type was standard hill. Scan duration and force were 120 s and 1 mg, respectively.

Fourier Transform Infrared Spectroscopy (FT-IR)

The integrity of azlactone groups present in the polymer after each fabrication process was verified using a Perkin Elmer ATR-FTIR. Spectra were analyzed using Perkin^{TM} software. A background spectrum of 32 scans of the clean diamond crystal was first collected. Ethanol was used for cleaning of crystal prior to analysis of each sample. All spectra were background-subtracted and baseline-corrected.

Atomic Force Microscopy (AFM)

To characterize the polymer brush heights, a PicoPlus atomic force microscope with a 100 μm multipurpose scanner and PicoScan software (Agilent Technologies, Tempe, AZ) operating in contact mode was used. Veeco MLCT-E cantilevers with a 0.5 N/m spring constant were used to image 30×30 μm areas of patterned polymer features. Scan speeds varied between 0.25 to 1 Hz.

Scanning Electron Microscopy (SEM)

Samples were placed on double sided conductive carbon sticky tap coated to aluminum SEM stub, sputtered with palladium atoms using Denton Vacuum Desk II sputter coater and

analyzed under the Hitachi S-3500N Scanning Electron Microscope (Hitachi Science Systems Ltd., Tokyo, Japan) at accelerating voltage of 5 kV.

3.4 Results and Discussion

3.4.1 Formation of Two-dimensional, Brush-like Patterns of PGMA-b-PVDMA

Patterning with conventional photoresists often results in chemical fouling over background regions after liftoff, limiting their use for chemical patterning applications. Parylene stencils are an attractive alternative, as parylene will preserve the underlying surface chemistry after liftoff.[21] Previous results have shown that parylene could be deposited over TPS backgrounds, and upon removal this hydrophobic chemical layer was preserved.[20] The goal here was to use this parylene patterning method to generate patterns consisting of 2-D films of PGMA-*b*-PVDMA. We define 2-D films as films approaching 90 nm, corresponding to brush-like structures with a GMA-rich region at the silicon interface and a PVDMA-rich region at the film interface.[16] Patterned 2-D films are desirable as they will closely mimic the physical topology of the underlying substrate. Controlling the 2-D pattern density of PGMA-*b*-PVDMA can also be used to modulate the overall chemical valency of the interface.

To develop this patterning approach, parylene was deposited on the silicon substrates at two different thicknesses (1 μm and 80 nm). After parylene stencil fabrication, PGMA-*b*-PVDMA spin coating, annealing, and parylene liftoff, patterned polymer was present on both substrates with minimal polymer in the background regions, as shown in Figure 3.2(a-b). It was observed that the parylene thicknesses influenced the overall thickness and uniformity of the patterned polymer films. 1 μm thick parylene generated thicker polymer films with lower uniformity. Here, it is likely that the thick edges of the parylene caused non-uniform polymer deposition during the spin coating step that was then crosslinked into a thicker film during annealing. In contrast, the thin 80 nm

parylene allows for a corresponding thin layer of the polymer to be deposited over the surface. After annealing and liftoff, the thin parylene mask creates uniform films with thicknesses of ~110 nm, which approaches the expected thicknesses for 2-D brushlike structures.[16] These results suggest that the parylene liftoff approach is most useful for generating thin, 2-D patterns of the polymer.

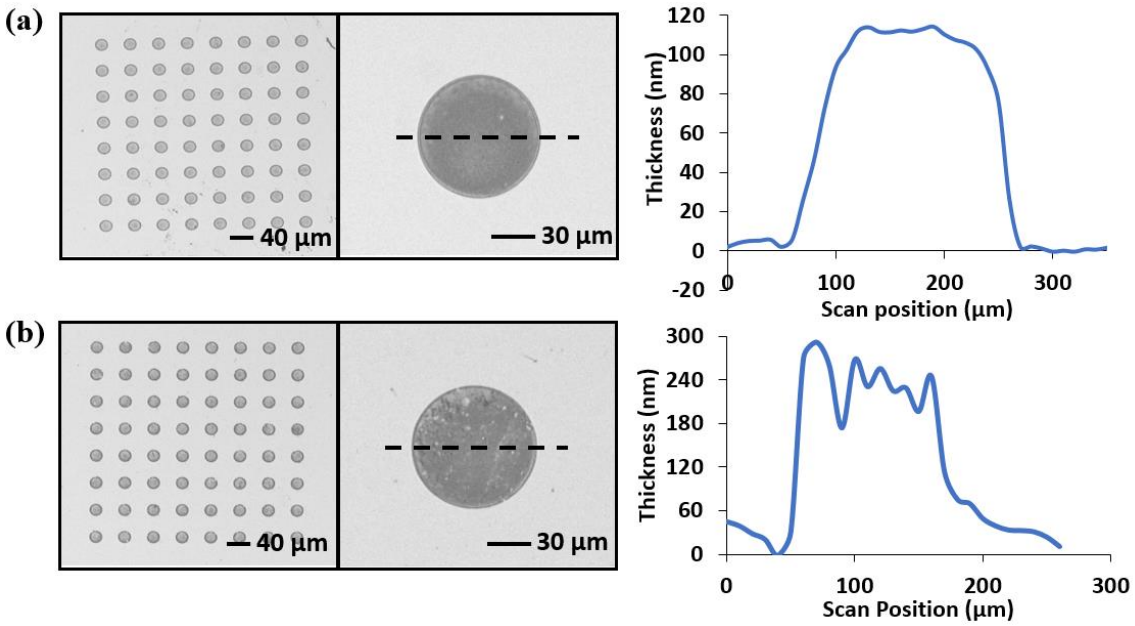

Figure 3.2 Parylene stencil thickness influences the PGMA-b-PVDMA film morphology. (a) Brightfield image and cross-sectional height profile of polymer generated from 80 nm thick parylene stencils shows patterns with uniform, brushlike thickness. (b) 1 µm thick parylene generated patterned films with non-uniform thickness.

Interface-directed assembly patterning techniques were explored as an alternative approach to generate 2-D patterned films. This bottom-up method relies on reactive oxide patterns to guide the assembly of polymer in the reactive regions, while background regions remain uncoupled to the polymer (Figure 3.1(b)). Brightfield and SEM images of these substrates show well-defined

PGMA-*b*-PVDMA pattern formation across the substrate, corresponding to the locations of oxide patterns etched into the TPS or PEG backgrounds (Figure 3.3(a)). Corresponding AFM measurements in Figure 3.3(b) show film heights of 90-100 nm, which agree with the expected thicknesses for brush-like structures of this polymer. ATR-FTIR was used to generate IR spectra on unpatterned PGMA-*b*-PVDMA films deposited under identical conditions over non-templated, clean Si surfaces. These spectra showed strong absorbance at 1818 cm^{-1}, verifying that azlactone functionality is preserved in this fabrication process (data not shown).

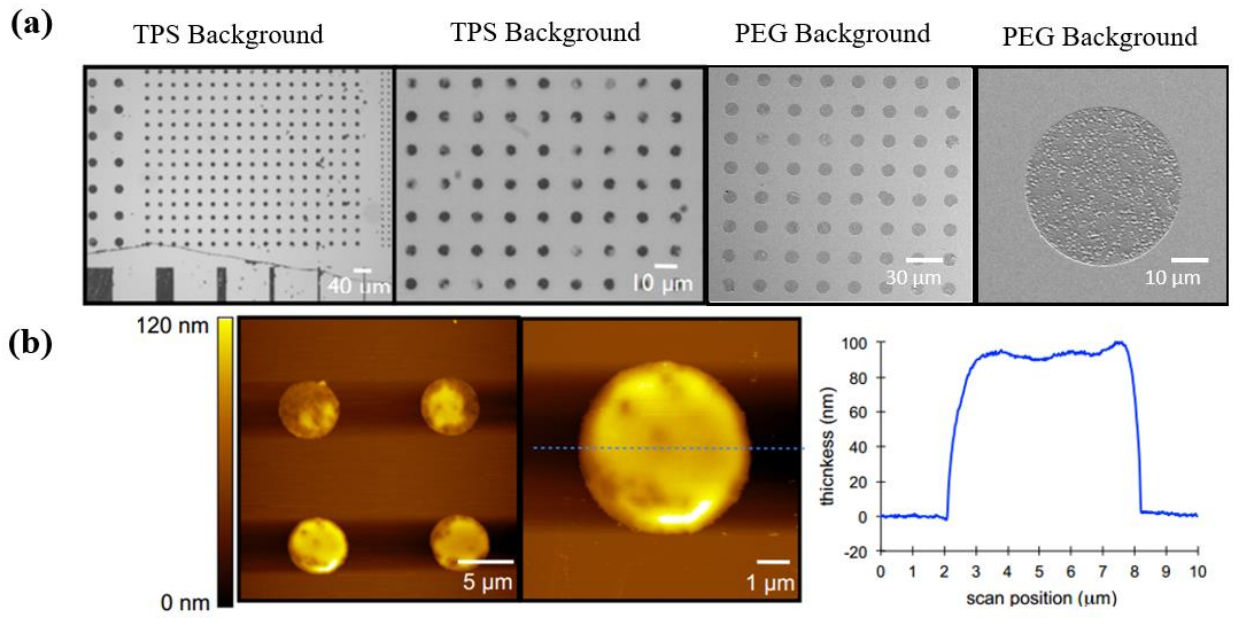

Figure 3.3 Interface directed assembly methods generate 2-D films of PGMA-*b*-PVDMA in chemically and biologically inert backgrounds. (a) Brightfield and SEM images of PGMA-*b*-PVDMA patterns on the chemically inert (TPS) and biologically inert (PEG) substrates. (b) AFM images of PGMA-*b*-PVDMA patterns on the patterned TPS surfaces and cross-sectional polymer height.

A key feature in both these co-patterning strategies is that the PGMA-*b*-PVDMA deposition, annealing, and sonication steps occur as the last steps of the fabrication. Attempting to modify background chemistry with silane-based reagents or other surface-reactive molecules in the presence of PGMA-*b*-PVDMA risks cross-reaction with highly reactive azlactone groups,

ultimately compromising polymer reactivity and functionality in downstream applications. The approaches reported here are specifically tailored to preserve azlactone functionality by requiring no further processing steps after patterning.

3.4.2 Formation of Three-dimensional Patterns of PGMA-b-PVDMA

To complement the 2-D patterning techniques, it was desired to also develop strategies for achieving 3-D PGMA-*b*-PVDMA patterns. We define 3-D films as those with film thicknesses greater that 90 nm, which requires crosslinking of GMA groups both to the surface and throughout the film to generate stable structures.[14] This feature would be advantageous in numerous applications; 3-D interfaces will achieve higher loading of target analytes in capture applications, higher sensitivity in sensing applications, and improved cell attachment, viability, and proliferation in cell culture applications.[28, 29] It was previously observed that epoxy crosslinking reactions that occur between GMA blocks in PGMA-*b*-PVDMA films during the annealing step can generate micron-thick, 3-D surface structures.[14] With this feature in mind, the spin-coating step previously used to deliver polymer to the surface was replaced with a customized μCP method, delivering higher amounts of the patterned PGMA-*b*-PVDMA to the surface and generating crosslinked 3-D structures on annealing.

Prior to μCP, PGMA-*b*-PVDMA was first loaded onto PDMS stamps through a custom inking process. Initial attempts at inking the stamp by pipetting 100 μl solution of PGMA-*b*-PVDMA in anhydrous chloroform resulted in non-uniform polymer deposition across the stamp due to rapid solvent evaporation (chloroform vapor pressure = 21.28 kPa at 20 ^{o}C)[30], compromising stamp reproducibility and efficiency.[31, 32] To deposit the polymer uniformly, stamps were instead completely submerged in polymer solution for 3 minutes and immediately pressed

over clean silicon substrates, annealed, and finally sonicated to remove loosely bound polymer. This resulted in well-defined polymer spots with micron-scale thicknesses stabilized to the surface, as shown in Figure. 3.4(a). As a control, substrates fabricated without the annealing step were also investigated. Sonication of these substrates in chloroform immediately washed away the polymer films (Figure 3.4(a,i)) verifying that GMA crosslinking was required to generate surface stable 3-D structures. Figure 3.4(b) shows the FTIR spectrum of silicon substrate before and after polymer transfer using a non-patterned PDMS stamp. The peak at 1818 cm^{-1} (corresponding to C=O bond of intact azlactone groups) directly confirmed that functional azlactone groups were present after transfer.

Finally, inking the PDMS stamp with varied concentrations of PGMA-*b*-PVDMA was investigated. Inking higher levels of the polymer resulted in delivery of more polymer to the surface, increasing the film heights as shown in Figure 3.4(c). Here, different concentrations of the inking solution (0.25-1% wt PGMA-*b*-PVDMA polymer) enabled polymer film formation between 3.5 ± 0.3 um and 6.5 ± 0.6 um. It would be expected that further dilution of the polymer would generate thinner structures.

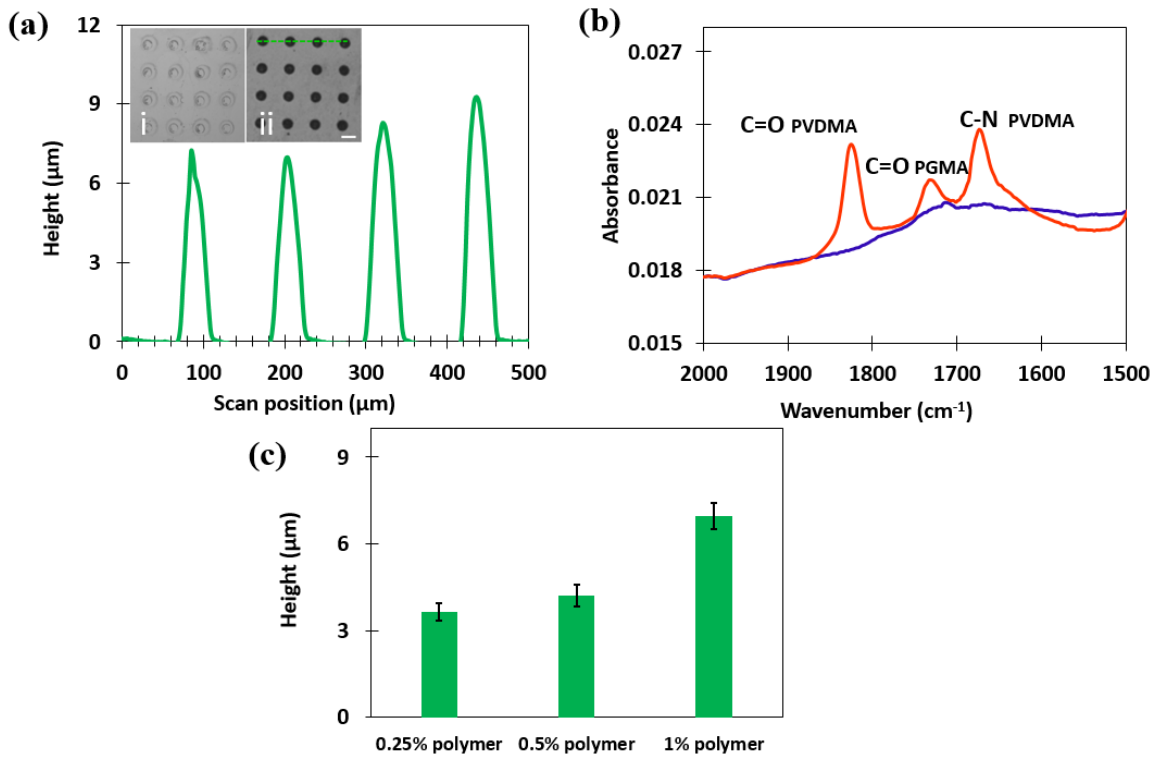

Figure 3.4 µCP can be used to generate 3-D PGMA-*b*-PVDMA structures. (A) Cross-sectional height profile of PGMA-*b*-PVDMA patterns (inset: brightfield images of PGMA-*b*-PVDMA patterned on silicon substrates (i) without annealing and (ii) with annealing, scale bar = 30 µm). (B) FTIR analysis of bare silicon (line without any significant peak) and PGMA-*b*-PVDMA (line with three significant peaks) transferred to the surface through the µCP method. (C) Average micropillar height for various inking concentrations.

The 3-D films generated by µCP appeared more uniform and more reproducible than the 3-D films generated from the parylene liftoff methods (Figure 3.2a), thus the µCP approach is the preferred fabrication method if thicker patterns are desired. However, we also investigated the potential to print these 3-D patterns over inert PEG backgrounds, and the polymer was unable to form stable surface attachment in this case (data not shown), presumably because the surface was unreactive to the polymer. Thus, the inability to pattern these structures into inert backgrounds is an inherent drawback of the µCP method.

3.5 Conclusion

In this report, we have successfully developed customized fabrication strategies that generate PGMA-*b*-PVDMA patterns for use in advanced material interfaces. The approaches detailed enable two significant advancements beyond previously published efforts: (1) functional PGMA-*b*-PVDMA can now be co-patterned into backgrounds that are chemically or biologically inert, and (2) PGMA-*b*-PVDMA can be patterned as 3-D surface structures. The capability to form precise 2-D PGMA-*b*-PVDMA patterns in chemically inert backgrounds enables one to precisely modulate the overall chemical reactivity of the surface by simply tuning the PGMA-*b*-PVDMA pattern density. Patterning these films within PEG-ylated backgrounds also advances its use in biointerface applications, as PGMA-*b*-PVDMA can now be functionalized with biological molecules (proteins, peptides, etc.) while minimizing non-specific background adsorption. Finally, generating 3-D structures using the facile μCP method reported will enable improved material capture and cell culture applications by generating PGMA-*b*-PVDMA with higher surface areas. We expect that this combined toolbox will progress the use of this material for advanced interface development. Future work is focused on developing these interfaces for improved capture and separation of biological analytes from complex mixtures for monitoring and diagnostic applications.

3.6 Acknowledgements

Support for this research was provided by Kansas State University. A portion of this research was conducted at the Center for Nanophase Materials Sciences, which is sponsored at Oak Ridge National Laboratory by the Scientific User Facilities Division, Office of Basic Energy Sciences and U.S. Department of Energy.

3.7 References

(1) B. Aden, C. M. Kite, B. W. Hopkins, A. Zetterberg, B. S. Lokitz, J. F. Ankner and S. M. Kilbey, *Macromolecules* **50**, 618 (2017).

(2) Q. Yu, J. Cho, P. Shivapooja, L. K. Ista and G. P. López, *ACS Appl. Mater. Interfaces* **5,** 9295 (2013).

(3) A. Olivier, F. Meyer, J. Raquez, P. Damman and P. Dubois, Prog. Polym. Sci. **37**, 157 (2012).

(4) A. H. Broderick, S. M. Azarin, M. E. Buck, S. P. Palecek and D. M. Lynn, *Biomacromolecules* **12**, 1998 (2011).

(5) A. Guyomard, D. Fournier, S. Pascual, L. Fontaine and J. Bardeau, *Eur. Polym. J.* **40**, 2343 (2004).

(6) Y. M. Zayas-Gonzalez and D. M. Lynn, *Biomacromolecules* **17**, 3067 (2016).

(7) S. K. Schmitt, D. J. Trebatoski, J. D. Krutty, A. W. Xie, B. Rollins, W. L. Murphy and P. Gopalan, *Biomacromolecules* **17**, 1040 (2016).

(8) M. W. Jones, S. Richards, D. M. Haddleton and M. I. Gibson, Polym. Chem. **4**, 717 (2013).

(9) B. Barkakaty, K. L. Browning, B. Sumpter, D. Uhrig, I. Karpisova, K. W. Harman, I. Ivanov, D. K. Hensley, J. M. Messman and S. M. Kilbey, *Macromolecules* **49**, 1523 (2016).

(10) S. K. Schmitt, A. W. Xie, R. M. Ghassemi, D. J. Trebatoski, W. L. Murphy and P. Gopalan, *Adv. Healthcare Mater*. **4**, 1555 (2015).

(11) S. P. Cullen, I. C. Mandel and P. Gopalan, *Langmuir* **24**, 13701 (2008).

(12) S. Yan, H. Shi, L. Song, X. Wang, L. Liu, S. Luan, Y. Yang and J. Yin, *ACS Appl. Mater. Interface* **8**, 24471 (2016).

(13) R. R. Hansen, K. R. Shubert, J. L. Morrell-Falvey, B. S. Lokitz, M. J. Doktycz and S. T. Retterer, *Biosensors* **4**, 63 (2014).

(14) R. R. Hansen, J. P. Hinestrosa, K. R. Shubert, J. L. Morrell-Falvey, D. A. Pelletier, J. M. Messman, S. M. Kilbey, B. S. Lokitz and S. T. Retterer, *Biomacromolecules* **14**, 3742 (2013).

(15) J. W. Choi, M. C. Carter, W. Wei, C. Kanimozi, F. W. Speetjens, M. K. Mahanthappa, D. M. Lynn and P. Gopalan, *Macromolecules* **49**, 8177 (2016).

(16) B. S. Lokitz, J. Wei, J. P. Hinestrosa, I. Ivanov, J. F. Browning, J. F. Ankner, S. M. Kilbey and J. M. Messman, *Macromolecules* **45**, 6438 (2012).

(17) B. S. Lokitz, J. M. Messman, J. P. Hinestrosa, J. Alonzo, R. Verduzco, R. H. Brown, M. Osa, J. F. Ankner and S. M. Kilbey, *Macromolecules* **42**, 9018 (2009).

(18) M. Veiseh, M. H. Zareie and M. Zhang, *Langmuir* **18**, 6671 (2002).

(19) J. Chalmeau, L. Salome, C. Thibault, C. Severac and C. Vieu, *Microelectron. Eng.* **84**, 1754 (2007).

(20) J. B. Boreyko, R. R. Hansen, K. R. Murphy, S. Nath, S. T. Retterer and C. P. Collier, *Sci. Rep.* **6**, 19131 (2016).

(21) C. P. Tan and H. G. Craighead, *Materials* **3**, 1803 (2010).

(22) C. P. Tan, B. R. Cipriany, D. M. Lin and H. G. Craighead, *Nano lett.* **10**, 719 (2010).

(23) T. Y. Chang, V. G. Yadav, S. De Leo, A. Mohedas, B. Rajalingam, C. Chen, S. Selvarasah, M. R. Dokmeci and A. Khademhosseini, *Langmuir* **23**, 11718 (2007).

(24) R. R. Hansen, A. C. Timm, C. M. Timm, A. N. Bible, J. L. Morrell-Falvey, D. A. Pelletier, M. L. Simpson, M. J. Doktycz and S. T. Retterer, *PloS One* **11**, 0160135 (2016).

(25) E. Vargis, C. B. Peterson, J. L. Morrell-Falvey, S. T. Retterer and C. P. Collier, *Biomaterials* **35**, 3999 (2014).

(26) D. Qin, Y. Xia and G. M. Whitesides, *Nat. Protoc.* **5**, 491 (2010).

(27) T. Kaufmann and B. J. Ravoo, *Poly. Chem-UK.* **1**, 371 (2010).

(28) P. Zhang, M. Gao and X. Zhang, *Talanscota* **153**, 366 (2016).

(29) L. Zheng, Y. Wan, P. Qi, Y. Sun, D. Zhang and L. Yu, *Talanta* **167**, 600 (2017).

(30) C. Credi, C. De Marco, E. Molena, M. P. Roca, J. S. Martí, J. Marques, X. Fernàndez-Busquets, M. Levi and S. Turri, *Colloid Surf., B* **146**, 250 (2016).

(31) Y. Li, Y. Sheng and H. Tsao, *Langmuir* **29**, 7802 (2013).

(32) L. Gonzalez-Macia, A. Morrin, M. R. Smyth and A. J. Killard, *Analyst* **135**, 845 (2010).

Chapter 4 - Fabricating Reactive Surfaces with Brush-like and Crosslinked Films of Azlactone-Functionalized Block Co-Polymers*

4.1 Overview

In this paper, fabrication methods that generate novel surfaces using the azlactone-based block co-polymer, poly (glycidyl methacrylate)-*block*-poly (vinyl dimethyl azlactone) (PGMA-*b*-PVDMA), are presented. Due to the high reactivity of azlactone groups towards amine, thiol, and hydroxyl groups, PGMA-*b*-PVDMA surfaces can be modified with secondary molecules to create chemically or biologically functionalized interfaces for a variety of applications. Previous reports of patterned PGMA-*b*-PVDMA interfaces have used traditional top-down patterning techniques that generate non-uniform films and poorly controlled background chemistries. Here, we describe customized patterning techniques that enable precise deposition of highly uniform PGMA-*b*-PVDMA films in backgrounds that are chemically inert or that have biomolecule-repellent properties. Importantly, these methods are designed to deposit PGMA-*b*-PVDMA films in a manner that completely preserves azlactone functionality through each processing step. Patterned films show well-controlled thicknesses that correspond to polymer brushes (~90 nm) or to highly crosslinked structures (~1-10 μm). Brush patterns are generated using either the parylene lift-off or interface directed assembly methods described and are useful for precise modulation of overall

---

* Manuscript appearing in: Masigol M., Barua N., Lokitz, B.S and Hansen, R.R. Fabricating Reactive Surfaces with Brush-like and Crosslinked Films of Azlactone-Functionalized Block Co-Polymers. *Journal of Visualized Experiments* 136, e57562 (2018). doi: 10.3791/57562
Reproduced with the permission from the *Journal of Visualized Experiments*.

chemical surface reactivity by adjusting either the PGMA-*b*-PVDMA pattern density or the length of the VDMA block. In contrast, the thick, crosslinked PGMA-*b*-PVDMA patterns are obtained using a customized micro-contact printing technique and offer the benefit of higher loading or capture of secondary material due to higher surface area to volume ratios. Detailed experimental steps, critical film characterizations, and trouble-shooting guides for each fabrication method are discussed.

4.2 Introduction

Developing fabrication techniques that allow for versatile and precise control of chemical and biological surface functionality is desirable for a variety of applications, from capture of environmental contaminants to development of next generation biosensors, implants, and tissue engineering devices[1, 2]. Functional polymers are excellent materials for tuning surface properties through "grafting from" or "grafting to" techniques[3]. These approaches allow for control of surface reactivity based on the chemical functionality of the monomer and molecular weight of the polymer[4-6]. Azlactone-based polymers have been intensely studied in this context, as azlactone groups rapidly couple with different nucleophiles in ring-opening reactions. This includes primary amines, alcohols, thiols and hydrazine groups, thereby providing a versatile route for further surface functionalization[7,8]. Azlactone-based polymer films have been employed in different environmental and biological applications including analyte capture[9, 10] cell culture[6, 11] and anti-fouling/anti-adhesive coatings[12]. In many biological applications, patterning azlactone polymer films at nano to micrometer length scales is desirable to facilitate spatial control of biomolecule presentation, cellular interactions, or to modulate surface interactions[13-18]. Therefore, fabrication methods should be developed to offer high pattern uniformity and well-controlled film thickness, without compromising chemical functionality[19].

Recently, Lokitz *et al.* developed a PGMA-*b*-PVDMA block copolymer which was capable of manipulating surface reactivity. PGMA blocks couple to oxide-bearing surfaces, yielding high and tunable surface densities of azlactone groups[20]. Previously reported methods for patterning this polymer for creation of biofunctional interfaces used traditional top-down photolithography approaches that generated non-uniform polymer films with background regions contaminated with residual photoresist material, causing high levels of non-specific chemical and biological interactions[21-23]. Here, attempts to passivate background regions caused cross-reaction with azlactone groups, compromising polymer reactivity. Considering these limitations, we recently developed techniques for patterning brush (~90 nm) or highly crosslinked (~1-10 mm) films of PGMA-*b*-PVDMA into chemically or biologically inert backgrounds in a manner that completely preserves the chemical functionality of the polymer[24]. These presented methods utilize parylene lift-off, interface-directed assembly (IDA), and a custom microcontact printing (mCP) techniques. Highly detailed experimental methods for these patterning approaches, as well as critical film characterizations and challenges and limitations associated with each technique are presented here in written and video format.

4.3 Experimental Section and Protocols

4.3.1 PGMA-b-PVDMA Synthesis

Synthesis of PGMA Macro-chain Transfer Agent (Macro-CTA)

(A) Use a 250-mL round-bottom reaction flask equipped with a polytetrafluoroethylene -coated magnetic stir bar.

(B) Combine 14.2 g of glycidyl methacrylate GMA (142.18 g/mol) with 490.8 mg of 2-cyano-2-propyl dodecyl trithiocarbonate (CPDT) (346.63 g/mol), and 87.7 mg of 2,2′-azobis (4-methoxy-

2,4-dimethyl valeronitrile) (V-70) (308.43 g/mol) (molar ratio of CPDT: V-70 = 5:1), and benzene (100 mL) into air free round bottom flask.

(C) Degas the reaction mixture using argon and stir for 30 min. Subsequently put the solution in a temperature-controlled oil bath at 30 °C and react for 18 h.

Note: The targeted molecular weight for the Macro-CTA is 10,000 g/mol.

Note: 18 hours was determined to be the time necessary to reach reasonable conversion.

Note: The color of the polymer solution is transparent light yellow.

(D) After 18 h, terminate the reaction by submerging the round bottom flask in liquid N_2.

(E) Precipitate the polymer by pouring the light yellow solution of polymer/benzene (~ 100 mL) into 400 mL of hexane.

(F) Stir the mixture for 5 min. Precipitate will be settled at the bottom of the beaker and is recovered by filtration.

(G) Dry the precipitate overnight under vacuum, then dilute it 400 mL tetrahydrofuran (THF). Re-precipitate in hexane.

(H) Dry this new precipitate again with argon overnight.

Note: Macro-CTA is a fine yellow powder. The product yield of the reaction will be ~ 43.8%. The M_n of the PGMA Macro-CTA is 7,990 g/mol with a polydispersity (PDI) of 1.506 (M_W = 12,030 g/mol).

Synthesis of PGMA-*b*-PVDMA

(A) VDMA must be fractionally distilled under reduced pressure, and the middle fraction (~70%) reserved for use.

Note: This is required to remove polymerization inhibitor.

Note: The distillation apparatus is attached to a schlenk line and the air seal valve is partially opened to the vacuum line. Minimal heat is applied using a varistat and heating mantle until the VDMA monomer begins distilling over at a rate of 1 drop per second.

(B) Combine the 2-Vinyl-4,4- dimethyl azlactone (VDMA) (139.15 g/mol) monomer (10.436 g) with the PGMA-macroCTA (1.669 g), V-70 (14.5 mg; molar ratio of PGMA-macroCTA: V-70 = 3:1) and benzene (75.0 mL) in a single-neck 250- mL round-bottom reaction flask equipped with a teflon-coated magnetic stir bar.

Note: Molecular weight information, PVDMA: 139.15 g/mol, PGMA-macroCTA: 12,030 g/mol, Benzene: 78.11 g/mol.

(C) Degas the mixture with high purity argon and stir for 30 min, and then put in oil bath at 32 °C for 18 h.

(D) Terminate the reaction by submerging the round bottom flask in liquid N_2.

(E) Precipitate the polymer three times into hexane and dry it at room temperature under vacuum.

(F) Characterize the molecular weight and PDI of the product by using size exclusion chromatography (SEC) according to the procedure in Lokitz et al.[20]

Note: SEC equipped with three 5 µm mixed-C columns (300 x 7.5 mm) in series, a refractive index detector (Wavelength= 880 nm), a photodiode array detector, multi-angle light scattering (MALS) detector (Wavelength= 660 nm), and a viscometer.

Note: All experiments performed in this manuscript used product with PGMA and PVDMA block lengths of 56 and 175, respectively. The molecular weight of the block copolymer was 37,620 g/mol and the PDI was 1.16.

4.3.2 Generation of Parylene Stencil Patterns Over Silicon Substrates

Parylene Coating

(A) Sonicate silicon wafers in 50% wt. acetone in water for 5 min followed by sonication in 50% wt. isopropanol (IPA) in water for 5 min.

(B) Rinse silicon wafers with deionized (DI) water and blow dry with gas N_2

(C) Deposit 80 nm and 1 µm thick parylene N on 4-inch silicon wafers using a parylene coater.

Note: Characterize the thickness of parylene films by using a surface profilometer.

(D) Calibrate parylene film thickness with parylene dimer mass for each individual parylene coating system.
Note: In the current system, ~80 mg and ~1000 mg parylene N dimer was required to obtain 80 nm and 1 µm film thickness, respectively (Based on the calibration curve obtained).
(E) Use the following settings during operation of the parylene coater: pressure: 80 mTorr, duration: 1 h, furnace temperature: 690 °C, vaporizer temperature: 160 °C.

Photolithography

(A) Bake wafers in an oven at 100 °C for 20 min then let wafers sit for another 3 min at room temperature.

Note: Additional wait time improves adhesion of the photoresist.

(B) Add 2 mL of positive photoresist and dispense at the center of the parylene-coated wafer. Spin coat the wafers with positive photoresist at 3000 rpm for 30 s.

Note: Spin coating must be done under hood.

(C) Wait 1 min, bake wafer on a hot plate at 105 °C for 1 min.

(D) Load photomask in a mask alignment system. Expose wafers to UV light (λ=325 nm) for 10 s with a dosage of 65 mJ/cm^2.

(E) Let the wafers sit for another 5 min at room temperature.

(F) Develop wafers by submerging in developer solution for 2 min, rinse the wafers with deionized water, then dry with N_2.

Note: Do this under a hood.

Note: After developing, photoresist appears completely removed from areas exposed to UV. Use an optical microscope to verify the wafers.

Reactive Ion Etching

(A) Use a reactive ion etching (RIE) tool to etch developed wafers with oxygen plasma.

(B) Apply an oxygen flow rate of 50 cm^3/min at a chamber pressure of 20 mTorr.

(C) For a parylene film thickness of 1 µm, use RF power of 50 W and inductively coupled plasma (ICP) power of 500 W for 100 s was to remove exposed parylene from patterned areas. This corresponded to a parylene etch rate of 1.0-1.15 µm/min.

(D) For a parylene thickness of 80 nm, use RF power of 50 W and ICP power of 200 W for 55 s to remove exposed parylene from patterned areas. This corresponds to a parylene etch rate of 570-620 nm/min.

Note: For efficient parylene removal, determine the parylene etch rate for each RIE system.

(E) Inspect etched substrates with an optical microscope. The silicon surface will appear shiny after the parylene is completely removed from exposed regions.

(F) Verify etch depth using a surface profilometer.

4.3.3 Parylene Lift-off Procedure

Preparation of Polymer Solutions

(A) Dissolve PGMA-*b*-PVDMA into chloroform (1% wt.). Chloroform should be anhydrous to prevent hydrolysis of azlactone groups.

Note: Chloroform is the preferred solvent because it has a high degree of solubility for the polymer, allowing for more uniform surface deposition of single polymer chains compared to other organic solvents[25].

Cleaning Parylene Stencils with the Plasma Cleaner

(A) Turn on the plasma cleaner main power and put the parylene-coated substrates in the plasma cleaner chamber.

(B) Turn on the vacuum pump and evacuate the air in the chamber until the pressure gauge is less than 400 mTorr.

(C) Slightly open the metering valve and allow the air to enter to the plasma cleaner until the pressure gauge shows 800-1000 mTorr.

(D) Select RF with “Hi” mode and expose the substrates for 3 min.

(E) At the end of process, turn off the RF power and vacuum pump.

(F) Turn off the plasma cleaner and remove the substrates.

Note: After plasma cleaning, the surface shows hydrophilic behavior (Figure 4.1B). The water contact angle of bare silicon surfaces before and after plasma cleaning are $27^{O} \pm 2^{O}$ and 0^{O}, respectively.

Spin-coating of PGMA-*b*-PVDMA, Annealing and Sonication over the Parylene Stencils

(A) Immediately spin-coat the substrates with 100 µL of 1% wt. PGMA-*b*-PVDMA in anhydrous chloroform at 1500 rpm, for 15 s using a spin coater.

Note: Perform spin-coating within 1-2 s of pipetting the polymer solution to minimize film non-uniformity caused by rapid chloroform evaporation.

(B) Anneal the polymer films at 110 °C in a vacuum oven for 18 h.

Note: Annealing allows for polymer microphase segregation and surface attachment of the GMA block to the surface[26].

(C) After the annealing, characterize the polymer coating by measuring the contact angle of substrates. Surfaces show a contact angle of $75^{O} \pm 1^{O}$ (Figure 4.1C)[20].

(D) Sonicate the substrates in 20 mL acetone or chloroform for 10 min to remove the parylene layer and any physisorbed polymer.

Note: Sonication conditions are, Ultra sonic power: 284 W, Operating frequency: 40 kHZ.

Note: Parylene can also be peeled off the substrate by applying a piece of tape at the edge of the substrate then pulling the tape away[27].

(E) Store the substrates under vacuum in a desiccator until characterization.

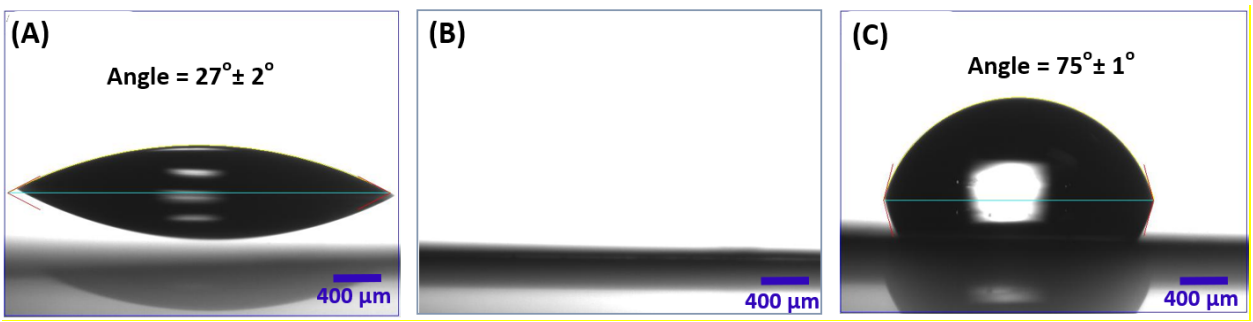

Figure 4.1 Contact angle measurements for treated silicon substrates. (A) Bare silicon, (B) Plasma-cleaned silicon, (C) Spin-coated silicon with PGMA-b-PVDMA (after annealing and sonication in chloroform).

4.3.4 PGMA-b-PVDMA Interface-Directed Assembly Procedure

Note: This procedure can be performed on substrates containing either a chemically inert background, or a biologically inert background, depending on the application.

Preparation of Chemically Inert Background on Silicon Substrates

(A) Use oxygen plasma cleaner to clean the bare silicon.

(B) Pipette 100 µL of trichloro(1H,1H,2H,2H-perfluorooctyl) silane (TPS) onto a petri dish, and place the silicon substrates inside a vacuum desiccator next to the petri dish.

(C) Apply vacuum (-750 Torr) for 1 h for chemical vapor deposition (CVD).

Caution: TPS is highly toxic and the CVD process should be performed inside a fume hood.

Note: After 1 h the substrate shows hydrophobic behavior. A contact angle of $109^{o} \pm 3^{o}$ is typically measured after the CVD process. The thickness of the TPS film is 1.5 ± 0.5 nm.

Note: TPS blocks reaction of the reactive surface oxide with PGMA-*b*-PVDMA.

(D) Coat the wafers with parylene (1 µm thickness). Perform photolithography and reactive ion etching to generate parylene patterns (section 4.3.2) and to etch away the TPS layer in the exposed regions.

Preparation of Polyethylene Glycol (PEG) Background on Silicon Substrates

(A) Use the oxygen plasma cleaner for 3 min to clean the bare silicon substrates.

(B) Perform CVD of TPS for 1 h.

(C) Immerse substrates into a 0.7% wt/v solution of Pluronic F-127 in ultrapure water for 18 h to generate a PEG layer on the surface[28, 29].

Note: Pluronic contains a hydrophobic polypropylene oxide (PPO) polymer block between two PEG chains. The PPO block anchors the polymer to the TPS surface while the PEG chains are exposed to solution[28].

(D) Wash and rinse the substrate for 5 min with 100 mL of ultrapure water.

(E) Deposit 80 nm and 1 μm thick parylene N on 4-inch silicon wafers using a parylene coater.

(F) Perform photolithography and reactive ion etching to generate parylene patterns (section 4.3.2).

Sonication, Spin-coating of PGMA-*b*-PVDMA Polymer, and Annealing the Substrates

(A) Sonicate chemically inert (TPS) substrates or PEG-functional substrates for 10 min in acetone to remove the parylene layer.

(B) Spin-coat the sonicated substrate with 100 μL of 1% wt. PGMA-*b*-PVDMA in anhydrous chloroform at 1500 rpm for 15 s.

(C) Anneal the polymer films at 110 °C under vacuum for 18 h.

(D) Sonicate the substrates in acetone or chloroform for 10 min to remove physisorbed polymer present in background regions on the surface.

(E) Store the substrates in a vacuum desiccator until further use.

4.3.5 Custom PGMA-b-PVDMA Micro-Contact Printing (μCP)

PDMS Stamp Fabrication

(A) Fabricate the silicon masters according to the standard photolithography procedure[30]. Use CVD process to deposit anti-adhesive TPS onto the silicon masters.

Note: The silicon mold should be treated with TPS the first time it is used, and re-applied after it has been used 5-10 times.

(B) Perform standard soft lithography methods for fabrication of stamps (PDMS precursor to curing agent mass ratio 10:1)[31].

Note: Stamps used in this study consist of micropillar arrays (diameter = 5-50 μm, height = 20 μm).

(C) Cut out a single stamp. Clean the stamp by sonicating for 10 min in HCl (1 M), 5 min in acetone, followed by 5 min in ethanol.

(D) Dry the stamps in a convection oven at 80 °C for 20 min to remove residual organic solvent.

Microcontact Printing of PGMA-*b*-PVDMA onto Silicon Substrates

(A) Deposit TPS onto the surface of PDMS stamps using the CVD process.

Note: The TPS layer is used to prevent coupling of the polymer to the stamp surface.

Note: Contact angle measurements can be used to characterize stamps after TPS adsorption, as shown in Figure 4.2 (Inset A, B).

(B) Dissolve the PGMA-*b*-PVDMA polymer into anhydrous chloroform at a concentration of 0.25-1% wt.

(C) Submerge the stamps into 5 mL of the polymer solution for 3 min.

(D) Plasma clean 2×2 cm bare silicon substrates for 3 min to clean surface for coupling with the PGMA blocks (section 4.3.3).

(E) Take out the polymer-coated stamps from the polymer solution.

Note: Stamps must be used for printing while they are still wet and a layer of solution exists over them.

(F) Put inked stamp directly on silicon substrate

(G) Use a manual drill press stand (Figure 4.3) to press the polymer-coated stamps onto the silicon surface to promote pattern transfer.

Note: Both the silicon and the PDMS stamp can be placed on double-sided tape backing to minimize PDMS stamp deformation due to non-uniform or high pressure stamping[32].

Note: Immediately apply the stamp to the substrate (within 1-2 s) after taking out the coated stamps from polymer solution.

(H) Apply conformal contact between polymer-inked stamp and silicon substrate for 1 min. Use the estimated pressure of 75 gr/cm^2 (7.35 kPa) to press.

(I) Gently separate the stamp from the silicon surface.

(J) Anneal the printed silicon substrates immediately in a vacuum oven at 110 ^{o}C for 18 h.

(K) Sonicate the printed silicon substrates in acetone or chloroform for 10 min to remove any physically-adsorbed PGMA-*b*-PVDMA and then dry with N_2.

Note: Perform surface characterization analysis for both PDMS stamp (after printing step) and printed-silicon (after annealing and sonication steps) to verify the successful transfer of PGMA-*b*-PVDMA.

Note: Surface profilometer and attenuated total reflectance fourier-transform infrared spectroscopy (ATR-FTIR) analysis could be used to analyze the printed-silicon substrate and PDMS stamp, respectively.

(L) Store the substrates under vacuum in a desiccator until characterization.

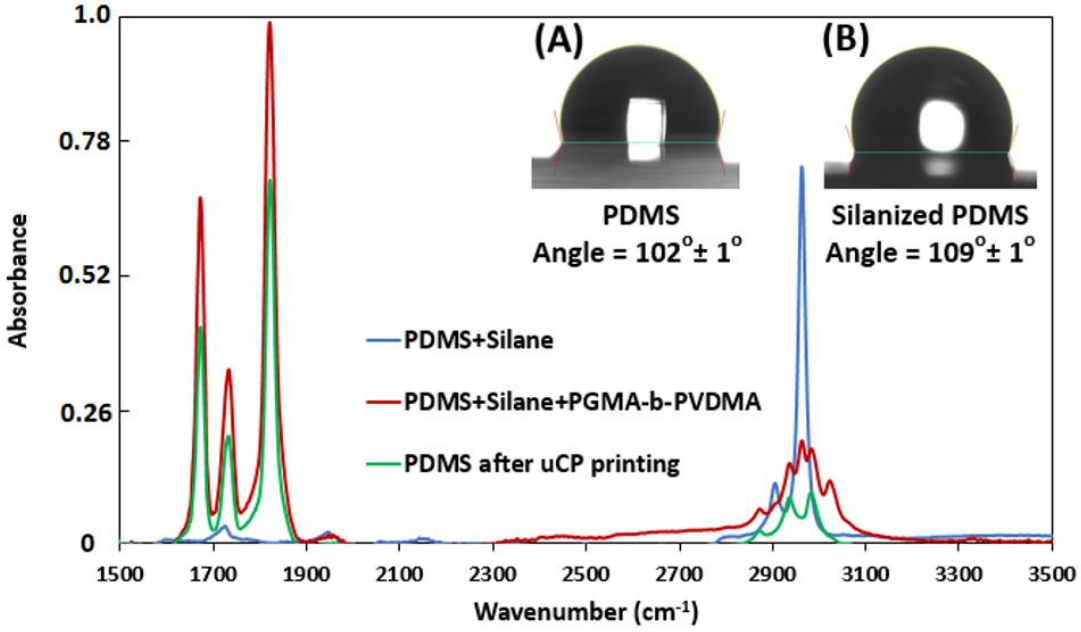

Figure 4.2 ATR-FTIR measurements for treated PDMS stamps (Relative intensity). (Inset A) Contact angle measurements for bare PDMS stamp. (Inset B) Contact angle measurements for TPS treated PDMS stamp.

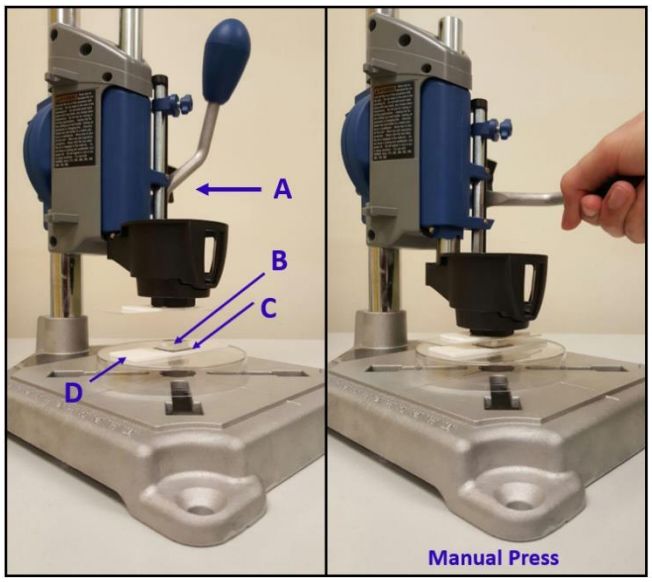

Figure 4.3 Setup for μCP of PGMA-*b*-PVDMA solutions onto silicon substrates. The procedure includes use of a **(A)** manual drill press, **(B)** a TPS-functionalized PDMS stamp coated with the PGMA-*b*-PVDMA polymer, **(C)** a plasma cleaned 2×2 cm silicon substrate, and **(D)** double-sided tape.

4.4 Representative Results

Contact angle measurements can be used to evaluate the functionalization of silicon with PGMA-b-PVDMA. Figure 4.1 depicts the contact angle of the silicon substrate during the different processing steps. Hydrophilic behavior of the plasma cleaned silicon substrate is shown in Figure 4.1B. The contact angle after polymer spin coating and annealing is $75^{o} \pm 1^{o}$ (Figure 4.1C) which is consistent with the values reported by Lokitz *et al*. for PVDMA surfaces[20].

Figure 4.2 shows the ATR-FTIR spectra and contact angle measurement of PDMS stamps during the different steps of the μCP procedure. After printing, the azlactone carbonyl stretching vibration at ~1818 cm^{-1} decreases by 34 ± 9%. Figure 4.2 (inset A, B) also depicts the change in hydrophobicity of PDMS stamps after TPS treatment. Stamp-substrate pressing is a critical step in μCP. Figure 4.3 exhibits different parts of the manual rotary tool necessary to achieve uniform contact between the polymer-coated stamp and silicon substrate.

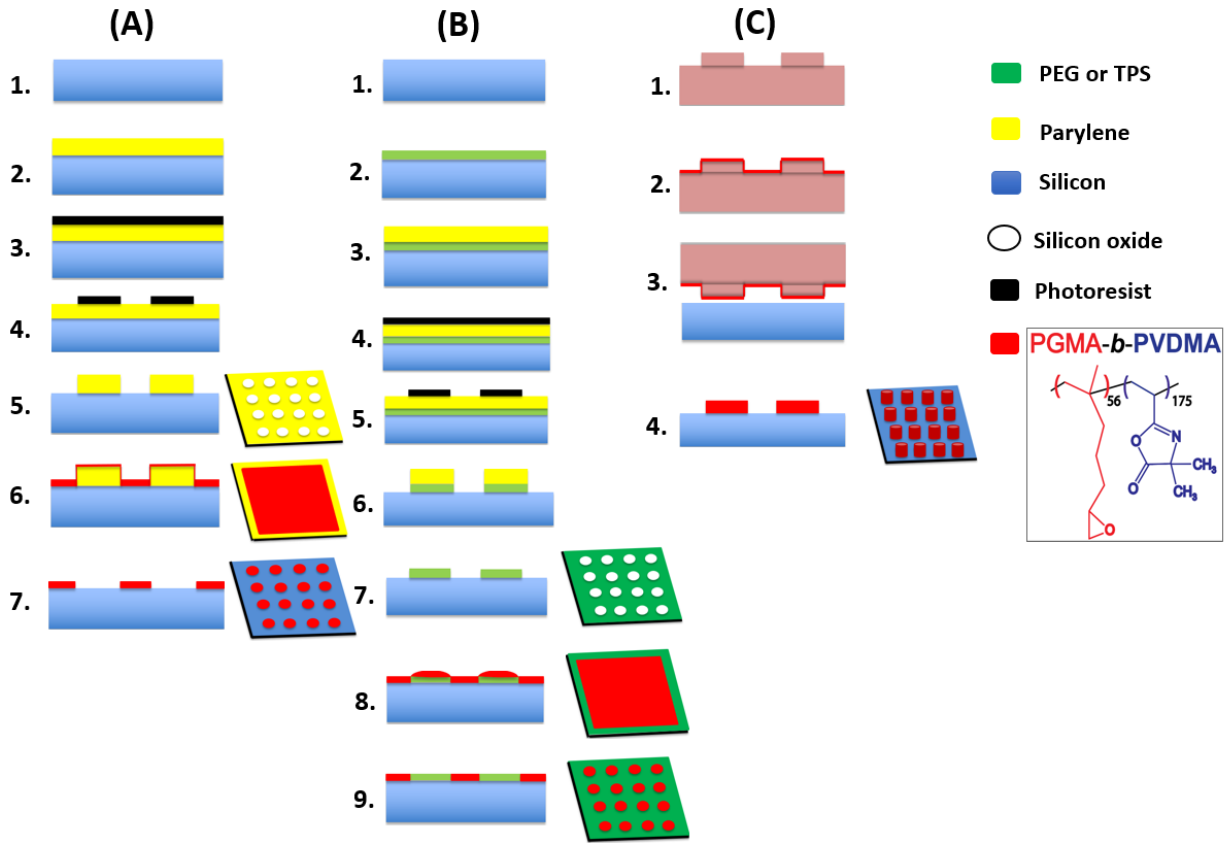

Figure 4.4 Details of the developed techniques for generating PGMA-*b*-PVDMA into patterned, crosslinked or brush films. This figure has been modified from Masigol *et al.*[24] (A) Schematic representation of the parylene lift-off protocol for patterning polymer brushes onto silicon substrates, 1. silicon wafer (w/native oxide), 2. parylene deposition (1 μm or 80 nm), 3. photoresist spin coating, 4. UV exposure and development, 5. oxygen plasma etching, 6. polymer spin coating, 7. annealing and parylene lift-off. (B) IDA procedure for patterning polymer brushes onto biological/chemical (PEG/TPS) inert substrates, 1. silicon wafer (w/native oxide), 2. PEG/TPS deposition, 3. parylene deposition (1 μm or 80 nm), 4. photoresist spin coating, 5. UV exposure and development, 6. oxygen plasma treatment, 7. parylene lift-off, 8. polymer spin coating, 9. annealing and sonication. (C) Generation of crosslinked polymer structures onto silicon using the μCP method, 1. soft-lithography for making PDMS stamp followed by TPS coating, 2. polymer inking on TPS-functionalized PDMS, 3. stamp/substrate contact, 4. annealing and sonication.

Figure 4.4 shows the step-by-step procedures for generating polymer patterns[24]. These procedures are designed to: (1) pattern uniform brush structures of PGMA-*b*-PVDMA polymers onto chemically/biologically inert substrates by applying parylene lift-off and IDA techniques (Figure 4.4(A,B)), or (2) generate thicker film patterns of micron-scale thickness (Figure 4.4C).

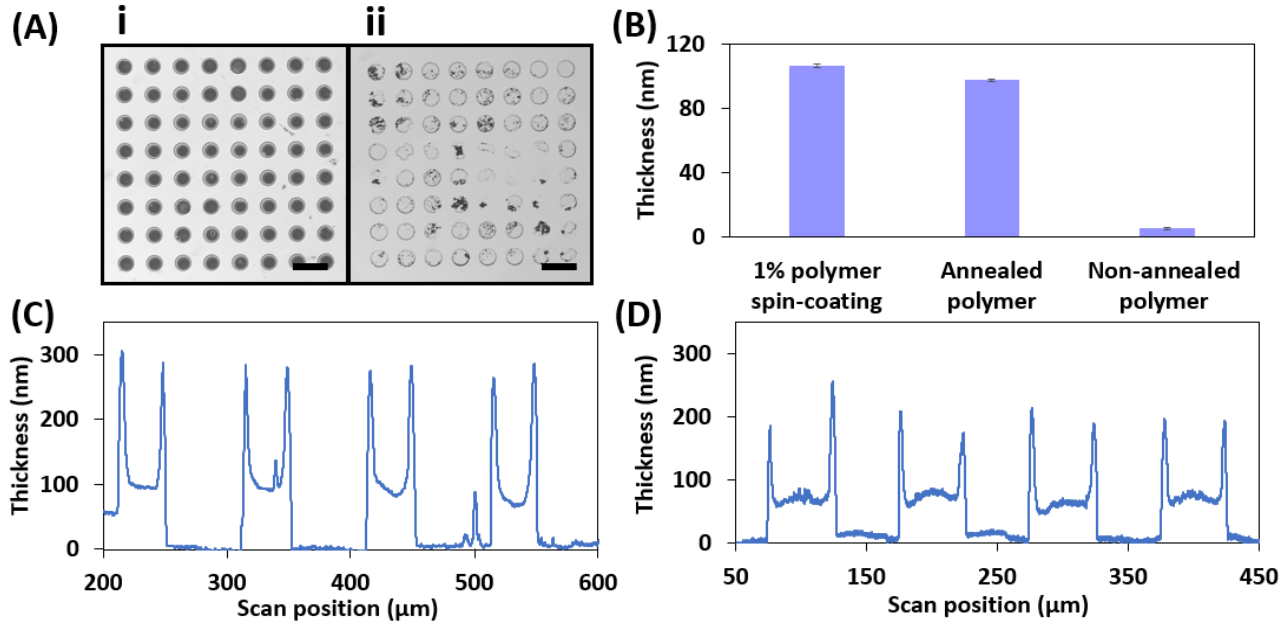

Figure 4.5 Representative results of the parylene lift-off procedure. **(A)** Brightfield images of PGMA-*b*-PVDMA polymer patterns on silicon with annealing **(inset i)** and without annealing **(inset ii)** (Scale bar = 40 µm). **(B)** Polymer thickness measured after 10 min sonication in chloroform with or without annealing. **(C)** Cross-sectional polymer height profile for 1 µm thick parylene stencils. **(D)** Cross-sectional polymer height profile for 80 nm thick parylene stencils.

The parylene lift-off technique can be used to achieve brush structures of PGMA-*b*-PVDMA block co-polymers, corresponding to ~90 nm film thickness. Figure 4.5A (inset i) depicts the patterned spots surrounded by polymer-free background. Annealing is the crucial step leading polymer phase-segregation and strong covalent surface attachment through reaction of epoxy groups on the GMA block with surface oxide[24]. As Figure 4.5A (inset ii) shows, without annealing, sonication in chloroform will remove much of the patterned polymer. To investigate the effect of annealing in more detail, a 1% wt. concentration of polymer in chloroform was spin-coated over a plasma-cleaned silicon substrate (without parylene). Polymer thickness was measured by ellipsometry. While sonication in chloroform led to the removal of most of the polymer from non-

annealed substrates, no significant change in thickness of polymer was observed for annealed substrates (Figure 4.5(B)). Compared to 1 μm parylene stencils, 80 nm parylene stencils generated higher film uniformity (Figure 4.5(C,D)).

The IDA technique can be used to co-pattern uniform films of the PGMA-*b*-PVDMA polymer over chemically or biologically inert backgrounds. (Chapter 3, Figure 3.3) shows the PGMA-*b*-PVDMA patterns on PEG/TPS backgrounds. This approach results in patterned films of 90-100 nm thickness without the edge defects observed from the prior method (Figures 4.5(C, D)). AFM profiles in Chapter 3, Figure 3.3 depict polymer film thicknesses obtained using the IDA method.

μCP was developed as the final approach to patterning PGMA-*b*-PVDMA polymers on silicon surfaces. In contrast to parylene lift-off and IDA techniques, this approach results in polymer films patterned at micron-scale thickness. There were several critical steps that were required to insure efficient transfer of polymer from the stamp to the substrate during the printing process. First, PDMS functionalization with TPS was required to inhibit PGMA-*b*-PVDMA coupling to the stamp (Figure 4.2 (inset A, B)). Second, plasma treatment on the substrate was required to form an oxide surface layer for reaction with epoxy groups present in the PGMA block of the polymer (Figure 4.1B). Finally, annealing of the stamped polymer films was required to promote crosslinking throughout the film; Figure 4.5A (inset i and ii) show annealed and non-annealed substrates after sonication, where significant damage to the non-annealed films was observed. Another requirement for the patterning technique was to preserve the azlactone functionality, which was verified by measuring the carbonyl stretching vibration at ~1818 cm^{-1} (Chapter 3 Figure 3.4 b). Finally, the μCP technique also enabled microscale control of polymer

thickness films by varying the concentrations of PGMA-*b*-PVDMA in chloroform during the inking step (Chapter 3 Figure 3.4 c).

4.5 Discussion

This article presents three approaches to patterning PGMA-*b*-PVDMA, each with its set of advantages and drawbacks. The parylene lift-off method is a versatile method for patterning block co-polymers at micro to nanoscale resolution, and has been used as a deposition mask in other patterning systems[33-35]. Due to its relatively weak surface adhesion, the parylene stencil can be easily removed from the surface by sonication in a solvent after polymer coating to expose the background regions. Background regions appear consistently clean and free of residual polymer. Since parylene is inert to a variety surfaces[36, 37] this approach is useful for depositing PGMA-*b*-PVDMA into a variety of different background surface chemistries. One factor that affected film uniformity was parylene stencil thickness. Two different parylene thicknesses (1 μm and 80 nm) were used (Method A, Figure 4.4) to investigate the effect of stencil thickness on the generated PGMA-*b*-PVDMA structures. Compared with 1 μm, 80 nm thick parylene created polymer films with higher uniformity, however, edge defects were observed around each polymer spot in both cases (Figure 4.5(C, D)). This is likely due to a build-up of polymer against the stencil during the spin-coating step, which was then crosslinked into thicker films at the pattern edges during the annealing step. However, annealing is critical for obtaining stable polymer patterns (Figure 4.5(A,B)), thus edge defects were unavoidable with this method.

As an alternative, the IDA patterning method uses parylene stencils to generate oxide patterns that guide the self-assembly of the PGMA-*b*-PVDMA polymer to the surface in a maskless deposition process (Method B, Figure 4.4). Physisorbed polymers present in the background regions immediately after the spin coating step are removed by sonication in organic

solvent. Brightfield, SEM, and AFM images after annealing and sonication in an organic solvent display well-defined PGMA-*b*-PVDMA patterns that correspond to the spatial locations of the silicon oxide patterns (Figure 6A). In contrast to the previous method, patterned films show high uniformity without edge-defects, as no mask was present during the spin coating step. The resulting thickness of the polymer films is 90-100 nm, in agreement with the reported thickness for brushes for PGMA-*b*-PVDMA polymer of this molecular weight[20]. This excellent characteristic enables precise manipulation of the chemical reactivity by adjusting either the PGMA-*b*-PVDMA pattern density, or the molecular weight of the PVDMA chain.

While the IDA method is preferred for applications where film uniformity is important, there are two inherent drawbacks to the method. First, formation of residual PGMA-*b*-PVDMA polymer in background regions can occur, as can be noted in the TPS background regions in Figure 6A. If background polymer is an issue, the chemical integrity of the background should first be checked with ATR-FTIR or water contact angle measurement[39]. Additional sonication may also be useful for removing residual polymer. Second, the IDA method is limited only to backgrounds that are unreactive to the PGMA or PVDMA groups in the polymer. Other backgrounds containing reactive moieties (amines, thiols, *etc*.) would likely to couple to the polymer, compromising pattern integrity.

To complement the parylene and IDA patterning methods, the customized μCP protocol generates thicker PGMA-*b*-PVDMA structures (Method C, Figure 4.4), providing higher surface-to-volume ratios that may enhance the loading of chemical or biological analytes in capture applications or improve cell attachment, viability, and proliferation in cell culture applications[41, 42]. Here, the surface chemistry of both the stamp and the substrate were essential to maintaining efficient polymer transfer while maintaining high pattern integrity. PGMA-*b*-PVDMA transfer

was facilitated by treating the stamp with a TPS layer to decrease the surface free energy of the stamp[44], while also treating the silicon substrates with oxygen plasma immediately before printing to provide reactive surface hydroxyl groups for coupling to epoxy groups present in the PGMA block[23].

A primary challenge in the μCP protocol comes from the use of chloroform solvent to prepare the polymer inking solution. Rapid solvent evaporation across the stamp can cause non-uniform polymer inking, compromising pattern reproducibility [24, 43]. To avoid this, it was critical that stamps were completely submerged into 5 mL volumes of the inking solution, as opposed to pipetting small volumes of the solution over the top of the stamp surface. Different submersion times were investigated and 3 min was found to be optimal for this process. It was necessary to then place the wet stamp directly on the top of the substrate within 1-2 seconds of removal from the solution and add manual pressure to the stamp (Figure 4.3). This process allowed for transfer under wet conditions, which was critical for maintaining transfer efficiency and uniformity. If patterning from this process still appears non-uniform, stamp deformation is likely. In this case, the ratio of PDMS base/curing agent in soft-lithography step can be changed to generate stiffer stamps[46].

In summary, the methods and results presented here describe multiple approaches for creating patterned interfaces with the PGMA-*b*-PVDMA polymer. The methods can be employed to generate patterned films with brush or crosslinked structures, depending on the application. Polymer can be patterned in chemically or biologically inert backgrounds. Because deposition of the polymer is the last step in the deposition process, the azlactone functionality is preserved in each patterning protocol. After patterning, substrates are ready for post-functionalization with other chemical or biological groups.

4.6 Acknowledgments

This research was supported by Kansas State University. A portion of this research was conducted at the Center for Nanophase Materials Sciences, which is sponsored at Oak Ridge National Laboratory by the Scientific User Facilities Division, Office of Basic Energy Sciences and U.S. Department of Energy.

4.7 References

(1) Faia-Torres, A., Goren, T., Textor, M. and Pla-Roca, M. Patterned Biointerfaces.Comprehensive biomaterials. 1st edition, Elsevier publications., 181-201 (2017).

(2) Ogaki, R., Alexander, M. and Kingshott, P. Chemical patterning in biointerface science. *Mater. Today*. 13 (4), 22-35 (2010).

(3) Rungta, A., Natarajan, B., Neely, T., Dukes, D., Schadler, L.S. and Benicewicz, B.C. Grafting bimodal polymer brushes on nanoparticles using controlled radical polymerization. *Macromolecules*. 45 (23), 9303-9311 (2012).

(4) Guyomard, A., Fournier, D., Pascual, S., Fontaine, L. and Bardeau, J. Preparation and characterization of azlactone functionalized polymer supports and their application as scavengers. *Eur. Polym. J.* 40 (10), 2343-2348 (2004).

(5) Zayas-Gonzalez, Y.M. and Lynn, D.M. Degradable Amine-Reactive Coatings Fabricated by the Covalent Layer-by-Layer Assembly of Poly (2-vinyl-4, 4-dimethylazlactone) with Degradable Polyamine Building Blocks. *Biomacromolecules*. 17 (9), 3067-3075 (2016).

(6) Schmitt, S.K., Trebatoski, D.J., Krutty, J.D., Xie, A.W., Rollins, B., Murphy, W.L. and Gopalan, P. Peptide Conjugation to a Polymer Coating via Native Chemical Ligation of Azlactones for Cell Culture. *Biomacromolecules*. 17 (3), 1040-1047 (2016).

(7) Yu, Q., Cho, J., Shivapooja, P., Ista, L.K. and López, G.P. Nanopatterned smart polymer surfaces for controlled attachment, killing, and release of bacteria. *ACS. Appl. Mater. Inter.* 5 (19), 9295-9304 (2013).

(8) Jones, M.W., Richards, S., Haddleton, D.M. and Gibson, M.I. Poly (azlactone) s: versatile scaffolds for tandem post-polymerisation modification and glycopolymer synthesis. *Polym. Chem-UK*. 4 (3), 717-723 (2013).

(9) Barkakaty, B., Browning, K.L., Sumpter, B., Uhrig, D., Karpisova, I., Harman, K.W., Ivanov, I., Hensley, D.K., Messman, J.M. and Kilbey, S.M. Amidine-Functionalized Poly (2-vinyl-4, 4-dimethylazlactone) for Selective and Efficient CO2 Fixing. *Macromolecules*. 49 (5), (2016).

(10) Cullen, S.P., Mandel, I.C. and Gopalan, P. Surface-anchored poly (2-vinyl-4, 4-dimethyl azlactone) brushes as templates for enzyme immobilization. *Langmuir*. 24 (23), 13701-13709 (2008).

(11) Schmitt, S.K., Xie, A.W., Ghassemi, R.M., Trebatoski, D.J., Murphy, W.L. and Gopalan, P. Polyethylene glycol coatings on plastic substrates for chemically defined stem cell culture. *Adv. Healthc. Mater.* 4 (10), 1555-1564 (2015).

(12) Yan, S., Shi, H., Song, L., Wang, X., Liu, L., Luan, S., Yang, Y. and Yin, J. Nonleaching Bacteria-Responsive Antibacterial Surface Based on a Unique Hierarchical Architecture. *ACS. Appl. Mater. Inter.* 8 (37), 24471-24481 (2016).

(13) Li, C., Glidle, A., Yuan, X., Hu, Z., Pulleine, E., Cooper, J., Yang, W. and Yin, H. Creating "living" polymer surfaces to pattern biomolecules and cells on common plastics. *Biomacromolecules*. 14 (5), 1278-1286 (2013).

(14) Brétagnol, F., Valsesia, A., Ceccone, G., Colpo, P., Gilliland, D., Ceriotti, L., Hasiwa, M. and Rossi, F. Surface functionalization and patterning techniques to design interfaces for biomedical and biosensor applications. *Plasma Process. Polym.* 3 (6-7), 443-455 (2006).

(15) Thery, M., Micropatterning as a tool to decipher cell morphogenesis and functions. *J. Cell. Sci.* 123 (Pt 24), 4201-4213 (2010).

(16) Robertus, J., Browne, W.R. and Feringa, B.L. Dynamic control over cell adhesive properties using molecular-based surface engineering strategies. *Chem. Soc. Rev.* 39 (1), 354-378 (2010).

(17) Kane, R.S., Takayama, S., Ostuni, E., Ingber, D.E. and Whitesides, G.M. Patterning proteins and cells using soft lithography. *Biomaterials.* 20 (23), 2363-2376 (1999).

(18) Cattani-Scholz, A., Pedone, D., Blobner, F., Abstreiter, G., Schwartz, J., Tornow, M. and Andruzzi, L. PNA-PEG modified silicon platforms as functional bio-interfaces for applications in DNA microarrays and biosensors. *Biomacromolecules*. 10 (3), 489-496 (2009).

(19) Nie, Z. and Kumacheva, E. Patterning surfaces with functional polymers. *Nat. Mater.* 7 (4), (2008).

(20) Lokitz, B.S., Wei, J., Hinestrosa, J.P., Ivanov, I., Browning, J.F., Ankner, J.F., Kilbey, S.M. and Messman, J.M. Manipulating interfaces through surface confinement of poly (glycidyl methacrylate)-block-poly (vinyldimethylazlactone), a dually reactive block copolymer. *Macromolecules*. 45 (16), 6438-6449 (2012).

(21) Kratochvil, M.J., Carter, M.C. and Lynn, D.M. Amine-Reactive Azlactone-Containing Nanofibers for the Immobilization and Patterning of New Functionality on Nanofiber-Based Scaffolds. *ACS. Appl. Mater. Inter.* 9 (11), 10243-10253 (2017).

(22) Wancura, M.M., Anex-Ries, Q., Carroll, A.L., Paola Garcia, A., Hindocha, P. and Buck, M.E. Fabrication, chemical modification, and topographical patterning of reactive gels assembled from azlactone-functionalized polymers and a diamine. *J. Polym. Sci.* Part A1. 55 (19), 3185-3194 (2017).

(23) Hansen, R.R., Hinestrosa, J.P., Shubert, K.R., Morrell-Falvey, J.L., Pelletier, D.A., Messman, J.M., Kilbey, S.M., Lokitz, B.S. and Retterer, S.T. Lectin-functionalized poly (glycidyl methacrylate)-block-poly (vinyldimethyl azlactone) surface scaffolds for high avidity microbial capture. *Biomacromolecules*. 14 (10), 3742-3748 (2013).

(24) Masigol, M., Barua, N., Retterer, S.T., Lokitz, B.S. and Hansen, R.R. Chemical copatterning strategies using azlactone-based block copolymers. *J. Vac. Sci. Technol B*. 35 (6), 06GJ01 (2017).

(25) Lokitz, B.S., Messman, J.M., Hinestrosa, J.P., Alonzo, J., Verduzco, R., Brown, R.H., Osa, M., Ankner, J.F. and Kilbey, S.M. Dilute solution properties and surface attachment of RAFT polymerized 2-vinyl-4, 4-dimethyl azlactone (VDMA). *Macromolecules.* 42 (22), 9018-9026 (2009).

(26) Aden, B., Kite, C.M., Hopkins, B.W., Zetterberg, A., Lokitz, B.S., Ankner, J.F. and Kilbey, S.M. Assessing Chemical Transformation of Reactive, Interfacial Thin Films Made of End-Tethered Poly (2-vinyl-4, 4-dimethyl azlactone)(PVDMA) Chains. *Macromolecules.* 50 (2), 618-630 (2017).

(27) Hansen, R.H., Timm, A.C., Timm, C.M., Bible, A.N., Morrell-Falvey, J.L., Pelletier, D.A., Simpson, M.L., Doktycz, M.J. and Retterer, S.T. Stochastic assembly of bacteria in microwell

arrays reveals the importance of confinement in community development. *PloS one.* 11 (5), e0155080 (2016).

(28) Vargis, E., Peterson, C.B., Morrell-Falvey, J.L., Retterer, S.T. and Collier, C.P. The effect of retinal pigment epithelial cell patch size on growth factor expression. *Biomaterials.* 35 (13), 3999-4004 (2014).

(29) Tzvetkova-Chevolleau, T., Yoxall, E., Fuard, D., Bruckert, F., Schiavone, P. and Weidenhaupt, M. Microscale adhesion patterns for the precise localization of amoeba. *Microelectron. Eng.* 86 (4), 1485-1487 (2009).

(30) Shelly, M., Lee, S., Suarato, G., Meng, Y. and Pautot, S. Photolithography-Based Substrate Microfabrication for Patterning Semaphorin 3A to Study Neuronal Development. Semaphorin Signaling: Methods and Protocols.1493, 321-343 (2017).

(31) McDonald, J.C., Duffy, D.C., Anderson, J.R., Chiu, D.T., Wu, H., Schueller, O.J. and Whitesides, G.M. Fabrication of microfluidic systems in poly(dimethylsiloxane). *Electrophoresis*. 21 (1), 27-40 (2000).

(32) Hansen, R.R., Wufsus, A.R., Barton, S.T., Onasoga, A.A., Johnson-Paben, R.M. and Neeves, K.B. High content evaluation of shear dependent platelet function in a microfluidic flow assay. *Annal. Biomed. Eng.* 41 (2), 250-262 (2013).

(33) Segalman, R.A., Yokoyama, H. and Kramer, E.J. Graphoepitaxy of spherical domain block copolymer films. *Adv. Mater.* 13 (15), 1152-1155 (2001).

(34) Stoykovich, M.P., Muller, M., Kim, S.O., Solak, H.H., Edwards, E.W., de Pablo, J.J. and Nealey, P.F. Directed assembly of block copolymer blends into nonregular device-oriented structures. *Science* (New York, N.Y.). 308 (5727), 1442-1446 (2005).

(35) Craig, G.S. and Nealey, P.F. Self-assembly of block copolymers on lithographically defined nanopatterned substrates. *J. Photopolym. Sci. Technol.* 20 (4), 511-517 (2007).

(36) Kodadek, T., Protein microarrays: prospects and problems. Chem. Biol. 8 (2), 105-115 (2001).

(37) Atsuta, K., Suzuki, H. and Takeuchi, S. A parylene lift-off process with microfluidic channels for selective protein patterning. *J. Micromech. Microeng*. 17 (3), 496 (2007).

(38) Ramanathan, M., Lokitz, B.S., Messman, J.M., Stafford, C.M. and Kilbey II, S.M. Spontaneous wrinkling in azlactone-based functional polymer thin films in 2D and 3D geometries for guided nanopatterning. *J. Mater. Chem.C.* 1 (11), 2097-2101 (2013).

(39) Kahp Y. Suh and Sangyong Jon, Control over wettability of polyethylene glycol surfaces using capillary lithography, *Langmuir*. 21 (15), 6836-6841 (2005).

(40) Buck, M.E. and Lynn, D.M. Layer-by-Layer Fabrication of Covalently Crosslinked and Reactive Polymer Multilayers Using Azlactone-Functionalized Copolymers: A Platform for the Design of Functional Biointerfaces. *Adv. Eng. Mater.* 13 (10), 343-352 (2011).

(41) Ma, L., Yang, G., Wang, N., Zhang, P., Guo, F., Meng, J., Zhang, F., Hu, Z., Wang, S. and Zhao, Y. Trap Effect of Three-Dimensional Fibers Network for High Efficient Cancer-Cell Capture. *Adv. Healthc. Mater.* 4 (6), 838-843 (2015).

(42) Massad-Ivanir, N., Shtenberg, G., Tzur, A., Krepker, M.A. and Segal, E. Engineering nanostructured porous SiO2 surfaces for bacteria detection via “direct cell capture”. *Anal. Chem.* 83 (9), 3282-3289 (2011).

(43) Ilic, B. and Craighead, H. Topographical patterning of chemically sensitive biological materials using a polymer-based dry lift off. *Biomed. Microdevices.* 2 (4), 317-322 (2000).

(44) Gates, B.D., Xu, Q., Stewart, M., Ryan, D., Willson, C.G. and Whitesides, G.M. New approaches to nanofabrication: molding, printing, and other techniques. *Chem. Rev.* 105 (4), 1171-1196 (2005).

(45) Jonas, U., del Campo, A., Kruger, C., Glasser, G. and Boos, D. Colloidal assemblies on patterned silane layers. *P. Natl. Acad. Sci.* USA. 99 (8), 5034-5039 (2002).

(46) Qin, D., Xia, Y. and Whitesides, G.M. Soft lithography for micro-and nanoscale patterning. *Nat. Protoc.* 5 (3), 491-502 (2010).

Chapter 5 - Identification of Critical Surface Parameters Driving Lectin-Mediated Capture of Bacteria from Solution*

5.1 Overview

Lectin-functional interfaces are useful for isolation of bacteria from solution because they are low cost and allow non-destructive, reversible capture. This study provides a systematic investigation of physical and chemical surface parameters that influence bacteria capture over lectin-functionalized polymer interfaces and then applies these findings to construct surfaces with significantly enhanced bacteria capture. The designer block copolymer, poly (glycidyl methacrylate)-*block*-poly (vinyldimethyl azlactone) was used as a lectin attachment layer, and lectin coupling into the polymer film through azlactone-lectin coupling reactions was first characterized. Here, experimental parameters including polymer areal chain density, lectin molecular weight, and lectin coupling buffer were systematically varied to identify parameters driving highest azlactone conversions and corresponding lectin surface densities. To introduce physical nanostructures into the attachment layer, nanopillar arrays (NPAs) of varied heights (300 and 2100 nm) were then used to provide an underlying surface template for the functional polymer layer. Capture of *Escherichia coli* on lectin-polymer surfaces coated over both flat and NPA surfaces was then investigated. For flat polymer interfaces, bacteria were detected on the surface

---

*Manuscript appearing in: Masigol M., Fattahi, N., Barua, N., Lokitz, B.S., Retterer S.T., Platt, T.G. and Hansen, R.R. Identification of Critical Surface Parameters Influencing Lectin-Mediated Capture of Bacteria from Solution, *Biomacromolecules*, 20 (7), 2852-2863 (2019). doi:10.1021/acs.biomac.9b00609
Reproduced with permission from the American Chemical Society. Copyright 2019 American Chemical Society.

after incubation at a solution concentration of 10^3 CFU/mL, and a corresponding detection limit of 1.7×10^3 CFU/mL was quantified. This detection limit was one order of magnitude lower than control lectin surfaces functionalized with standard, carbodiimide coupling chemistry. NPA surfaces containing 300 nm tall pillars further improved the detection limit to 2.1×10^2 CFU/mL, but also reduced the viability of captured cells. Finally, to investigate the impact of cell surface parameters on capture, we used *Agrobacterium tumefaciens* cells genetically modified to allow manipulation of exopolysaccharide adhesin production levels. Statistical analysis of surface capture levels revealed that lectin surface density was the primary factor driving capture, as opposed to exopolysaccharide adhesin expression. These findings emphasize the critical importance of the synthetic interface and the development of surfaces that combine high lectin densities with tailored physical features to drive high levels of capture. These insights will aid in design of biofunctional interfaces with physicochemical surface properties favorable for capture and isolation of bacteria cells from solution.

KEYWORDS: Bacteria isolation, affinity based capture, lectin, azlactone polymers, nanopillars

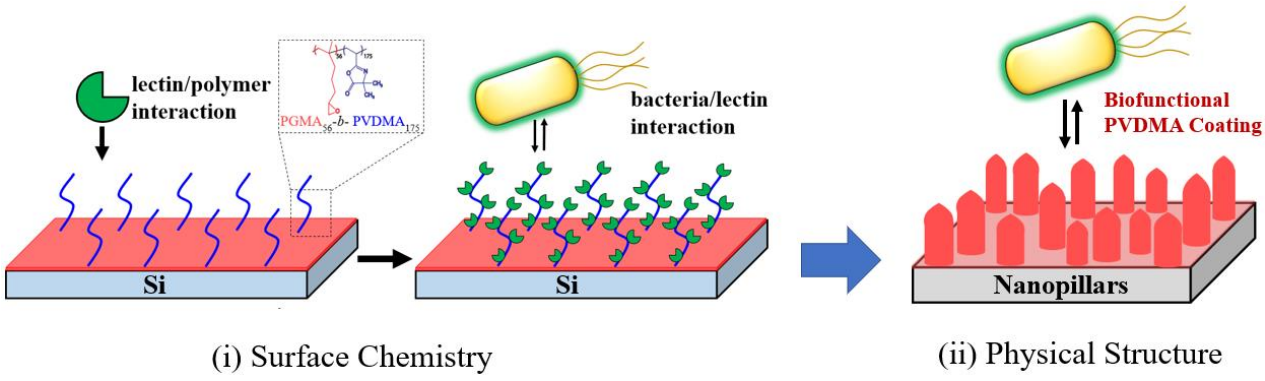

Scheme 5.1 Lectin functional polymer interface for capture of bacteria from solution. (i) Surface chemistry optimized to achieve maximum lectin density on the Si surfaces. (ii) Surfaces were further engineered to contain nanopillar structures that allowed to introduce well-controlled, nanoscale surface features to the functional interfaces

5.2 Introduction

Developing synthetic biological interfaces that enable reliable and rapid capture and enrichment of microorganisms is useful for applications in food and water monitoring, clinical diagnostics, applied medicine, and industrial and environmental monitoring.[1-3] Microbe capture and enrichment support rapid, culture-free detection and thus faster, more informed responses.[4,5] While synthetic interfaces functionalized with antibodies targeting microbial surface antigens are most commonly used for capture,[6-8] carbohydrate recognition with lectin-functionalized interfaces has been increasingly considered as an alternative approach, as microorganisms express extracellular surface carbohydrates in the form of lipopolysaccharides, glycolipids, and glycoproteins.[2,5] Lectins have advanced glycomic research, as they can be used to understand the role of glycans in a variety of cellular processes.[9-11] With respect to cell capture, lectin interfaces have been used for isolating and enriching cancerous cells from whole blood,[12,13] bacterial pathogens from food and environmental samples,[14] and for removal of microbial pathogens from whole blood for sepsis therapy.[15] However, limitations in capture efficiency often arise due to the fact that carbohydrate-protein interactions are inherently weaker than antibody-antigen interactions,[16,17] with equilibrium dissociation constants (K_D) higher by a factor of 10^2-10^3.[1] Thus, developing physicochemically tunable interfaces with improved control of lectin density, orientation, and stability is key for utilizing lectin-carbohydrate interactions for cell capture and other glycomic research applications.[18-20]

Synthetic, biofunctional polymers have been used to tune physicochemical and biological interface properties to improve cell capture and surface viability.[21,22] For example, polymer films containing reactive azlactone groups have been used to immobilize a suite of biomolecules (lectins, proteins, and peptides) through rapid coupling with amine or thiol groups.[23,24] Compared to other

bioconjugation chemistries (e.g. EDC-NHS), the higher hydrolytic stability of azlactones, combined with one-step "click" reactions with biomolecules make it a robust route to biofunctionalization.[25,26] Azlactone-functionalized copolymers have been used to generate reliable platforms for cell culture investigations. For instance, Schmitt *et al.* presented a peptide-coupled interface using a triblock copolymer consisting of glycidyl methacrylate, polyethylene glycol (PEG), and azlactone-based polymers for Human mesenchymal stem cell adhesion and growth. The polymer coatings generated a highly stable biointerface, allowing for long-term (>2 week) cell culture experiments.[24] Other amine-functionalized biomolecules can be coupled to polyvinyl dimethyl azlactone (PVDMA) surfaces as well. Broderick *et al.* presented a top-down fabrication method using poly (ethylamine) (PEI)/PVDMA multilayer surfaces to generate patterned arrays of amine-terminated oligonucleotides for DNA hybridization studies. Azlactone-bearing background regions were passivated by treatment with D-glucamine to prevent non-specific biomolecule adsorption.[27] Neri *et al*. used azlactone-bearing polymers to modulate the chemical properties of graphene. They generated the azlactone-graphene interface for the selective attachment of chemical and biological targets such as glutathione disulfide.[28]

In order to address limitations associated with lectin binding, Hansen *et al*. applied the dually-reactive block copolymer, poly(glycidyl methacrylate)-*block*-poly(vinyl dimethyl azlactone) (PGMA-*b*-PVDMA) to generate three-dimensional, microscale patterns of lectins over surfaces for bacteria capture, and demonstrated that these polymer treatments could couple high lectin densities and capture significantly more bacteria from solution compared to surfaces containing physisorbed lectins.[29,30] However, these polymer coatings were unoptimized, as lectin-polymer and lectin-cell interactions were not studied. In fact, few reports have provided a detailed understanding of how experimental parameters, such as pH or polymer surface density affect

biomolecule coupling in these systems.[31] The work presented here builds off the previous system,[29] and provides a fundamental understanding of the critical surface and coupling parameters that influence lectin-polymer functionalization over PVDMA-based coatings. In addition to these chemical parameters, physical surface features such as nanoscale architecture also impact capture by providing increased surface area for bacteria interaction.[32] For example, Friedlander *et al.* recently showed that sub-micron surface crevices increase *E. coli*-surface adhesion by providing anchoring sites for flagella.[33] Given this premise, we used nanofabrication methods to generate nanopillar arrays (NPAs)[34] with controlled pillar heights to provide the interface with tailored nanostructure. This allowed for further investigation on the impact of nanoscale surface features on lectin-based capture in this system. The combination of favorable physical and chemical surface features were then used to construct surfaces providing improved gains in sensitivity and capture efficiency.

Finally, the effect of exopolysaccharide production levels on capture over these interfaces is investigated, which is important since capture is also influenced by surface properties of the bacterial cell, such as amount of extracellular polymeric substances (EPS) present.[35] For these studies, *Agrobacterium tumefaciens* was selected as model microbe since it can release a broad range of exopolysaccharides such as cellulose, succinoglycan, β-1,2 glucan, β-1,3 glucan and unipolar polysaccharides (UPP).[36,37] Prior research has established an *A. tumefaciens* strain whose UPP adhesin production can be experimentally manipulated in the absence of other exopolysaccharides.[37,38] This biological resource allowed for an experimental evaluation of the relative importance of lectin surface density and adhesin production to bacterial cell capture.

5.3 Experimental Section

5.3.1 Materials

Sodium carbonate (Na_2CO_3), sodium bicarbonate ($NaHCO_3$), 2-(N-Morpholino) ethanesulfonic acid hemisodium salt (MES), 4-(2-Hydroxyethyl) piperazine-1-ethanesulfonic acid (HEPES), manganese (II) chloride ($MnCl_2$), calcium chloride ($CaCl_2$), anhydrous toluene, 3-aminopropyl triethoxysilane (APTES), N-(3-dimethylaminopropyl)-N′-ethylcarbodiimide (EDC), N-hydroxysuccinimide (NHS), dimethylformamide (DMF), succinic anhydride (SA), triethylamine (TEA), isopropyl β-D-1-thiogalactopyranoside (IPTG), and glutaraldehyde solution (25 wt.% in water) were purchased from Sigma-Aldrich. *Triticum vulgare* lectin (Wheat germ agglutinin, WGA), *Helix pomatia lectin* (HPA), and Concanvaline A from *Canavalia ensiformis* (ConA) were purchased from Sigma-Aldrich and diluted to specific concentrations in buffer and stored at −20 °C. WGA-FITC conjugate and HPA-Alexa Fluor 488 conjugate were purchased from Fisher Scientific, diluted to the desired concentration in 1X PBS and stored at −20 °C. 1X PBS buffer (pH 7.4), carbonate/bicarbonate buffer (pH 9.3, pH 10.0, and pH 10.4), HEPES buffer (pH 8.0), and MES buffer (pH 6.0) were made using standard recipes.[39] WGA and HPA were dissolved in the buffers with pH 7.4, 9.3, and 10.4. ConA was dissolved in the buffers with pH 6.0, 8.0, and 10.0 that contained 100 μM of $MnCl_2$ and $CaCl_2$ (Mn^{+2} and Ca^{+2} are critical for the carbohydrate interaction).[40] *E. coli* K12-mCherry and *A. tumefaciens* JX110 (Δ*crdS*Δ*cel*Δ*exoA*Δ*chvAB* mutant of strain C58) carrying pJW110 (encoding an IPTG inducible P_{lac}-*pleD*) were stored in 25% glycerol stocks at −80 °C.[37,38] $PGMA_{56}$-*b*-$PVDMA_{175}$ was synthesized as reported by Lokitz *et al.*,[41] stored at −20 °C until use. A LIVE/DEAD BacLight Bacterial Viability Kit was purchased from ThermoFisher Scientific and stored at −20 °C until use. Silicon (Si) wafers were purchased from WRS Materials.

5.3.2 Polymer Cross-linking Over Flat Si Substrates and Lectin Functionalization

Flat Si wafers (9 × 9 mm) were treated with oxygen plasma (3 min), then treated with Piranha solution (3:1 v/v H_2SO_4 / 30% H_2O_2 at 120 ºC for 30 min) (*Caution! Strongly corrosive*) for cleaning and to generate surface hydroxyl groups to be reacted with epoxy group existing in the PGMA block.[42] Wafers were then washed with ultrapure water and used within 24 hr of cleaning. $PGMA_{56}$-*b*-$PVDMA_{175}$ polymer was dissolved in anhydrous chloroform at the specified concentration. 100 µL of the solution was spin coated over wafers (1500 rpm, 15 sec), substrates were then placed in a vacuum oven for 18 hr (annealing temperature: 110 °C). Cross-linking of PGMA epoxy groups to surface hydroxyl groups allowed for covalent attachment to the Si substrate.[41] After annealing, acetone was used to sonicate the polymer-coated surfaces for 10 min to remove physiosorbed polymer. The substrates were dried with N_2 and stored at vacuum condition until further use. Using the ellipsometry data, the areal chain density has been calculated using of the following equation:[41,42]

$$\sigma = \frac{h\rho N_a}{M_n} \tag{5.1}$$

In this equation, *h* corresponds to polymer film thickness (nm), ρ is the density of the block-co-polymer (gr/cm^3), N_a and M_n represent Avogadro's number and polymer molecular weight (34,231 g/mol), respectively. Lectin functionalization to the PVDMA chains (Scheme 5.2) was conducted by incubating solutions of WGA, HPA, or ConA in their appropriate buffers over azlactone-functionalized substrates for 1 hr. Substrates were incubated in 100 µL volumes at 0.1 mg/mL lectin concentrations unless otherwise noted. A 0.05% solution of Tween 20 in appropriate

buffer was used to wash the substrates. Identical protocols were followed for functionalization over polymer-coated nanopillar surfaces from Section 5.3.3.

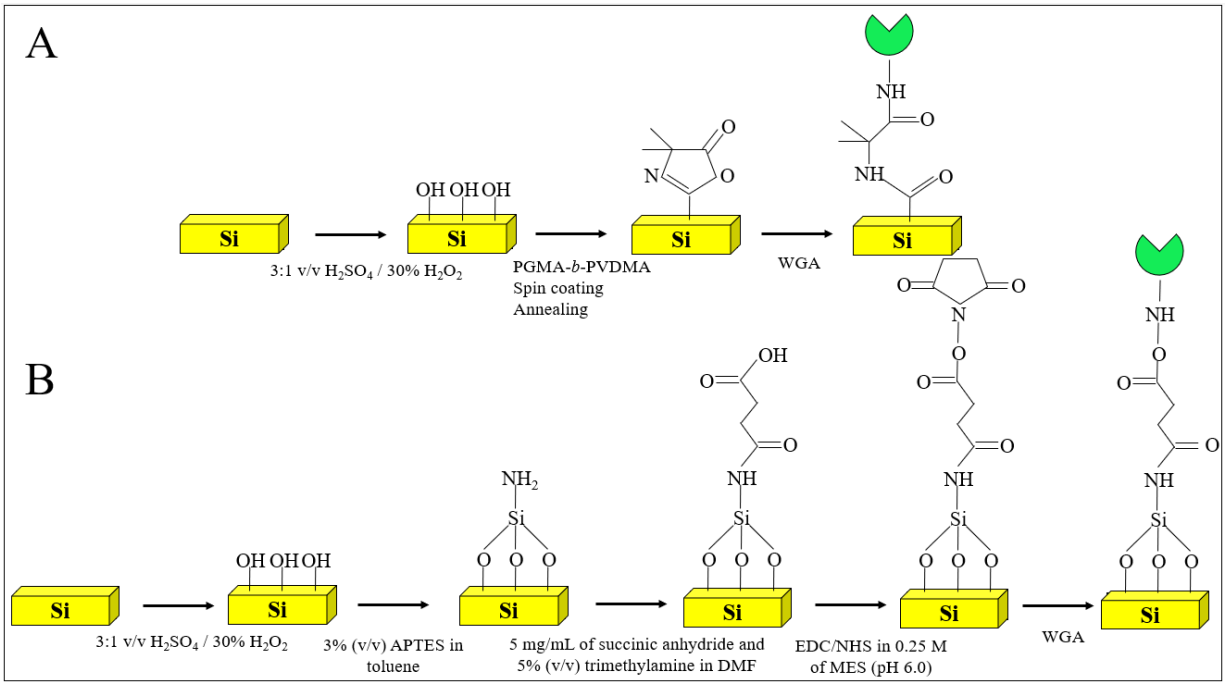

Scheme 5.2: Surface functionalization schemes. **(A)** PGMA-*b*-PVDMA. **(B)** EDC-NHS procedures.

5.3.3 Fabrication of Nanopillar Array Surfaces

Nanopillar array (NPA) surfaces were created using a combination of mask-less reactive ion etching (RIE) and plasma enhanced chemical vapor deposition (PECVD). Clean 4" <100> silicon wafers were etched in an Oxford Plasmalab 100 RIE system (Oxford Instruments, Concord, MA) for the desired time (3.3 or 10.3 minutes) using a 'black silicon'[43] etch recipe (100 W DC Bia, 1000 W ICP RF Power, 20 ^{o}C, 35 mT, 65 sccm SF_6, 45 sccm O_2). This etch process simultaneously generates random SiO_2 micromasks across the sample surface while removing exposed silicon, creating nanopillar texturing. A thin (~32 nm) layer of SiO_2 was then deposited

on the samples via PECVD to provide an oxide attachment layer for the $PGMA_{56}$-*b*-$PVDMA_{175}$ polymer. Samples were placed in an Oxford Plasmalab 100 PECVD system (Oxford Instruments, Concord, MA) and coated with SiO_2 at approximately 1.1 nm/min for 30 seconds (350 ºC, 1000 mT, 20 W RF power, 170 sccm 5% silane in Ar, 170 sccm N_2O). Samples were imaged in a FEI Novalab Dual Beam system prior to being coated with SiO_2. Coating of $PGMA_{56}$-*b*-$PVDMA_{175}$ on samples was performed according to the procedure described in Section 5.3.2. Polymer-coated nanopillars surfaces are referenced according to their pillar dimensions as low aspect ratio NPA (LAR-NPA) and high aspect ratio NPA (HAR-NPA).

5.3.4 Preparation of Bacterial Samples and Capture Conditions

Liquid cultures were prepared by inoculating a single colony of *E. coli* K12-mCherry in 3 mL of LB media (37 °C, 215 rpm). Bacteria were harvested by centrifugation, washed and re-suspended in 1X PBS solution. *E. coli*-mCherry solution with desired OD was incubated over the lectin-functionalized substrates by gentle rocking. After incubation of 1 mL of microbe solution for 1 hr, the substrates were immersed in 1X PBS buffer (0.05% Tween 20) to remove unattached bacteria followed by fixing the attached cells using 2.5% glutaraldehyde in ultrapure water. The substrates were then washed using ultrapure water and dried by aspirating water off the surface. Bacteria concentration in solution was quantified using optical density (OD_{600}) measurements. *A. tumefaciens* was cultured in AT minimal media supplemented with 0.5% glucose (w/v), 15 mM $(NH_4)_2SO_4$, and 100 mg/mL gentamicin.[44,45] For each culture a single colony of *A. tumefaciens* JX110 pJW110 was inoculated into 2 mL media and cultured for 22-24 hr (28 °C, 215 rpm). We then used 10 µL of this culture to inoculate 2 mL of fresh media supplemented with either 0, 50, 100, 200, or 400 µM IPTG. These cultures grew for an additional 10 -14 hr such that log phase

cultures could be used for subsequent experiments. A growth curve verified that these cells were taken in the log phase after this amount of time (Figure 5.1).

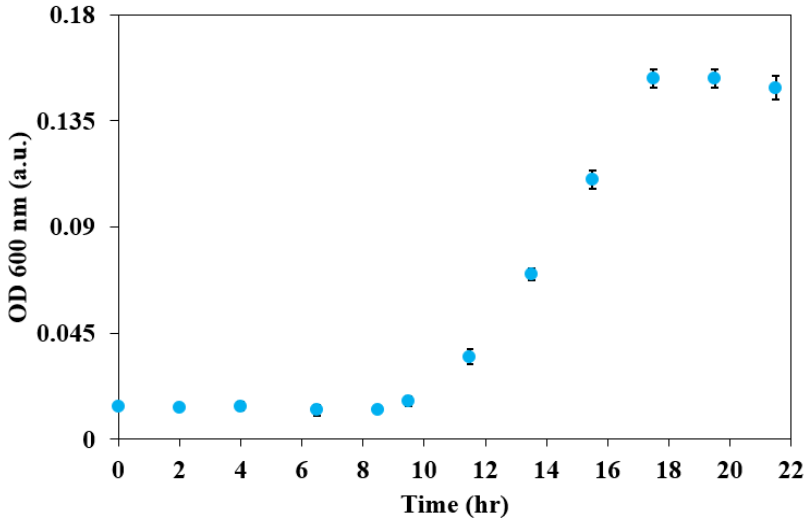

Figure 5.1 Growth curve of the *A. tumefaciens* JX110 culture solution. The 22-24 hr initial culture was spun down (4000 rpm, 10 min), re-suspended in fresh medium, diluted (10 µL in 2 mL fresh media), and OD_{600} measurements were then started. Culturing conditions: 28 ^{o}C, 22 hr, 215 rpm.

5.3.5 Lectin Binding Assay

The UPP production by *A. tumefaciens* JX110 pJW110 was visualized by using WGA labelled with FITC.[37] 1.0 mL of washed cell solution was incubated with 10 µg/mL solutions of WGA-FITC (1.0 mg/mL) for 1.5 hr at 25 °C while shaking at 200 rpm. Lectins unattached to the bacteria were removed by spinning down the cell suspension (4000 rpm, 10 min) and washing the solution twice. The solution was resuspended to an OD_{600} of 0.1 and 10 µL of the labelled cell suspension was pipetted between a glass slide (75×75 mm) and a coverslip (20×20 mm). The fluorescent intensity of the labelled cells was determined using a fluorescent microscope (Nikon Eclipse *Ti-E*).

5.3.6 EDC-NHS Coupling

Lectins were coupled to the Si wafer surfaces using EDC-NHS chemistry (Scheme S1B) following a standardized coupling protocol described in the works of Kim *et al.*[46] and Patel *et al*.[47] Briefly, Si wafers were cleaned in Piranha solution (3:1 v/v H_2SO_4 / 30% H_2O_2) at 120 °C for 30 min (*Caution! Strongly corrosive*), then incubated with a 3% (v/v) solution of APTES in anhydrous toluene for 24 hr to make an APTES film on the surface. Toluene was used to sonicate the substrates for 20 min. Surfaces then cured at 100 °C for 24 hr, followed by sonication in ultrapure water for 20 min. Substrates were then incubated in DMF including 5 mg/mL of succinic anhydride and 5% (v/v) trimethylamine for 4 hr. Surfaces immersed in a solution of EDC (50 mg/mL) and NHS (5 mg/mL) in 0.25 M of MES (pH 6.0) for 3 hr to introduce NHS ester groups over the substrates. Functionalized surfaces were then immobilized with WGA (same as PVDMA surfaces) followed by incubation with different concentrations of *E. coli* cell suspensions.

5.3.7 Limit of Detection (LOD) Determination

LOD is reported in terms of a solution concentration and was calculated according to the International Conference on Harmonisation (ICH) definition. This uses a combination of (1) microscopic evaluation of cells captured on a surface after incubation at a given solution concentration, and (2) standard deviation and slope of the response ($3\times\sigma/m$), where σ is the standard deviation from the replicates analysis near the detection limit, and m is the slope of the calibration curve.[48-50]

5.3.8 Live/Dead Assay

A live/dead assay was used to measure bacteria viability after surface capture following the procedure described in the LIVE/DEAD BacLight Bacterial Viability Kit, L7012.[51] Briefly, 2 µL of SYTO 9 and 2 µL of propidium iodide fluorescent dyes were added to 1 mL of NaCl 0.85 wt. % solution and thoroughly mixed. Flat and nanopillar surfaces were spin coated (1500 rpm, 15 sec) with a 0.75 wt.% solution of $PGMA_{56}$-*b*-$PVDMA_{175}$ and then functionalized with WGA. 1 mL of *E. coli* solution (10^4 CFU/mL) was then incubated on the surfaces. After 1 hr, bacteria on each surface were stained with the 200 µL of SYTO 9/ propidium iodide mixture for 15 min in a light-protected environment. SYTO 9 penetrates into the membrane of all cells, while propidium iodide only permeates dead cells and reduces SYTO 9 fluorescence when both dyes are present.[51,52] Samples were then washed with the buffer to remove unattached dye and imaged with a fluorescent microscope.

5.3.9 Instrumentation

Fourier transform infrared spectroscopy (FTIR). A Perkin Elmer ATR-FTIR was used to generate IR spectra and measure the peak intensity of azlactone carbonyl group at 1818 cm^{-1}. Before analyzing the samples, ethanol was used to clean the crystal and background spectrum of the diamond crystal was obtained (64 scans). The spectra acquired was examined, background-subtracted, and baseline-corrected by using Perkin™ software.

Ellipsometry. J.A. Woollam M-2000U variable angle spectroscopic ellipsometer was used to determine the polymer film thickness spin-coated over the Si wafers (Wavelength range 245-999 nm). Optical properties were explained by Cauchy model, considering: (1) polymer layer

represented a uniform layer and (2) the refractive indices for PVDMA and PGMA at 632 nm were considered as 1.52 and 1.50, respectively.[41]

Brightfield and fluorescence microscopy. An upright microscope (BX51, Olympus) and a fluorescent microscope (Eclipse *Ti-E*, Nikon) were used to take brightfield and fluorescent images of surfaces containing fluorescent lectins or captured bacteria. Lectin levels were quantified using NIS-Element software and reported as average fluorescent intensity per area ± standard deviation.

Scanning Electron Microscopy (SEM). Characterization of surfaces was performed using a SEM (FEI VERSA 3D DUAL BEAM) at 10 kV under 25,000 and 65,000 magnification. Bacteria were fixed for 15 min with 2.5% glutaraldehyde, and dehydrated in isopropanol solution (70 wt.%) for 15 min. Prior to SEM analysis, the surfaces were coated with a thin gold film (3.2 nm) using an EMS 150R plus rotary pumped coater (Electron Microscopy Science).

5.3.10 Image Analysis

ImageJ software was used to count the number of attached bacteria on the surfaces. Five to six representative images of each substrate were taken at different locations and reported as average ± standard deviation.

5.3.11 Statistical Analysis of Data

One-way ANOVA was used to compare group means and to test whether there was any statistical evidence that the associated population means were significantly different.[53] Post-hoc Tukey's tests were used to make pair-wise comparisons.[54] The statistical significance of the results

was confirmed at 95% confidence level. Calculations were performed by MINITAB 17^{TM} software and all values reported as the mean with the standard deviation.

5.4 Results and Discussion

5.4.1 Investigation of Lectin - Polymer Interactions on Flat Substrates

The goal of this study was to investigate the effect of PVDMA chain density on lectin coupling in effort to identify the polymer chain densities that provide the highest levels of azlactone conversion and highest corresponding lectin density. While higher PVDMA chain densities, and thus higher densities of azlactone groups would be expected to increase lectin surface loading, other factors including steric hindrance of polymer brushes or changes in polymer morphology could render higher fractions of azlactone groups inaccessible for coupling. To investigate this, different concentrations of polymer (0.25-1 wt.%) were first spin-coated over Si wafers followed by annealing and sonication.[55,56] Polymer film thickness and IR spectra of each sample were then measured (Figure 5.2, Figure 5.3) and subsequent calculation of areal chain densities was calculated using Equation 5.1. Film thickness and areal chain density showed a linear increase with polymer solution concentration, consistent with Lokitz *et al.,*[41] The overall range of thickness was found to be 30-110 nm while the areal chain density was 0.5-2.2 chains/nm^2. Further ATR-FTIR characterization of these substrates after WGA lectin coupling showed the expected decrease in the peak at 1818 cm^{-1} due to the ring opening, covalent reaction between azlactones and lectins,[29,57] and a corresponding appearance of an amide peak at ~1600 cm^{-1} (Figure 5.3).

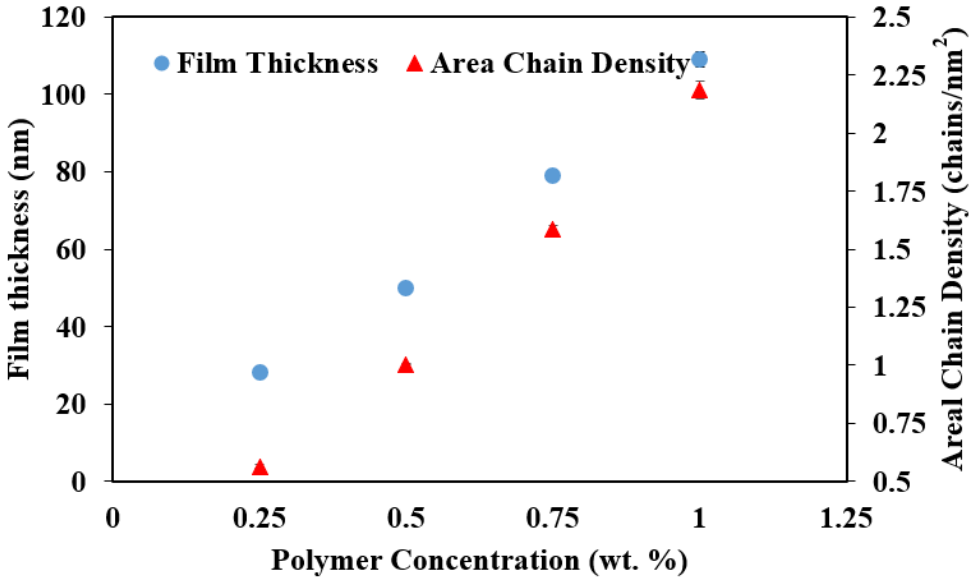

Figure 5.2 Film thickness and corresponding areal chain density of the polymer obtained via spin coating of different concentrations of $PGMA_{56}$-b-$PVDMA_{175}$ from chloroform.

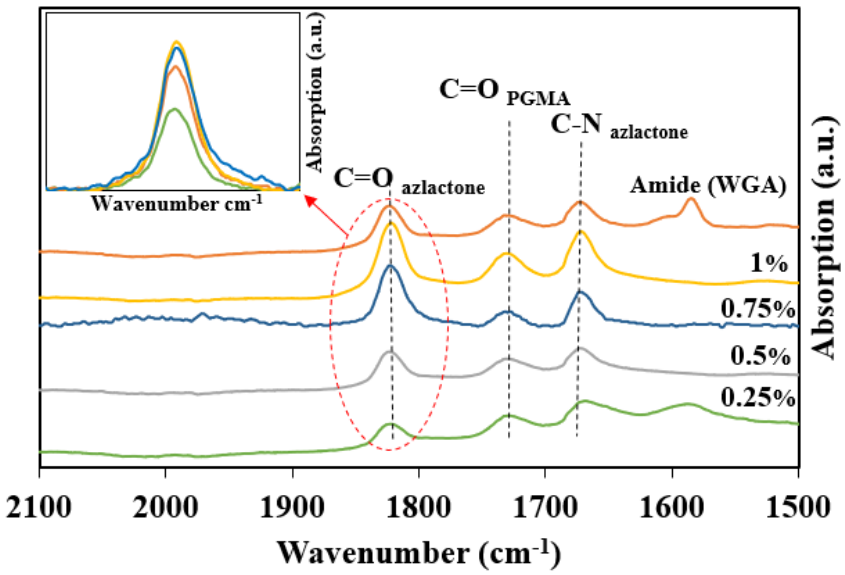

Figure 5.3 ATR-FTIR analysis of surface coated with different polymer concentrations (0.25-1 wt. %). The orange line shows the IR spectra of 0.75 wt. % polymer films incubated with WGA in 1X PBS. All spectra were background subtracted from bare silicon substrates.

Azlactone conversion measured for each PVDMA chain density is shown in Figure 5.4(A) as well as representative FTIR spectra of azlactone peak absorbance (inset). To account for the

fact that azlactone hydrolysis from aqueous buffer could also cause a decrease in absorbance, control substrates that were incubated with coupling buffer only (1X PBS) were also measured, and showed 6-7% hydrolysis in every case, independent of PVDMA chain density. With lectin coupling, a significant portion of azlactone groups remained unreacted at each polymer density. While this is partially due to the hydrophobic nature of the polymer that results in collapse of VDMA chains, a decrease in azlactone conversion with higher PVDMA chain densities is also noted. This trend suggests that as polymer chains become more compact, steric hindrance reduces the intermolecular interaction between lectin and polymer brushes.[58-60] Comparison of P-values from azlactone conversion data in Figure 5.4(A) reveals the most significant impact of polymer chain density occurred between 1.0 to 1.6 chains/nm^2. Comparable trends have been noted with other PVDMA systems. For example, Aden *et al.* studied the surface properties and the reaction of PVDMA films with molecule amines (hexylamine, tetradecylamine, and octadecylamine) and concluded that the degree of functionalization is lowered when chain density of polymer increases.[61] In another work, neutron reflectometry analysis of PVDMA brushes coupled with amines indicated that the degree of functionalization of polymer decreases when the grafting density of brush chains increases.[42] We further estimated the resulting lectin density on these surfaces by assuming that conversion of one azlactone group was equivalent to attachment of one lectin, shown in Figure 5.4(B). As evident, applying higher polymer concentrations results in more lectin density up to a polymer density of 1.6 chains/nm^2; beyond this point there was no change.

To verify the trends in Figures 5.4(A) and 5.4(B), independent fluorescent measurements of lectin density were also performed using fluorescently-labeled lectins (WGA-FITC and HPA-Alexa 488). Figure 5.4(C) shows the fluorescent intensity of polymer-functionalized substrates before and after treatment with solutions of WGA. The plot reveals increases in lectin density due

to higher fluorescent intensity with increasing polymer concentration up to 1.6 chains/nm^2, followed by saturation at higher densities, consistent with the trend in Figure 5.4(B), providing additional evidence of steric hindrance at higher polymer densities. To investigate if similar trends were noted with other lectins, analogous studies were performed with a significantly larger lectin (HPA ~70 kDa compared to WGA ~35 kDa), which showed a similar trend. It is worth mentioning that the intention of Figure 5.4(C) is not to compare the florescent intensity of WGA-FITC with HPA-Alexa fluor 488 at each polymer concentration, since each has been conjugated with a different type and number of fluorophores. These combined results led us to use surfaces with a chain density of 1.6 chains/nm^2 in order to provide maximum lectin loading for further use.

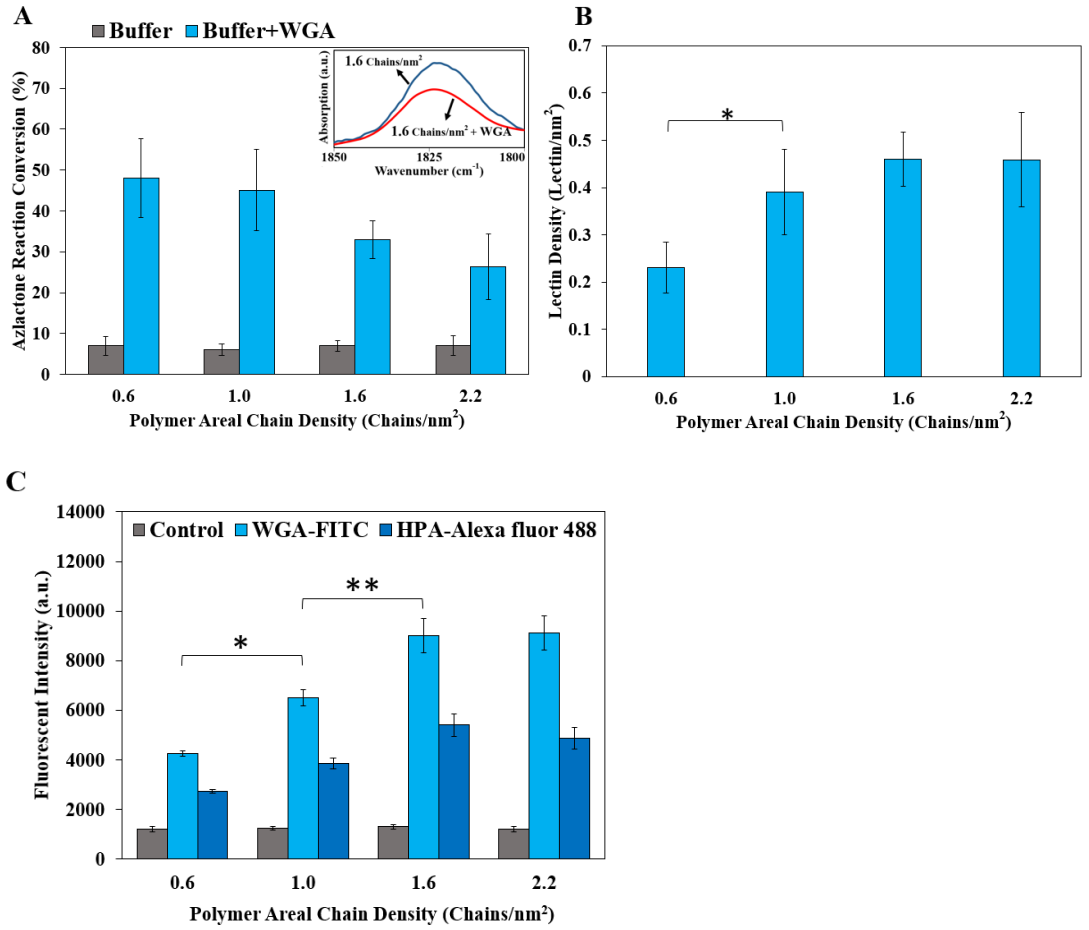

Figure 5.4 Surface characterization of lectin functionalized PGMA$_{56}$-*b*-PVDMA$_{175}$ films using ellipsometry, ATR-FTIR, and fluorescent microscopy. (A) Azlactone reaction conversion after

WGA coupling at each polymer surface density before and after WGA functionalization. (A Inset) IR spectra of surfaces functionalized with 0.75 wt.% polymer (blue line) and then coupled with WGA (red line). (B) WGA density measured for surfaces pre-coated with different polymer concentrations. (C) Fluorescent intensity of polymer-functionalized surfaces immobilized with 0.1 mg/mL of WGA-FITC or HPA-A488 in 1X PBS. (Control: 1X PBS without lectin incubated over substrates). ** = $P < 0.01$, * = $P < 0.05$, statistical differences apply to both WGA and HPA data sets. n = 3 independent substrates per condition. Values are the average ± standard deviation.

5.4.2 Investigation of a Lectin Panel for PVDMA Coupling and Microbe Capture

Despite the wide-spread potential to functionalize PVDMA-based polymers with biomolecules, coupling buffers that maximize PVDMA conversion with lectins has not been studied. Schmitt *et al*. reported that peptide coupling was significantly affected by change in pH, as an increase of pH from 7.4 to 9.5 enabled optimum coupling efficiency of cRGDfK peptides to PVDMA.[31] Here, the effect of coupling buffers on WGA, HPA, and ConA lectins was investigated using buffers with pH values commonly used in the literature.[40,62-65] The selection of these three lectins and the pH values tested were based on differences in molecular weight, isoelectric point, number of azlactone-reactive lysine residues, and sugar specificity (Table S1). While higher pH buffers favor nucleophilic addition with primary amino nucleophiles, the rate of azlactone hydrolysis will also increase and consequently compromise the reactive groups available. Figures 5.5(A-C) demonstrate the effect of solution pH on hydrolysis and aminolysis of the azlactone ring. Here, azlactone reaction conversion was again measured using ATR-FTIR to identify the optimum pH leading to the highest conversion for each lectin. Polymer-functionalized surfaces were also exposed to each buffer without lectin to quantify the effect from azlactone hydrolysis. The percentage decrease in the 1818 cm^{-1} peak can be attributed to the sum of the reactions of azlactone with amines and hydroxyl groups. Net contribution of amines then can be calculated by subtracting

the summation from hydrolysis data. As can be seen for all three lectins, increasing pH to an intermediate level (pH 9.3 or 8.0) enhanced the lectin-azlactone reaction conversion marginally, reaching ~30%. The optimal pH found at 9.3 is likely due to the fact that this is slightly above the pKa of lysine residues present on the protein (pKa = 8.95),[66] resulting in deprotonated amino groups that most efficiently couple with the azlactones. The lower levels of HPA coupling compared to the other lectins may be due to the lower number of lysine residues present.

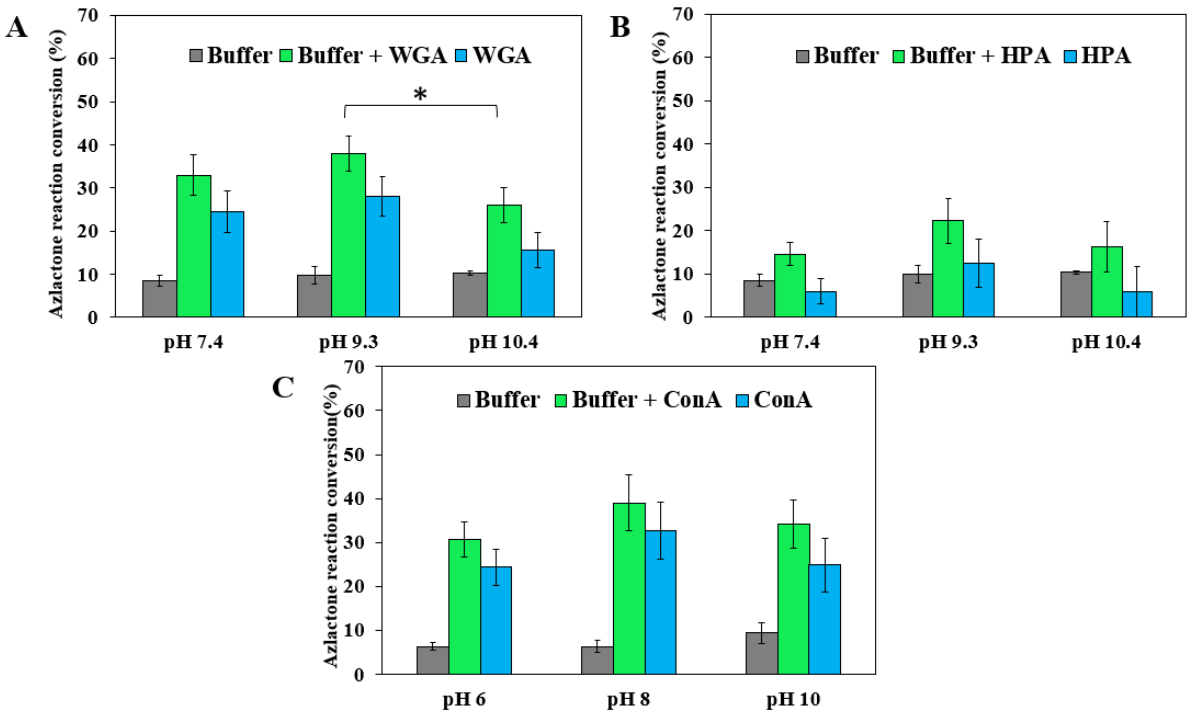

Figure 5.5 Results demonstrating the lectin addition and hydrolysis of azlactone groups at various pH. Variation of azlactone reaction conversion with different pH levels calculated by the percentage decrease in the height of IR spectra peak at 1818 cm^{-1} due to (A) WGA immobilization, (B) HPA, and (C) ConA. Contribution of each lectin was measured by subtracting the summation (buffer + lectin) from hydrolysis data (buffer). * = $P < 0.05$, n = 3 independent substrates per condition. Values are the average ± standard deviation.

To identify lectins that enable the highest bacteria capture levels, this panel of lectins was coupled to polymer surfaces at the pH showing highest levels of coupling, and capture levels for

model *E. coli* mCherry cells at high concentrations (10^8 CFU/mL) were quantified. As lectins provide valuable interfaces for glycoprofiling cell-surfaces, proteins, and other glycoconjugates,[67] the secondary goal here was to verify that polymer-functionalized surfaces coupled with different lectins could produce a differential binding response consistent with literature. The results in Figure 5.6 indicate that *E. coli* capturing capacity of WGA is higher than HPA and ConA, suggesting that WGA lectin had higher binding affinity for *E. coli* than HPA and ConA. The difference in capture ability might be due to the lectin size, sugar specificity, or the composition of the bacteria cell wall.[68] Similarly, Wang *et al.* described a surface plasmon resonance sensor coupled with WGA and ConA lectins for *E. coli* O157:H7 capture, also indicating higher capture of *E. coli* by WGA compared to ConA.[3] Hsu *et al.* reported a lectin microarray for fast analysis of the carbohydrates present on bacterial cell surfaces, and demonstrated that lectin surfaces produced differential binding levels, with WGA-functional surfaces capturing more *E. coli* compared to ConA.[69]

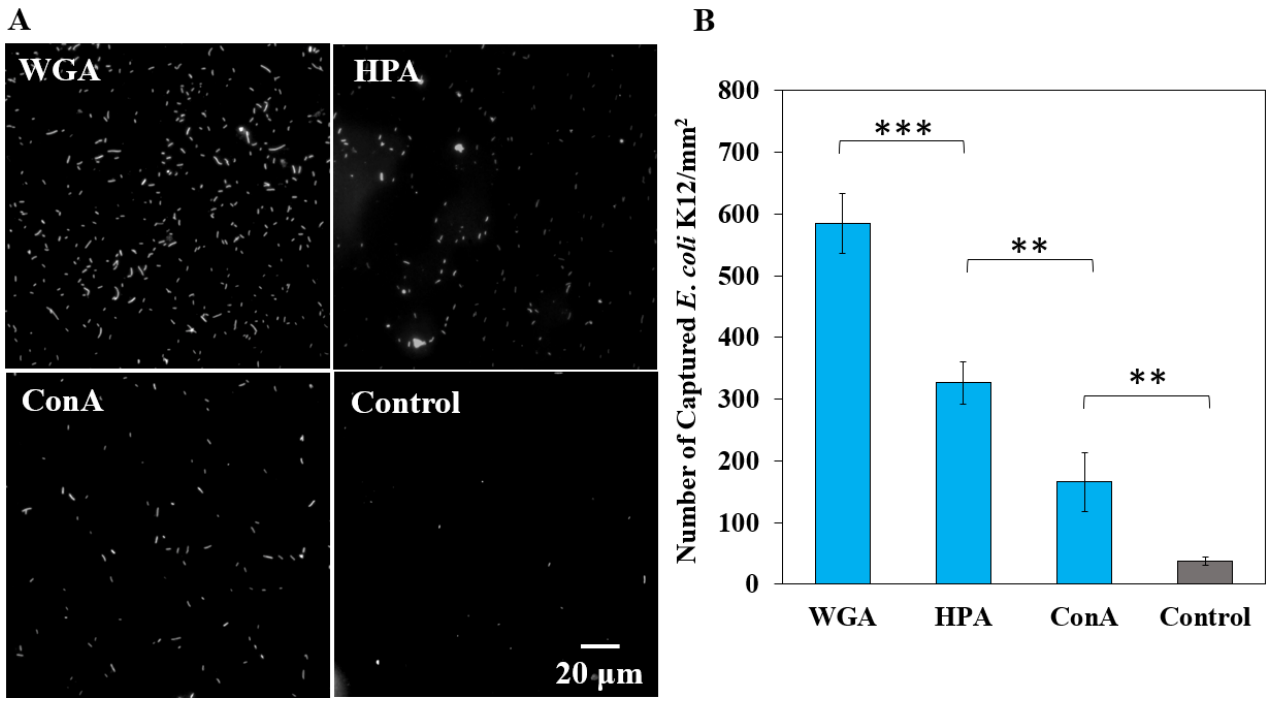

Figure 5.6 (A) Representative fluorescent images of *E. coli*-mCherry captured by the polymer surfaces immobilized with WGA, HPA and ConA at high concentrations (10^8 CFU/mL). As the control, BSA solution (1 wt.%) was incubated on the PVDMA substrates to account for non-specific binding of cells to the surface under these conditions. (B) Calculated number of captured *E. coli* on the surface via using ImageJ. The values were given as the mean of five different surface locations from three independent surfaces. *** = $P < 0.001$, ** = $P < 0.01$. Values are the average ± standard deviation.

5.4.3 Characterization of PVDMA-coated Nanopillar Array Surfaces

In order to integrate physical nanostructures into our capture surfaces, we generated high-density NPAs on silicon surfaces using RIE etching, as described in Section 5.3.3. These structures were designed to serve as an underlying surface template for the PVDMA polymer films, providing the interface with pronounced nanoscale architecture. Etch times were varied to generate a low-aspect ratio nanopillar array (LAR-NPAs) and a high-aspect ratio nanopillar array (HAR-NPAs). Figure 5.7(A) and (B) show SEM images of substrates with LAR-NPA surfaces prior to the PVDMA coating step. These nanopillars appear to be 300 ± 59 nm in height with an average

diameter of 73 ± 9 nm. After PVDMA spin coating and annealing, the polymer appears visible on the nanopillars, as shown in Figure 5.7(C). An increase in average pillar diameter to 120 ± 6 nm due to addition of the polymer coating was measured and pillar aggregation was also noted. The apparent thickness of the polymer films on non-aggregated pillars (~ 47 nm) was less than the polymer film thickness measured after spin-coating onto flat Si surfaces (80 nm, Figure 5.1), likely due to the fact that the spin-coating process is non-conformal. HAR-NPA surfaces appeared to have similar pillar diameters as their LAR-NPA counterparts before coating, but pillars were 2100 ± 126 nm in height, as shown in Figures 5.7(D) and (E). After spin coating over these surfaces, the polymer again appeared to cause nanopillar aggregation, as shown in Figure 5.7(F). Because of excessive pillar aggregation here, we were unable to quantify the increase in individual pillar diameter due to the polymer. Instead, to further confirm the presence of the PVDMA polymer on the nanopillars, additional qualitative characterizations were made, including EDX to verify a change in surface composition and fluorescence measurements of the coated substrates (Figure 5.8), which detected an increase in fluorescence after the spin coating and annealing steps due to the fact that the polymer is weakly auto-fluorescent.

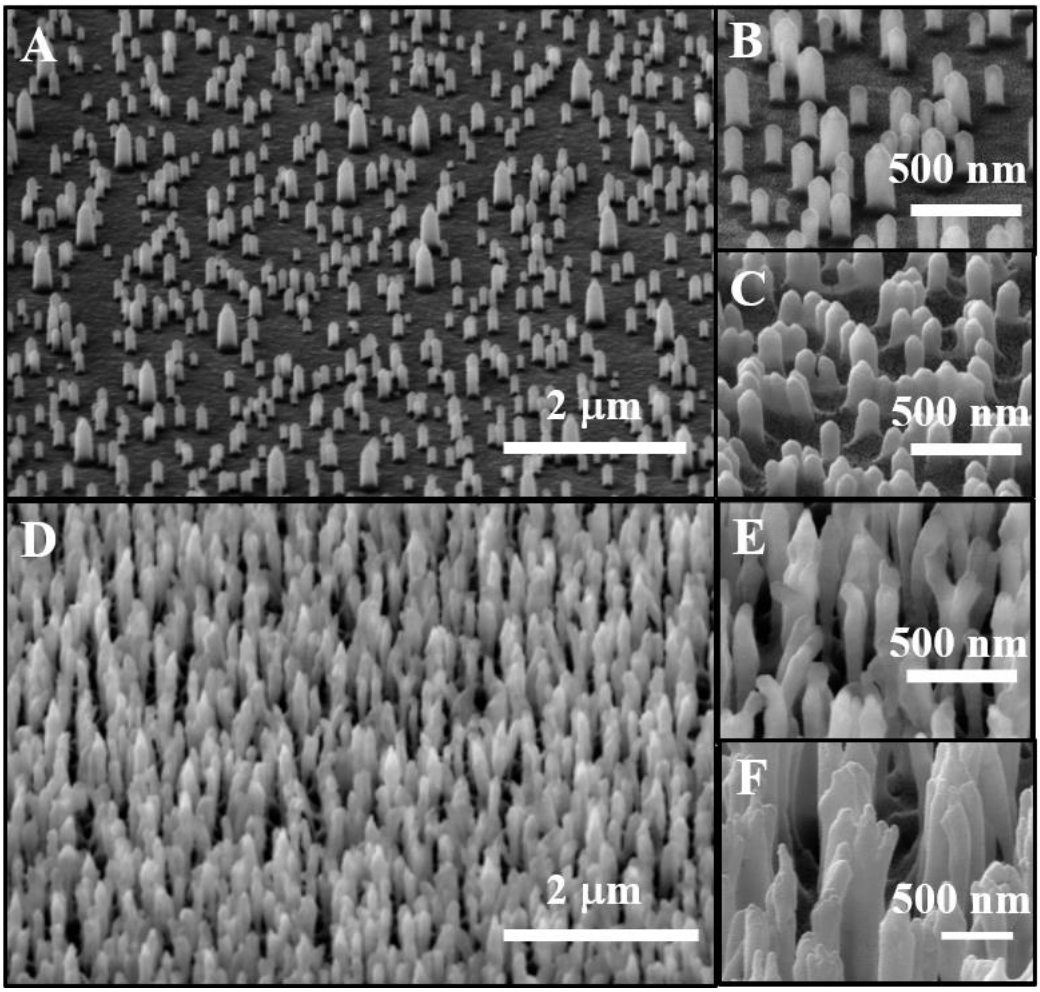

Figure 5.7 Scanning electron micrographs of NPAs before and after PVDMA spin coating. (A and B) Uncoated LAR-NPA surfaces; (C) PVDMA-coated LAR-NPA surfaces; (D and E) Uncoated HAR-NPA surfaces; (F) PVDMA-coated HAR-NPA surfaces. Spin coating used a 0.75 wt.% PVDMA solution followed by annealing at 110 °C.

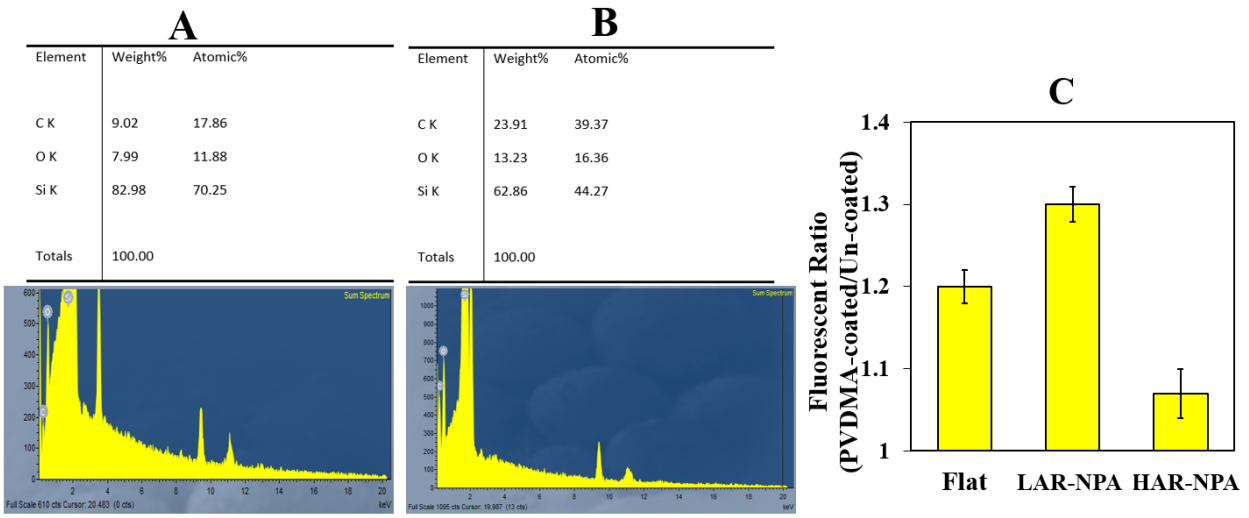

Figure 5.8 Characterization of flat and nanopillar surfaces with SEM-EDX and auto-fluorescent measurements. (A) Composition analysis and sum spectrum of the bare LAR-NPA by SEM-EDX (B) Composition analysis and sum spectrum of the PVDMA-coated LAR-NPA surface by SEM-EDX (C) Autofluorescence measurements of uncoated and PVDMA-coated surfaces. (0.75 wt.% PVDMA solution in chloroform). Spin coating conditions: 1500 rpm, 15 sec. A ratio greater than 1 indicates an increase in autofluorescence compared to the uncoated substrate.

5.4.4 Sensitivity and Quantitative Detection of *E. coli*

Results obtained from Sections 5.4.1 to 5.4.3 were applied to generate both flat and NPA surfaces coated with lectin-functional PVDMA for assessment of capture sensitivity. All polymer films were functionalized under conditions showing highest levels of lectin coupling and bacteria capture at high concentrations (0.75 wt.% PVDMA spin coating, WGA lectin, pH 9.3 coupling buffer) and a set of capture experiments was performed to quantify the limit of detection (LOD).

To first benchmark the gains in sensitivity from the flat polymer surfaces against standardized capture substrates, a side-by-side comparison of capture levels was performed using lectin substrates functionalized with an EDC-NHS coupling chemistry protocol.[46] Different concentrations of bacterial culture (ranging from 10^2 to 10^5 CFU/mL) were contacted with WGA

functionalized to either flat PVDMA or EDC-NHS surfaces and incubated for 1 hr (Figure 5.9 (A,i) and (ii)). For wider observation of these surfaces, see Figure 5.10.

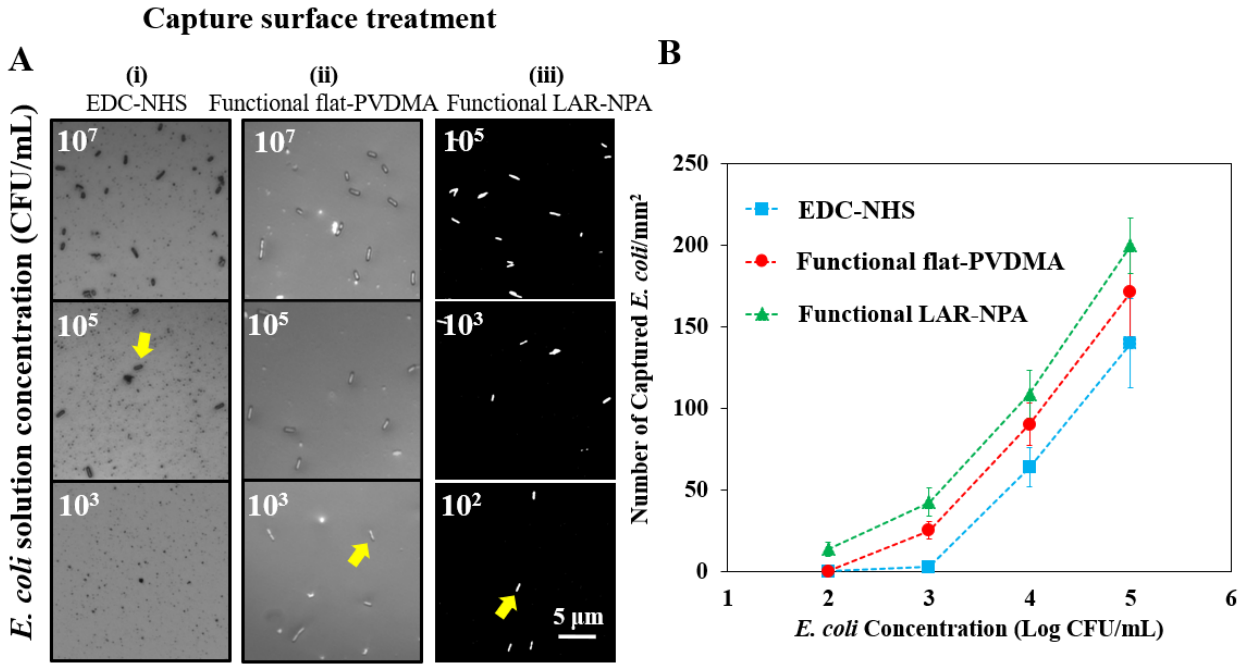

Figure 5.9 (A) Representative microscopic images of *E. coli* captured by the WGA immobilized on EDC-NHS surfaces, functional flat-PVDMA surfaces, and functional LAR-NPA surfaces after contact with bacteria at different concentrations. Yellow arrows indicate a representative bacteria cell on the surface. (B) Corresponding analysis of the number of captured *E. coli* for different bacteria solution concentrations. The values were given as the mean of five different locations from three independent surfaces. Values are the average ± standard deviation.

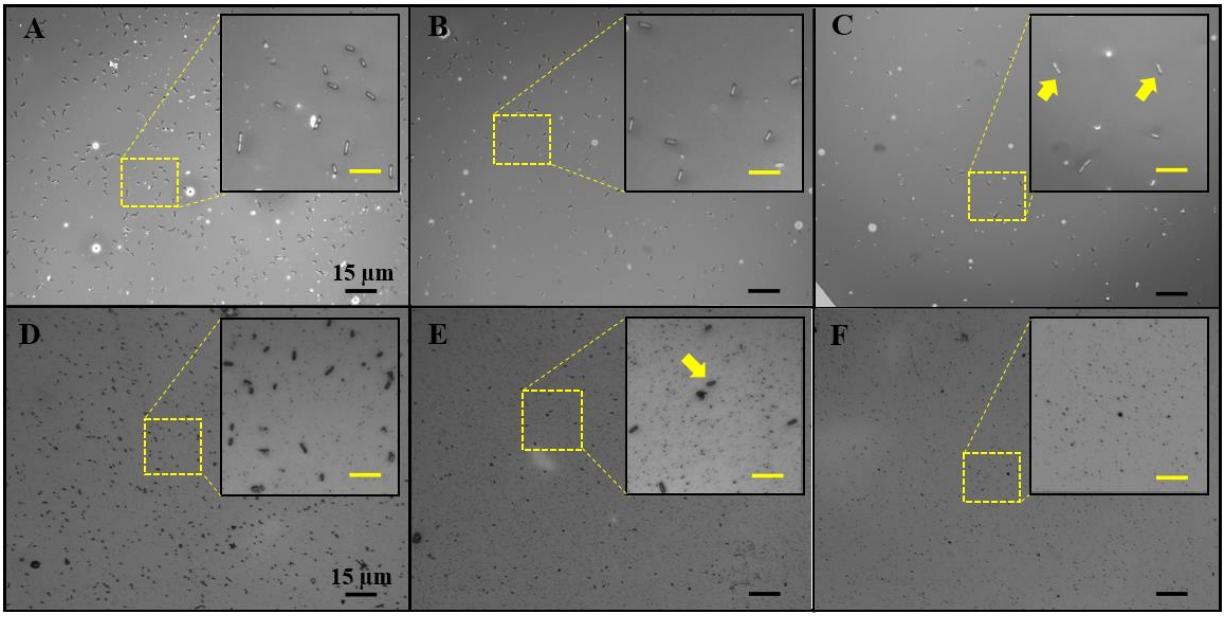

Figure 5.10 (A-C) Representative microscopic images of *E. coli* captured by WGA immobilized on $PGMA_{56}$-*b*-$PVDMA_{175}$ surfaces incubated with different bacteria concentration. (A) 10^7 CFU/mL, (B) 10^5 CFU/mL, (C) 10^3 CFU/mL (near the estimated LOD). (D-F) Representative microscopic images of *E. coli* captured by WGA immobilized on EDC-NHS surfaces incubated with different bacteria concentration. (D) 10^7 CFU/mL, (E) 10^5 CFU/mL, (F) 10^3 CFU/mL (One order of magnitude below the estimated LOD) (Inset scale bar: 5 µm). Both methods treated with the same bacteria but the efforts to increase the contrast and quality of images by ImageJ made the bacteria in EDC-NHS darker. Yellow arrows demonstrate the location of representative bacteria cells on the surface.

For flat, WGA-functionalized PVDMA surfaces (herein referred to as functional flat-PVDMA), the number of cells captured was significantly higher at concentrations between 10^3 and 10^4 CFU/mL ($P<0.01$), as shown in Figure 5.9(B). An estimated detection limit of 1.7×10^3 CFU/mL was calculated and a linear correlation between the number of captured bacteria and the logarithm of *E. coli* concentration was also observed. The result at 10^3 CFU/mL (Figure 5.9(A,ii)) was presented to demonstrate bacteria capture near the LOD. For control EDC-NHS substrates, no bacteria were observed at a concentration of 10^3 CFU/mL, and the LOD was estimated as 1.6×10^4 CFU/mL. Compared with the EDC-NHS cross-linking protocol, the functional flat-PVDMA

surface exhibited lower detection limit by roughly one order of magnitude. This improvement in sensitivity is attributed to the increased lectin density and uniformity over the PVDMA polymer. We quantified that a 41.9% increase in lectin density was present relative to the control, based on fluorescence measurement (Figure 5.11). Further comparison of capture levels at diluted bacteria concentrations (10^4 CFU/mL) also shows that capture efficiency, defined as the number of cells captured on the surface compared to the number of cells initially in solution, improved from 51.8% to 72.9%.

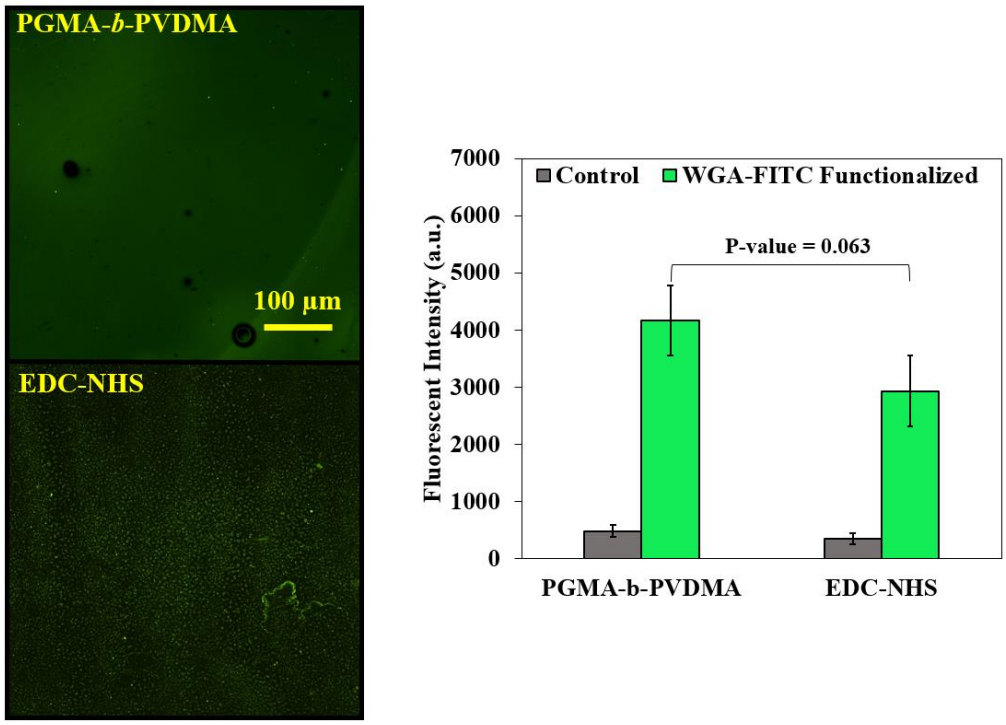

Figure 5.11 (A) Representative fluorescent images of lectin surfaces treated with EDC-NHS and PGMA-b-PVDMA and functionalized by a labeled lectin (WGA-FITC) (B) Corresponding fluorescent intensity measurements of each surface.

This comparison quantifies the gains in sensitivity that can be achieved using the polymer compared to conventional interface chemistry. Additional advantages of using the polymer relative to the standard substrates include (1) high hydrolytic stability of PVDMA compared to NHS esters,

which are susceptible to hydrolysis,[25] making it a more robust platform for biofunctionalization; (2) a facile, one-step protein bioconjugation using a rapid "click" reaction with no byproducts; and (3) facile control of reactive site densities through modulating the polymer solution deposition procedure (Figure 5.2). This last benefit is particularly useful, as it enables one to modulate the range and strength of the cell binding interaction.

To access the impact of incorporating nanostructure into the lectin-functionalized polymer films, the sensitivity was accessed in analogous fashion for NPA surfaces after PVDMA coating and WGA functionalization, these surfaces are herein referred to as "functional NPAs". Figure 5.9 demonstrates additional gains in capture efficiency and sensitivity using the functional LAR-NPA surfaces, as cell capture levels were significantly increased at all solution concentrations between 10^2 and 10^4 CFU/mL ($P<0.01$). With the addition of the LAR-NPAs, the LOD using the PVDMA coatings improved from 1.7×10^3 to 2.1×10^2 CFU/mL. Binary fluorescent images instead of brightfield images are provided for the functional LAR-NPA surfaces for image clarity (Figure 5.9 (A,iii)). To check for non-specific capture of bacteria due to the presence of the nanostructures, a negative control was performed by instead passivating LAR-NPA surfaces with BSA. Here, capture of *E. coli* was minimal (12 ± 3 cells/mm^2) at a solution concentrations of 10^4 CFU/mL. Capture on functional HAR-LAR surfaces was not quantified, as distinctive changes in cell morphology were noted; this will be discussed in Section 5.4.5.

The positive effects from the nanostructure are consistent with multiple findings from the literature. For example, Jalali *et al.* presented a micro-fluidic device containing three-dimensional, shrub-like nano-micro islands (NMI) for capture and detection of *E. coli* and *Staphylococcus aureus*. The fluorescent intensity of both captured on 3D NMI structures was improved compared to flat platforms.[70] With respect to eukaryotic cell capture, Wang *et al*. reported Si NPAs

immobilized with epithelial-cell adhesion-molecule antibodies to isolate circulating tumor cells and found that the functionalized NPAs increased cell adhesion 10-fold compared to smooth Si substrates.[71] Chen *et al*. measured a similar increase in CTC capture by increasing the roughness of the capture surface from 1 to 150 nm.[72]

The gains in sensitivity quantified for lectin-based capture from (i) use of the PVDMA polymer and (ii) addition of nanostructure give these interfaces relevance to variety of different diagnostic applications where lectin-based bacteria capture is traditionally limited. For example, contaminated water samples containing fecal coliforms such as *Enterococci* and *Escherichia* bacteria generally range in concentrations from 10^3-10^5 CFU/mL.[73,74] With respect to clinical applications, urinary tract infections (UTI) often require detection on the order of 10^3 CFU/mL, depending on the type of bacteria present.[75] Both flat and NPA surfaces are applicable for UTI diagnosis. Finally, literature reports the initial symptoms of sepsis in an adult when bacteria are present in blood at 1-100 CFU/mL.[76,77] Lectins have been shown to be particularly useful for isolation of bacteria from blood; for example, engineered mannose binding lectin was recently applied to remove Gram negative and Gram positive pathogens from blood at high specificity in a blood cleansing device.[15] Our highest sensitivity surfaces, achieved with functional LAR-NPAs surfaces, achieves a LOD on the order of 10^2 CFU/mL, approaching the upper-end of the sensitivity requirement for applications to blood infections. While further development is required for bacteria isolation directly from clinical or environmental samples, we have observed similar capture levels between buffer and LB media (Figure 5.12), suggesting that these surfaces are useful for capture from more complex media.

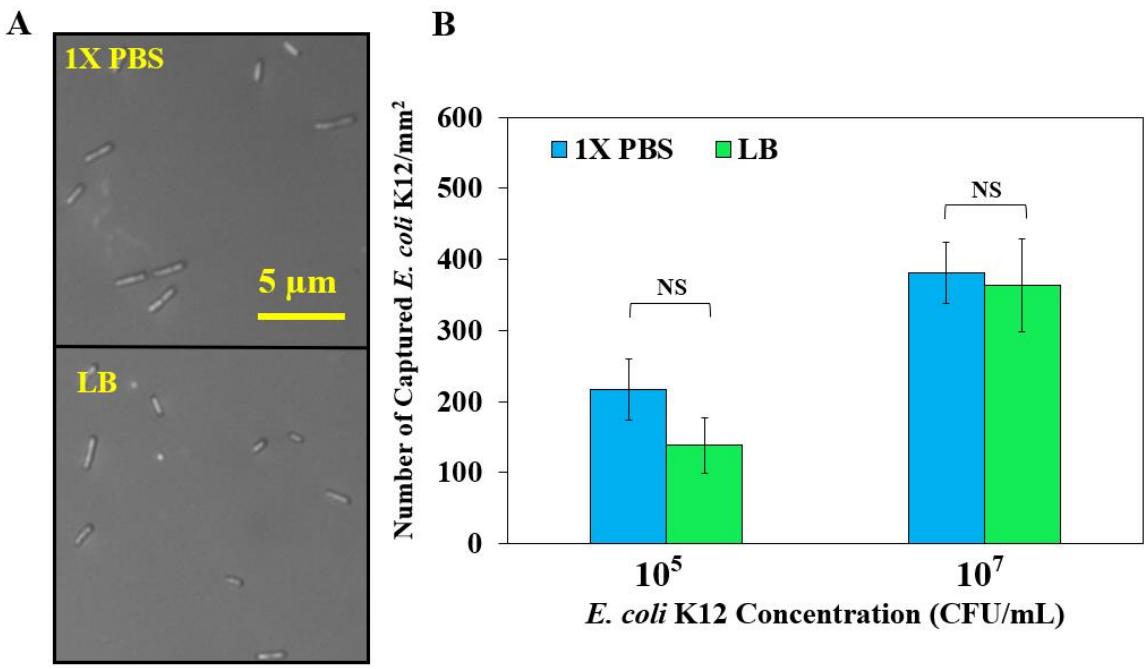

Figure 5.12 Comparison of bacteria capture levels on flat functional PVDMA surfaces using 1X PBS and LB media as the capture solution. (A) Representative brightfield images, and (B) surface density of captured bacteria at each solution concentration tested. NS = no statistical difference.

5.4.5 Bacteria Viability After Capture on Functional Nanopillar Array Surfaces

While functional NPAs improved cell capture, nanopillars may also have bactericidal properties as they can cause mechanical cell deformation and lysis by puncturing and rupturing the cell membrane on contact.[78] To characterize the effect of the nanopillar structure on cell viability, both SEM images and live/dead assays were used. Figure 5.13(A) shows the SEM images of *E. coli* after capture on functional LAR-NPA and functional HAR-NPA surfaces. While the cell structure was maintained on LAR-NPA surfaces (Figure 5.13(A,i)), significant deformation in cell morphology becomes apparent on HAR-NPA surfaces. Here, intact bacteria appear more stretched and deformed across the pillars (Figure 5.13(A,ii)) and cellular debris also becomes visible across the surface (Figure 5.13(A,iii)), indicating that cell lysis is occurring. Live-dead assays indicate that while 48 ± 6.8% of the attached *E. coli* cells remained alive after contact on the flat PVDMA

surfaces, viability decreased upon contact with the NPAs; 12 ± 4.5% of cells were live on LAR-NPAs and 9 ± 4% of intact cells were alive on HAR-NPAs (Figure 5.13(B)). Taken together, the combined results in Figures 5.9 and 5.13 emphasize the potential trade-offs offered by each capture surface. For applications where only capture and detection sensitivity are important, LAR-NPA surfaces are most beneficial. However, for applications requiring retrieval of live cells for culture-based follow-up analysis (e.g. enrichment for genotyping, testing for antibiotic resistance, etc.), non-structured, flat PVDMA surfaces may be more beneficial.

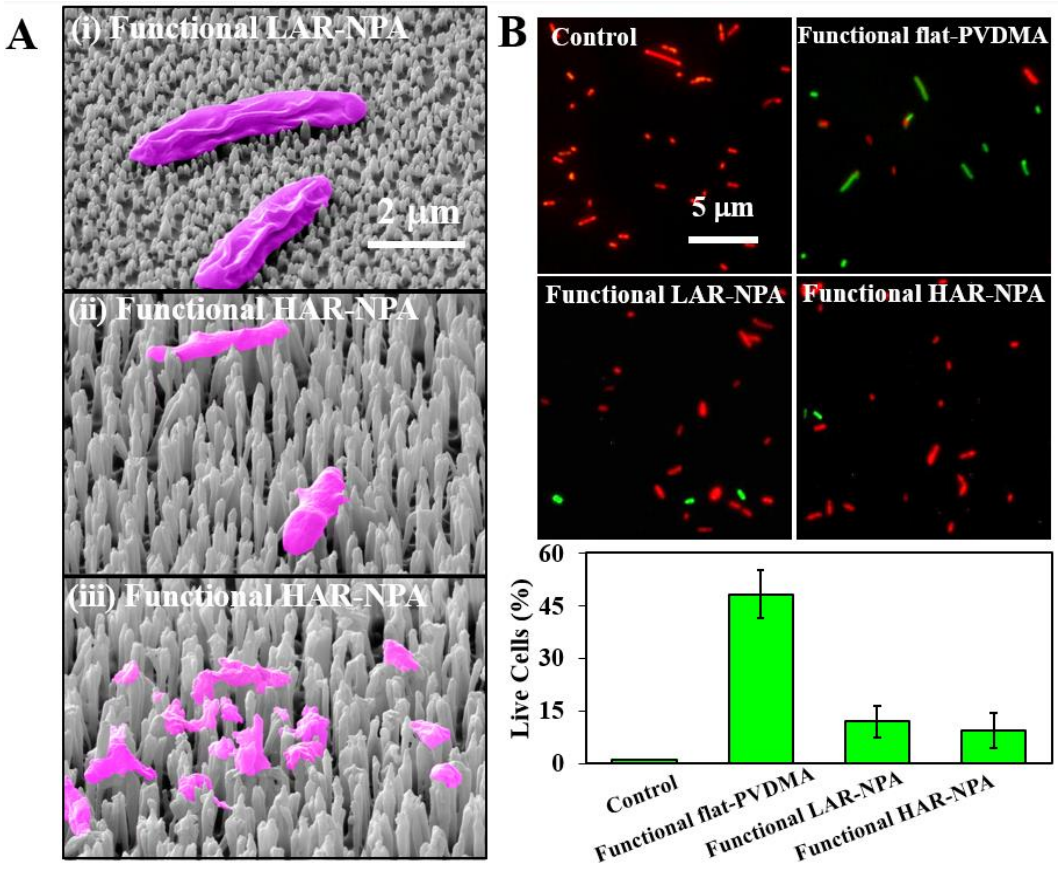

Figure 5.13 (A) Scanning electron micrographs and microscopic images of *E. coli* after capture onto functional NPA surfaces. Bacteria or cellular debris were colored pink to distinguish them from the pillars. (B) Representative fluorescent images and % of live cells after capture to each surface. Control: Attached bacteria were exposed to a 2.5% glutaldehyde solution and 70% isopropanol solution to verify that dead cells could be detected with the live/dead assay. Live/dead assay images were adjusted with ImageJ to maximize color contrast.

5.4.6 Importance of Bacteria UPP Expression vs Lectin Density on Capture

While lectin density is key for improving bacteria capture, the structure and composition of the bacteria's extracellular surface can also play a significant role.[36] Here, we systematically modulated production of an exopolysaccharide adhesin, a critical bacterial cell surface feature, to understand its effect on lectin-based surface capture. This was achieved using *A. tumefaciens* JX110 pJW110, a mutant strain that produces modulated levels of unipolar polysaccharide (UPP) adhesin in response to varied degree pleD gene expression. The UPP adhesin is localized to one pole of *A. tumefaciens* cells and plays a key role in initiating stable surface attachment.[36,79] Extracellular UPP levels can be controlled by varying IPTG inducer concentration in culture media. Without IPTG induction, very low levels of UPP are inherently present and this strain also lacks other major exopolysaccharides produced by *A. tumefaciens*. Upon induction, UPP is produced and binds WGA lectin due to the fact that it is partly composed of N-acetyl glucosamine (GlcNAc) components. Consequently, this system allows us to experimentally manipulate the degree to which bacterial cells present extracellular surface features required for capture by lectin-functional interfaces. Further, this experimental system allows us to manipulate these features over a broad and quantitative range, including levels exceeding that of unmanipulated, planktonic *A. tumefaciens* cells.[37]

It was first verified that UPP expression could be modulated by culturing JX110 pJW110 in culture media supplemented with either 0, 50, 100, 200, or 400 μM IPTG. Similar experimental conditions reported in Xu *et al.* were sufficient to produce substantial overexpression of the UPP adhesin relative to uninduced controls.[37] Extracellular glycan levels were then characterized with a solution-phase lectin binding assay using WGA-FITC, binding to GlcNAc components present on the extracellular surface.[29] As shown in Figure 7A, increasing the IPTG concentration resulted

in proportionally higher UPP production consistent with the results of Xu *et al*.[37] Post hoc Tukey's test was applied to identify three groups with significantly different fluorescence levels (denoted by groups a, b, and c in Figure 5.14(A)). Based on this, we used IPTG concentrations of 0, 200, and 400 μM for subsequent experiments in which cells produced varying levels of UPP ($P < 0.05$). Across this range of IPTG concentrations, a wide range of UPP levels was achieved for further study; increasing IPTG from 0 to 200 μM raised the cell fluorescent intensity by 96%, while an additional increase to 400 μM increased cell fluorescence another 35%. To measure the impact that UPP production levels had on capture, WGA surface density was held constant (0.46 lectins/nm^2) and capture was measured by incubating the surfaces with JX110 pJW110 populations cultured at each of the three different IPTG concentrations identified from Figure 5.14(A). Each population was incubated over the lectin-functional surface at the same concentration (OD_{600} = 0.1) and experimental conditions. As shown in Figure 5.14(B), a slight increase in bacteria capture was measured as UPP expression increased. However, the difference was not statistically significant ($P > 0.05$). To compare these changes to changes caused by varying the WGA surface density, populations of cells showing intermediate levels of UPP expression (IPTG = 200 μM) were cultured, then their capture was measured across surfaces with varied WGA densities (Figure 5.14(C)). JX110 pJW110 populations were incubated over the surface at the same concentration as in the previous experiment (OD_{600} = 0.1). Here, the number of captured bacteria showed a strong dependence on WGA density, as increasing WGA densities from 0.23 to 0.39 or to 0.46 WGA/nm^2 generated significant increases in capture ($P < 0.05$). Results from Figures 5.14(A) and (B) demonstrate that bacteria capture increases as both the levels of extracellular adhesin increase and as lectin surface densities increase, which is consistent with other reports,[9,80-82] and with the theory that multi-valent lectin-oligosaccharide interactions increase binding strength.[18,83] Comparing the

two different factors, it appears that lectin surface densities had a greater impact on capture efficiency as a 2-fold increase in lectin density generated a statistically significant increase in capture level, while a 3-fold increase in extracellular glycosylation levels did not. This finding is highly favorable, because in real capture applications the lectin surface density on the synthetic interface can be easily manipulated using the parameters discussed previously, while the extracellular glycan levels of the targeted bacteria cannot be controlled. This highlights the importance of the synthetic interface for driving capture and for loading high levels of lectin to the surface in order to efficiently capture bacteria as they encounter the surface.

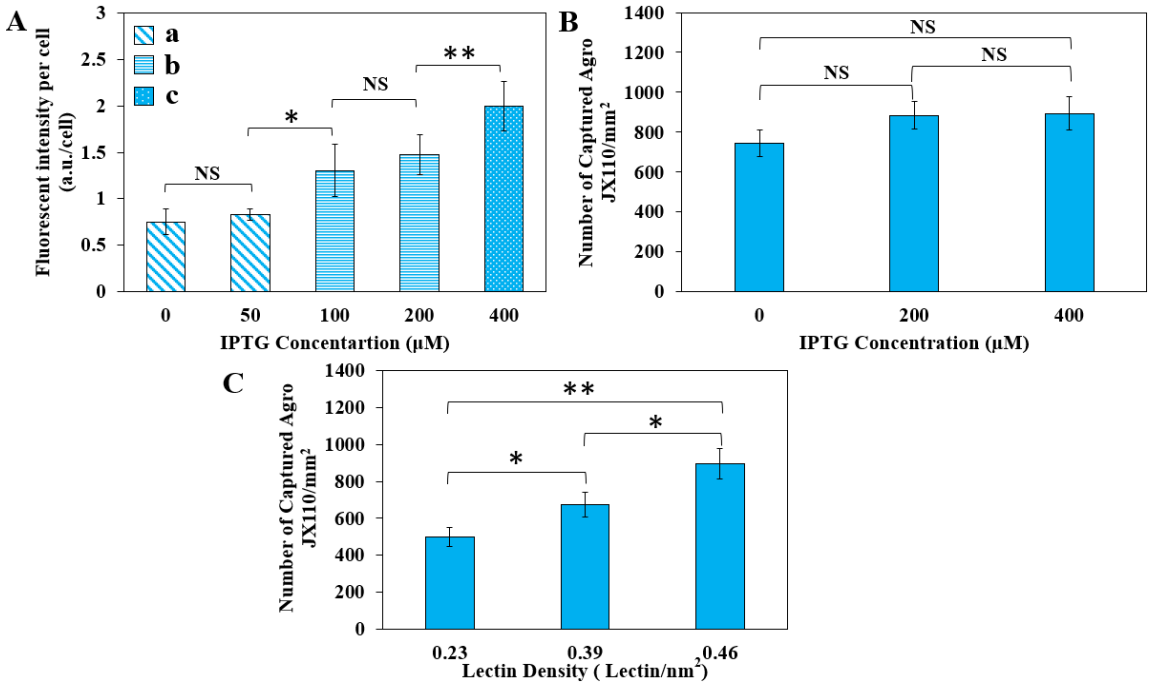

Figure 5.14 (A) Variation of fluorescent intensity of *A. tumefaciens* JX110 cells after culturing at different IPTG concentrations and labeling with FITC-conjugated WGA lectins. ANOVA one-way and Tukey's test were applied to measure overall and pairwise p-values, respectively. Tukey test categorized IPTG concentrations into 3 different groups (a, b, and c). (B) Number of captured *A. tumefaciens* JX110 cells on the surface at different IPTG concentrations. All solutions of JX110 cells were incubated on the surface at OD 0.1 and lectin density was held constant at 0.46 WGA/nm^2. (C) Number of captured *A. tumefaciens* JX110 on the surface at different the lectin densities. All solutions were again incubated over the surface at OD 0.1 and IPTG concentration was kept constant at 200 µM. The values were given as the mean of five different locations from

three independent surfaces. ** = $P < 0.01$, * = $P < 0.05$, NS = Not Significant. Values are the average ± standard deviation.

5.5 Conclusion

Lectin proteins bind extracellular glycan structures with high specificity and can be functionalized to synthetic interfaces for non-destructive cell capture and glycomic profiling. In the present research we performed a systematic study of parameters that influence lectin coupling to the azlactone-functional block copolymer, $PGMA_{56}$-*b*-$PVDMA_{175}$, and used these findings to construct capture surfaces with maximized lectin density and pronounced nanoscale surface structures for highest capture efficiency and detection sensitivity at 10^2 CFU/mL. It was shown that applying higher polymer concentrations led to higher lectin surface density up to a polymer density of 1.6 chains/nm^2, further increases did not impact lectin density, likely due to steric hindrance. Functional NPA surfaces were able to provide more interaction area with cells to enhance cell capture. Gains in *E. coli* capture on flat and nanopillar surfaces were quantified, and compared to standard carbodiimide (EDC-NHS) coupling (LOD: 1.6×10^4 CFU/mL), a one order of magnitude improvement in detection sensitivity was achieved by introducing the functional polymer to flat surfaces (LOD: 1.7×10^3 CFU/mL), while a two order of magnitude improvement in detection sensitivity was measured for the nanopillar surface (LOD: 2.1×10^2 CFU/mL). The range of detection sensitivities achieved for our flat and NPA surfaces offer potential use in a variety of applications including diagnosis of UTI, blood infections, and detection of bacterial pathogens in water - applications where lectin-based capture has traditionally been limited. Finally, our experiments indicate that lectin surface density, modulated by the underlying polymer chain density, allows for one to efficiently tune the strength of the binding interaction, and that this parameter had a greater impact than extracellular glycosylation levels on bacterial cell capture.

Taken together, this work emphasizes the critical role of the synthetic interface design for efficient isolation of bacteria from solutions.

5.6 Acknowledgements

This research was supported by Kansas State University. A portion of this research was conducted at the Center for Nanophase Materials Sciences, which is sponsored at Oak Ridge National Laboratory by the Scientific User Facilities Division, Office of Basic Energy Sciences and U.S. Department of Energy. We thank Dr. Clay Fuqua (Department of Biology, Indiana University, Bloomington) for providing bacteria strains. We also would like to express our appreciation to Dr. André J. van der Vlies for his valuable and constructive comments during the planning and development of the presented work and Dr. Prem Thapa (Microscopy and Analytical Imaging, Laboratory at University of Kansas) for assistance with SEM imaging.

5.7 References

(1) Shen, Z.; Huang, M.; Xiao, C.; Zhang, Y.; Zeng, X.; Wang, P. G. Nonlabeled Quartz Crystal Microbalance Biosensor for Bacterial Detection using Carbohydrate and Lectin Recognitions. *Anal. Chem.* **2007**, *79*, 2312-2319.

(2) Dechtrirat, D.; Gajovic-Eichelmann, N.; Wojcik, F.; Hartmann, L.; Bier, F. F.; Scheller, F. W. Electrochemical Displacement Sensor Based on Ferrocene Boronic Acid Tracer and Immobilized Glycan for Saccharide Binding Proteins and E. Coli. *Biosensors and Bioelectronics* **2014**, *58*, 1-8.

(3) Wang, Y.; Ye, Z.; Si, C.; Ying, Y. Monitoring of Escherichia Coli O157: H7 in Food Samples using Lectin Based Surface Plasmon Resonance Biosensor. *Food Chem.* **2013**, *136*, 1303-1308.

(4) Zheng, L.; Wan, Y.; Qi, P.; Sun, Y.; Zhang, D.; Yu, L. Lectin Functionalized ZnO Nanoarrays as a 3D Nano-Biointerface for Bacterial Detection. *Talanta* **2017**, *167*, 600-606.

(5) Serra, B.; Gamella, M.; Reviejo, A.; Pingarron, J. Lectin-Modified Piezoelectric Biosensors for Bacteria Recognition and Quantification. *Analytical and bioanalytical chemistry* **2008**, *391*, 1853-1860.

(6) Poonlapdecha, W.; Seetang-Nun, Y.; Wonglumsom, W.; Tuitemwong, K.; Erickson, L. E.; Hansen, R. R.; Tuitemwong, P. Antibody-Conjugated Ferromagnetic Nanoparticles with Lateral Flow Test Strip Assay for Rapid Detection of Campylobacter Jejuni in Poultry Samples. *Int. J. Food Microbiol.* **2018**, *286*, 6-14.

(7) Thepwiwatjit, N.; Thattiyaphong, A.; Limsuwan, P.; Tuitemwong, K.; Tuitemwong, P. jovejjRubpy Dye-Doped Silica Nanoparticles as Signal Reporter in a Dot Fluorescence Immunoassay Strip. *Journal of Nanomaterials* **2014**, *2014*, 23.

(8) Tansub, W.; Tuitemwong, K.; Limsuwan, P.; Theparoonrat, S.; Tuitemwong, P. Synthesis of Antibodies-Conjugated Fluorescent Dye-Doped Silica Nanoparticles for a Rapid Single Step Detection of Campylobacter Jejuni in Live Poultry. *Journal of Nanomaterials* **2012**, *2012*, 60.

(9) Gamella, M.; Campuzano, S.; Parrado, C.; Reviejo, A.; Pingarrón, J. Microorganisms Recognition and Quantification by Lectin Adsorptive Affinity Impedance. *Talanta* **2009**, *78*, 1303-1309.

(10) Huang, C.; Chen, C.; Shiang, Y.; Lin, Z.; Chang, H. Synthesis of Fluorescent Carbohydrate-Protected Au Nanodots for Detection of Concanavalin A and Escherichia Coli. *Anal. Chem.* **2009**, *81*, 875-882.

(11) Sharon, N. Lectins: Carbohydrate-Specific Reagents and Biological Recognition Molecules. *J. Biol. Chem.* **2007**, *282*, 2753-2764.

(12) Vickers, D. A.; Kulik, M.; Hincapie, M.; Hancock, W. S.; Dalton, S.; Murthy, S. K. Lectin-Functionalized Microchannels for Characterizing Pluripotent Cells and Early Differentiation. *Biomicrofluidics* **2012**, *6*, 024122.

(13) Vickers, D. A.; Hincapie, M.; Hancock, W. S.; Murthy, S. K. Lectin-Mediated Microfluidic Capture and Release of Leukemic Lymphocytes from Whole Blood. *Biomed. Microdevices* **2011**, *13*, 565-571.

(14) Campuzano, S.; Orozco, J.; Kagan, D.; Guix, M.; Gao, W.; Sattayasamitsathit, S.; Claussen, J. C.; Merkoçi, A.; Wang, J. Bacterial Isolation by Lectin-Modified Microengines. *Nano letters* **2011**, *12*, 396-401.

(15) Kang, J. H.; Super, M.; Yung, C. W.; Cooper, R. M.; Domansky, K.; Graveline, A. R.; Mammoto, T.; Berthet, J. B.; Tobin, H.; Cartwright, M. J. An Extracorporeal Blood-Cleansing Device for Sepsis Therapy. *Nat. Med.* **2014**, *20*, 1211.

(16) Bewley, C. A.; Shahzad-ul-Hussan, S. Characterizing Carbohydrate–protein Interactions by Nuclear Magnetic Resonance Spectroscopy. *Biopolymers* **2013**, *99*, 796-806.

(17) Liang, P.; Wang, S.; Wong, C. Quantitative Analysis of Carbohydrate− Protein Interactions using Glycan Microarrays: Determination of Surface and Solution Dissociation Constants. *J. Am. Chem. Soc.* **2007**, *129*, 11177-11184.

(18) Klukova, L.; Bertok, T.; Kasak, P.; Tkac, J. Nanoscale-Controlled Architecture for the Development of Ultrasensitive Lectin Biosensors Applicable in Glycomics. *Analytical Methods* **2014**, *6*, 4922-4931.

(19) Templier, V.; Roux, A.; Roupioz, Y.; Livache, T. Ligands for Label-Free Detection of Whole Bacteria on Biosensors: A Review. *TrAC Trends in Analytical Chemistry* **2016**, *79*, 71-79.

(20) Belicky, S.; Katrlik, J.; Tkac, J. Glycan and Lectin Biosensors. *Essays Biochem.* **2016**, *60*, 37-47.

(21) Zayas-Gonzalez, Y. M.; Lynn, D. M. Degradable Amine-Reactive Coatings Fabricated by the Covalent Layer-by-Layer Assembly of Poly (2-Vinyl-4, 4-Dimethylazlactone) with Degradable Polyamine Building Blocks. *Biomacromolecules* **2016**, *17*, 3067-3075.

(22) Buck, M. E.; Lynn, D. M. Layer-by-Layer Fabrication of Covalently Crosslinked and Reactive Polymer Multilayers using Azlactone-Functionalized Copolymers: A Platform for the Design of Functional Biointerfaces. *Advanced Engineering Materials* **2011**, *13*.

(23) Zayas-Gonzalez, Y. M.; Ortiz, B. J.; Lynn, D. M. Layer-by-Layer Assembly of Amine-Reactive Multilayers using an Azlactone-Functionalized Polymer and Small-Molecule Diamine Linkers. *Biomacromolecules* **2017**, *18*, 1499-1508.

(24) Schmitt, S. K.; Trebatoski, D. J.; Krutty, J. D.; Xie, A. W.; Rollins, B.; Murphy, W. L.; Gopalan, P. Peptide Conjugation to a Polymer Coating Via Native Chemical Ligation of Azlactones for Cell Culture. *Biomacromolecules* **2016**, *17*, 1040-1047.

(25) Cullen, S. P.; Mandel, I. C.; Gopalan, P. Surface-Anchored Poly (2-Vinyl-4, 4-Dimethyl Azlactone) Brushes as Templates for Enzyme Immobilization. *Langmuir* **2008**, *24*, 13701-13709.

(26) Kratochvil, M. J.; Carter, M. C.; Lynn, D. M. Amine-Reactive Azlactone-Containing Nanofibers for the Immobilization and Patterning of New Functionality on Nanofiber-Based Scaffolds. *ACS Applied Materials & Interfaces* **2017**, *9*, 10243-10253.

(27) Broderick, A. H.; Carter, M. C.; Lockett, M. R.; Smith, L. M.; Lynn, D. M. Fabrication of Oligonucleotide and Protein Arrays on Rigid and Flexible Substrates Coated with Reactive Polymer Multilayers. *ACS applied materials & interfaces* **2012**, *5*, 351-359.

(28) Neri, G.; Scala, A.; Barreca, F.; Fazio, E.; Mineo, P.; Mazzaglia, A.; Grassi, G.; Piperno, A. Engineering of Carbon Based Nanomaterials by Ring-Opening Reactions of a Reactive Azlactone Graphene Platform. *Chemical Communications* **2015**, *51*, 4846-4849.

(29) Hansen, R. R.; Hinestrosa, J. P.; Shubert, K. R.; Morrell-Falvey, J. L.; Pelletier, D. A.; Messman, J. M.; Kilbey, S. M.; Lokitz, B. S.; Retterer, S. T. Lectin-Functionalized Poly (Glycidyl Methacrylate)-Block-Poly (Vinyldimethyl Azlactone) Surface Scaffolds for High Avidity Microbial Capture. *Biomacromolecules* **2013**, *14*, 3742-3748.

(30) Hansen, R. R.; Shubert, K. R.; Morrell-Falvey, J. L.; Lokitz, B. S.; Doktycz, M. J.; Retterer, S. T. Microstructured Block Copolymer Surfaces for Control of Microbe Adhesion and Aggregation. *Biosensors* **2014**, *4*, 63-75.

(31) Schmitt, S. K.; Xie, A. W.; Ghassemi, R. M.; Trebatoski, D. J.; Murphy, W. L.; Gopalan, P. Polyethylene Glycol Coatings on Plastic Substrates for Chemically Defined Stem Cell Culture. *Advanced healthcare materials* **2015**, *4*, 1555-1564.

(32) Valle, J.; Burgui, S.; Langheinrich, D.; Gil, C.; Solano, C.; Toledo-Arana, A.; Helbig, R.; Lasagni, A.; Lasa, I. Evaluation of Surface Microtopography Engineered by Direct Laser Interference for Bacterial Anti-Biofouling. *Macromolecular bioscience* **2015**, *15*, 1060-1069.

(33) Friedlander, R. S.; Vlamakis, H.; Kim, P.; Khan, M.; Kolter, R.; Aizenberg, J. Bacterial Flagella Explore Microscale Hummocks and Hollows to Increase Adhesion. *Proc. Natl. Acad. Sci. U. S. A.* **2013**, *110*, 5624-5629.

(34) Agapov, R. L.; Boreyko, J. B.; Briggs, D. P.; Srijanto, B. R.; Retterer, S. T.; Collier, C. P.; Lavrik, N. V. Asymmetric Wettability of Nanostructures Directs Leidenfrost Droplets. *Acs Nano* **2013**, *8*, 860-867.

(35) Donlan, R. M. Biofilms: Microbial Life on Surfaces. *Emerg. Infect. Dis.* **2002**, *8*, 881-890.

(36) Tomlinson, A. D.; Fuqua, C. Mechanisms and Regulation of Polar Surface Attachment in Agrobacterium Tumefaciens. *Curr. Opin. Microbiol.* **2009**, *12*, 708-714.

(37) Xu, J.; Kim, J.; Koestler, B. J.; Choi, J.; Waters, C. M.; Fuqua, C. Genetic Analysis of A Grobacterium Tumefaciens Unipolar Polysaccharide Production Reveals Complex Integrated Control of the Motile-to-sessile Switch. *Mol. Microbiol.* **2013**, *89*, 929-948.

(38) Xu, J.; Kim, J.; Danhorn, T.; Merritt, P. M.; Fuqua, C. Phosphorus Limitation Increases Attachment in Agrobacterium Tumefaciens and Reveals a Conditional Functional Redundancy in Adhesin Biosynthesis. *Res. Microbiol.* **2012**, *163*, 674-684.

(39) Gueffroy, D. E. Guide for the Preparation and use of Buffers in Biological Systems. **1975**.

(40) Zhuang, M.; Wang, C.; Xu, M.; Ling, X.; Shen, J.; Zhang, Y. Using ConcanavalinA as a Spacer for Immobilization of E. Coli Onto Magnetic Nanoparticles. *Int. J. Biol. Macromol.* **2017**.

(41) Lokitz, B. S.; Wei, J.; Hinestrosa, J. P.; Ivanov, I.; Browning, J. F.; Ankner, J. F.; Kilbey, S. M.; Messman, J. M. Manipulating Interfaces through Surface Confinement of Poly (Glycidyl Methacrylate)-Block-Poly (Vinyldimethylazlactone), a Dually Reactive Block Copolymer. *Macromolecules* **2012**, *45*, 6438-6449.

(42) Aden, B.; Kite, C. M.; Hopkins, B. W.; Zetterberg, A.; Lokitz, B. S.; Ankner, J. F.; Kilbey, S. M. Assessing Chemical Transformation of Reactive, Interfacial Thin Films made of End-Tethered Poly (2-Vinyl-4, 4-Dimethyl Azlactone)(PVDMA) Chains. *Macromolecules* **2017**, *50*, 618-630.

(43) Steglich, M.; Käsebier, T.; Zilk, M.; Pertsch, T.; Kley, E.; Tünnermann, A. The Structural and Optical Properties of Black Silicon by Inductively Coupled Plasma Reactive Ion Etching. *J. Appl. Phys.* **2014**, *116*, 173503.

(44) Tempe, J.; Petit, A.; Holsters, M.; Montagu, M.; Schell, J. Thermosensitive Step Associated with Transfer of the Ti Plasmid during Conjugation: Possible Relation to Transformation in Crown Gall. *Proc. Natl. Acad. Sci. U. S. A.* **1977**, *74*, 2848-2849.

(45) Morton, E. R.; Platt, T. G.; Fuqua, C.; Bever, J. D. Non-Additive Costs and Interactions Alter the Competitive Dynamics of Co-Occurring Ecologically Distinct Plasmids. *Proc. Biol. Sci.* **2014**, *281*, 20132173.

(46) Kim, J. Chemical Modifications of Amino-Terminated Organic Films on Silicon Substrates and Controlled Protein Immobilization by FT-IR and Ellipsometry. *Spectroscopy-Eugene* **2012**, *25*, 26.

(47) Patel, N.; Davies, M. C.; Hartshorne, M.; Heaton, R. J.; Roberts, C. J.; Tendler, S. J.; Williams, P. M. Immobilization of Protein Molecules Onto Homogeneous and Mixed Carboxylate-Terminated Self-Assembled Monolayers. *Langmuir* **1997**, *13*, 6485-6490.

(48) Rengaraj, S.; Cruz-Izquierdo, Á; Scott, J. L.; Di Lorenzo, M. Impedimetric Paper-Based Biosensor for the Detection of Bacterial Contamination in Water. *Sensors Actuators B: Chem.* **2018**, *265*, 50-58.

(49) Shrivastava, A.; Gupta, V. B. Methods for the Determination of Limit of Detection and Limit of Quantitation of the Analytical Methods. *Chronicles of Young Scientists* **2011**, *2*, 21.

(50) Asadpour-Zeynali, K.; Mollarasouli, F. Novel Electrochemical Biosensor Based on PVP Capped CoFe2O4@ CdSe Core-Shell Nanoparticles Modified Electrode for Ultra-Trace Level Determination of Rifampicin by Square Wave Adsorptive Stripping Voltammetry. *Biosensors and Bioelectronics* **2017**, *92*, 509-516.

(51) Probes, M. LIVE/DEAD BacLight Bacterial Viability Kit (L7012), Instruction Manual with Appendix. Molecular Probes. *Inc., Eugene, Oreg* **1994**.

(52) Ivanova, E. P.; Hasan, J.; Webb, H. K.; Gervinskas, G.; Juodkazis, S.; Truong, V. K.; Wu, A. H.; Lamb, R. N.; Baulin, V. A.; Watson, G. S. Bactericidal Activity of Black Silicon. *Nature communications* **2013**, *4*, 2838.

(53) Park, H. M. Comparing Group Means: T-Tests and One-Way ANOVA using Stata, SAS, R, and SPSS. **2009**.

(54) Traunspurger, W.; Bergtold, M.; Goedkoop, W. The Effects of Nematodes on Bacterial Activity and Abundance in a Freshwater Sediment. *Oecologia* **1997**, *112*, 118-122.

(55) Masigol, M.; Barua, N.; Retterer, S. T.; Lokitz, B. S.; Hansen, R. R. Chemical Copatterning Strategies using Azlactone-Based Block Copolymers. *Journal of Vacuum Science & Technology B, Nanotechnology and Microelectronics: Materials, Processing, Measurement, and Phenomena* **2017**, *35*, 06GJ01.

(56) Masigol, M.; Barua, N.; Lokitz, B. S.; Hansen, R. R. Fabricating Reactive Surfaces with Brush-Like and Crosslinked Films of Azlactone-Functionalized Block Co-Polymers. *JoVE (Journal of Visualized Experiments)* **2018**, e57562.

(57) Carter, M. C.; Lynn, D. M. Covalently Crosslinked and Physically Stable Polymer Coatings with Chemically Labile and Dynamic Surface Features Fabricated by Treatment of Azlactone-Containing Multilayers with Alcohol-, Thiol-, and Hydrazine-Based Nucleophiles. *Chemistry of Materials* **2016**, *28*, 5063-5072.

(58) Catrouillet, S.; Fonteneau, C.; Bouteiller, L.; Delorme, N.; Nicol, E.; Nicolai, T.; Pensec, S.; Colombani, O. Competition between Steric Hindrance and Hydrogen Bonding in the Formation of Supramolecular Bottle Brush Polymers. *Macromolecules* **2013**, *46*, 7911-7919.

(59) Han, Y.; Cui, J.; Jin, J.; Jiang, W. Hydrogen Bonding Induced Protein Adsorption on Polymer Brushes: A Monte Carlo Study. *Journal of Materials Chemistry B* **2017**, *5*, 8479-8486.

(60) Ruckenstein, E.; Li, B. Steric Interactions between Two Grafted Polymer Brushes. *J. Chem. Phys.* **1997**, *107*, 932-942.

(61) Aden, B.; Street, D. P.; Hopkins, B. W.; Lokitz, B. S.; Kilbey, S. M. Tailoring Surface Properties through in Situ Functionality Gradients in Reactively Modified Poly (2-Vinyl-4, 4-Dimethyl Azlactone) Thin Films. *Langmuir* **2018**, *34*, 5204-5213.

(62) Li, Z.; Fu, Y.; Fang, W.; Li, Y. Electrochemical Impedance Immunosensor Based on Self-Assembled Monolayers for Rapid Detection of Escherichia Coli o157: H7 with Signal Amplification using Lectin. *Sensors* **2015**, *15*, 19212-19224.

(63) Mikaelyan, M. V.; Poghosyan, G. G.; Hendrickson, O. D.; Dzantiev, B. B.; Gasparyan, V. K. Wheat Germ Agglutinin and Lens Culinaris Agglutinin Sensitized Anisotropic Silver Nanoparticles in Detection of Bacteria: A Simple Photometric Assay. *Anal. Chim. Acta* **2017**.

(64) Kirkeby, S.; Friis, M.; Mikkelsen, H.; Cayé-Thomasen, P. Bacterial Adherence in Otitis Media: Determination of N-Acetylgalactosamine (GalNAc) Residues in the Submucosal Glands and Surface Epithelium of the Normal and Diseased Eustachian Tube. *Microb. Pathog.* **2011**, *51*, 48-57.

(65) Ajish, J. K.; Kumar, K. A.; Ruhela, A.; Subramanian, M.; Ballal, A. D.; Kumar, M. AIE Based Fluorescent Self Assembled Glycoacrylamides for E. Coli Detection and Cell Imaging. *Sensors Actuators B: Chem.* **2018**, *255*, 1726-1734.

(66) Skoog, B.; Wichman, A. Calculation of the Isoelectric Points of Polypeptides from the Amino Acid Composition. *Trac-Trends in Analytical Chemistry* **1986**, *5*, 82-83.

(67) Hu, S.; Wong, D. T. Lectin Microarray. *PROTEOMICS–Clinical Applications* **2009**, *3*, 148-154.

(68) Mandenius, C.; Wang, R.; Aldén, A.; Bergström, G.; Thébault, S.; Lutsch, C.; Ohlson, S. Monitoring of Influenza Virus Hemagglutinin in Process Samples using Weak Affinity Ligands and Surface Plasmon Resonance. *Anal. Chim. Acta* **2008**, *623*, 66-75.

(69) Hsu, K.; Mahal, L. K. A Lectin Microarray Approach for the Rapid Analysis of Bacterial Glycans. *Nature protocols* **2006**, *1*, 543.

(70) Jalali, M.; AbdelFatah, T.; Mahshid, S. S.; Labib, M.; Sudalaiyadum Perumal, A.; Mahshid, S. A Hierarchical 3D Nanostructured Microfluidic Device for Sensitive Detection of Pathogenic Bacteria. *Small* **2018**, *14*, 1801893.

(71) Wang, S.; Wang, H.; Jiao, J.; Chen, K.; Owens, G. E.; Kamei, K.; Sun, J.; Sherman, D. J.; Behrenbruch, C. P.; Wu, H. Three-Dimensional Nanostructured Substrates Toward Efficient Capture of Circulating Tumor Cells. *Angewandte Chemie* **2009**, *121*, 9132-9135.

(72) Chen, W.; Weng, S.; Zhang, F.; Allen, S.; Li, X.; Bao, L.; Lam, R. H.; Macoska, J. A.; Merajver, S. D.; Fu, J. Nanoroughened Surfaces for Efficient Capture of Circulating Tumor Cells without using Capture Antibodies. *ACS nano* **2012**, *7*, 566-575.

(73) Toze, S. PCR and the Detection of Microbial Pathogens in Water and Wastewater. *Water Res.* **1999**, *33*, 3545-3556.

(74) Francy, D. S.; Stelzer, E. A.; Bushon, R. N.; Brady, A. M.; Mailot, B. E.; Spencer, S. K.; Borchardt, M. A.; Elber, A. G.; Riddell, K. R.; Gellner, T. M. Quantifying Viruses and Bacteria in Wastewater—results, Interpretation Methods, and Quality Control. *US Geological Survey scientific investigations report* **2011**, *5150*.

(75) Groen, J.; Pannek, J.; Diaz, D. C.; Del Popolo, G.; Gross, T.; Hamid, R.; Karsenty, G.; Kessler, T. M.; Schneider, M.; Blok, B. Summary of European Association of Urology (EAU) Guidelines on Neuro-Urology. *Eur. Urol.* **2016**, *69*, 324-333.

(76) Puttaswamy, S.; Lee, B. D.; Sengupta, S. Novel Electrical Method for Early Detection of Viable Bacteria in Blood Cultures. *J. Clin. Microbiol.* **2011**, *49*, 2286-2289.

(77) Yagupsky, P.; Nolte, F. S. Quantitative Aspects of Septicemia. *Clin. Microbiol. Rev.* **1990**, *3*, 269-279.

(78) Lin, N.; Berton, P.; Moraes, C.; Rogers, R. D.; Tufenkji, N. Nanodarts, Nanoblades, and Nanospikes: Mechano-Bactericidal Nanostructures and Where to Find Them. *Adv. Colloid Interface Sci.* **2018**, *252*, 55-68.

(79) Thompson, M. A.; Onyeziri, M. C.; Fuqua, C. Function and Regulation of Agrobacterium Tumefaciens Cell Surface Structures that Promote Attachment. **2018**.

(80) Li, G.; Brown, P. J.; Tang, J. X.; Xu, J.; Quardokus, E. M.; Fuqua, C.; Brun, Y. V. Surface Contact Stimulates the Just-in-time Deployment of Bacterial Adhesins. *Mol. Microbiol.* **2012**, *83*, 41-51.

(81) Tsang, P. H.; Li, G.; Brun, Y. V.; Freund, L. B.; Tang, J. X. Adhesion of Single Bacterial Cells in the Micronewton Range. *Proc. Natl. Acad. Sci. U. S. A.* **2006**, *103*, 5764-5768.

(82) Merritt, P. M.; Danhorn, T.; Fuqua, C. Motility and Chemotaxis in Agrobacterium Tumefaciens Surface Attachment and Biofilm Formation. *J. Bacteriol.* **2007**, *189*, 8005-8014.

(83) Liu, X.; Lei, Z.; Liu, F.; Liu, D.; Wang, Z. Fabricating Three-Dimensional Carbohydrate Hydrogel Microarray for Lectin-Mediated Bacterium Capturing. *Biosensors and Bioelectronics* **2014**, *58*, 92-100.

Chapter 6 - Polymer Surface Dissection for Investigation of the Early Stage Biofilm Formation on AnMBR Membranes*

6.1 Overview

Anerobic membrane bioreactors (AnMBRs) are an energy-efficient and high-performance technology used to treat wastewater and to produce particle-free effluent by combining membrane separation and biological treatment techniques[1]. The critical drawback associated with AnMBRs is formation of biofilms on the membrane surfaces, resulting in dramatic decrease in performance efficiencies characterized by high transmembrane pressure (TMP) and lower net flux of treated water. The goal of this work is to develop a method that can be used to isolate members of wastewater communities that attach to membranes early in AnMBR systems. The technique developed, termed polymer surface dissection (PSD), uses a photodegradable PEG-based hydrogel functionalized with affinity ligands for detachment of microbes from membrane surface. The approach is designed to be non-destructive to both cells and the membrane support. Subsequent exposure of targeted cells within the hydrogel using patterned UV light allows for release into solution and isolation. The method is demonstrated for isolation of small aggregates from PVDF membranes based on floc size and will allow for follow-up molecular characterization of principal organisms by 16S rRNA sequencing, PCR, and EPS/SMP analysis. This knowledge will enable the identification of wastewater sub-communities that adhere to the membrane early in the biofouling process.

---

* Manuscript: Polymer Surface Dissection for Investigation of Early Stage Biofilm Formation on Membrane Surfaces, *In preparation*.

6.2 Introduction

Anaerobic processes are applied to treat a broad range of industrial, pharmaceutical, and agricultural wastewaters[2]. Anaerobic membrane bioreactors (AnMBRs), with the capability of producing high-quality water can successfully provide an energy-efficient approach to wastewater treatment, as there is no need of aerobic conditions for sustainable water treatment and reuse[3,4]. In addition to reducing biological and chemical oxygen demand (BOD, COD), AnMBRs are also able to produce and capture methane biogas, which highlights their role as an alternative source of supplemental energy[5,6]. One operational challenge in AnMBR technology is formation of biofilms on the membrane substrates. Fouling causes a significant drop in membrane and bioreactor performance and usually requires expensive, labor intensive, and time-consuming physicochemical cleaning protocols as well as operational shutdown periods[7,8]. Biofouling also results in decreased membrane lifespan, increases in replacement costs, as well as energy required to recirculate sludges[9], and accounts for ~50% of the total energy consumption in typical AnMBR systems[10]. Membrane biofouling processes are caused by attachment of bacteria from wastewater communities, initiating the formation and development of biofilms on the surface. Biofouling is defined by formation of complex, multi-species communities such as bacteria and microorganisms and their associated organics such as extracellular polymeric substances (EPS), including bound EPS and soluble EPS also known as soluble microbial products (SMP)[11,12]. This accounts for more than 60% of total fouling, the other contributions are from inorganic scaling[13]. Considering the research reports focused on the central mechanisms involved in AnMBR biofouling, there is scare experimental data and a lack of understanding in the fundamental mechanisms that drive biofilm formation over these membrane surfaces[7,14]. For instance, while Jeison et al.,[15] proposed the formation and consolidation of cake layers as the major parameter governing biofouling in

anaerobic submerged membrane bioreactors (AnSMBR), Hwang et al.,[16] highlighted the spatiotemporal changes of foulant composition (EPS and SMP) in the bio-cake as the main factor promoting biofouling on the membrane surfaces in MBRs. The role of EPS and SMP to expedite accumulation of organic/inorganic materials, cake compression, and interception of active pores are other factors involved[17]. Achieving knowledge on dominant fouling mechanisms in AnMBR systems may facilitate the design of effective control and mitigation strategies. Although membrane autopsies are able to characterize some biofouling phenomena and determine the identity of foulants, this is a bulk measurement and end-point information only, it does not provide any mechanistic insight or reveal the major players that initiate the biofouling[18]. Besides, autopsies generally are conducted after membrane failure or at the end of AnMBR process[19,20].

The central goal of this research is to develop a method that will enable one to examine the early-stage colonizers and mechanisms that initiate membrane biofouling on membrane materials used in AnMBR systems. The polymer surface dissection (PSD) approach is developed with the capability of detaching then isolating specified cells or biofilm aggregates adhered to AnMBR membranes (Figure 6.1). The critical advantages of PSD technique are (1) cells can be removed from surfaces at micron-scale resolution (2) flocs can be isolated based on their size, and (3) cells/floc detachment and isolation occurs without damaging cells or underlying membrane supports. This enables isolation of important organisms for their characterization which may include DNA sequencing and other molecular characterization methods to analyze the spatiotemporal aspects of EPS/SMP in the community and to gain information on microorganism identification.

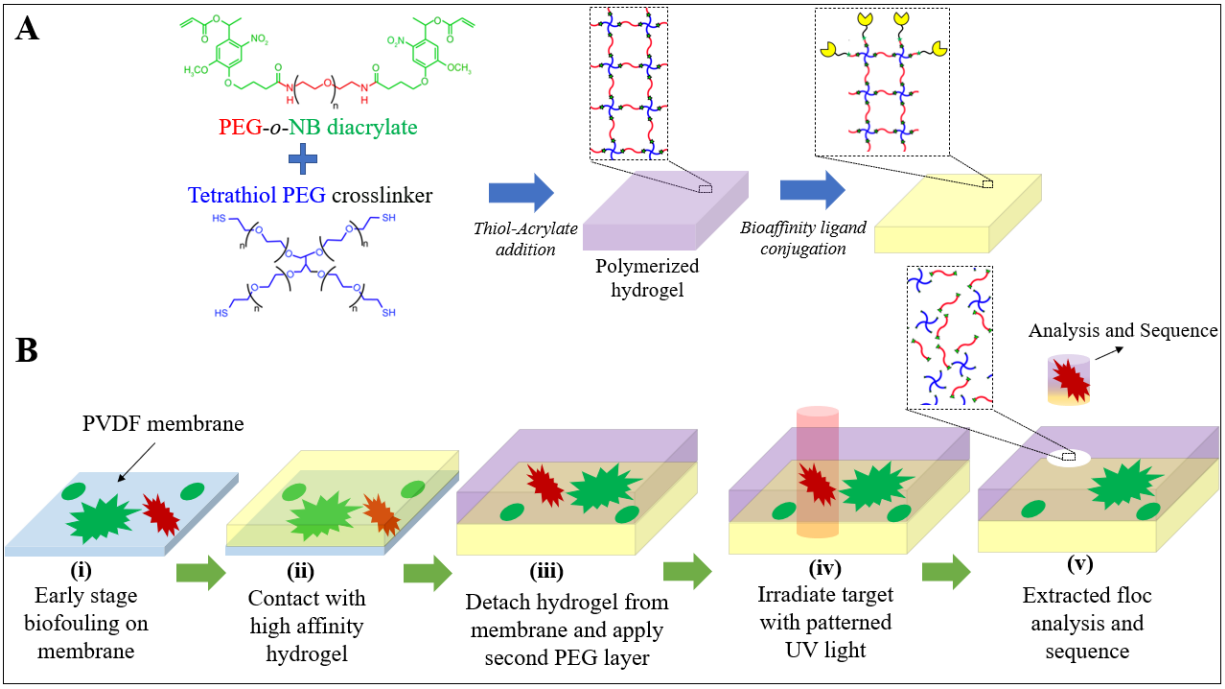

Figure 6.1 (A) Hydrogel preparation and bioaffinity ligand conjugation. (B) Schematic of the PSD method. (i) PVDF Membranes are contacted with wastewater solutions and cell attachment to the surface is characterized using an optical microscope. (ii) The substrate is then contacted with a pre-formed polymer gel loaded with bacteria affinity ligands for flocs transfer (iii) The hydrogel is removed from the membrane surfaces and a second pre-formed hydrogel is placed on the first hydrogel to trap not-desired flocs and ensure clean extraction. (iv) Cells of interest are sectioned from the base hydrogel using patterned UV light. (v) The sectioned cell(s) are lifted off the base hydrogel for molecular analysis.

6.3 Experimental Section

6.3.1 Materials

3-aminopropyl triethoxysilane (APTES), N-(3-dimethylaminopropyl)-N′-ethylcarbodiimide (EDC), N-hydroxysuccinimide (NHS), and glutaraldehyde solution (25 wt % in water) were purchased from Sigma-Aldrich. Triticum vulgare lectin (wheat germ agglutinin, WGA) and poly-L-lysine were purchased from Sigma-Aldrich and diluted to specific concentrations in buffer and stored at −20 °C. WGA−Alexa Fluor 488 conjugate was purchased from Fisher Scientific, diluted to the desired concentration in 1× phosphate-buffered saline (PBS),

and stored at −20 °C. 1× PBS buffer (pH 7.4). *E. coli* JM 109 was stored in 25% glycerol stocks at −80 °C. A LIVE/ DEAD BacLight Bacterial Viability Kit was purchased from ThermoFisher Scientific and stored at −20 °C until use. PVDF membranes were purchased from Novavem. PEG-diacrylate (PEGDA, MW 3400) was purchased from Laysan Bio.

6.3.2 Thiol SAM formation

Coverslips were treated with oxygen plasma and further hydroxylated by using Piranha solution, a 30:70 (v/v) mixture of H_2O_2 and H_2SO_4 at 60-80 ºC for 30 min. *(Cation! strongly corrosive*) Thiol groups were functionalized on the surfaces by immersing coverslips into 269 mM of (3-Mercaptopropyl) trimethoxysilane (MPTS) solution in toluene (5% v/v) for 4 hrs following by washing substrates with solution of ethanol/toluene. Coverslips were then stored in ethanol at 4 ºC.

6.3.3 Flocs Transfer from Membrane to Hydrogel

Wastewater solutions (Manhattan Wastewater Treatment Plant, KS) were washed and resuspended in 1× PBS solution. Solutions were kept on the bench for 10 min for complete sludge participation. 3 mL of solution from top of the container were harvested. 12 µg/mL solutions of FM-1-43 lipid dye (1 mg/mL) was added to the solution to label the flocs while shaking at 200 rpm for 30 min at 25 ºC. 0.8 × 0.8 cm^2 Novamem membrane filters (PVDF20, 0.02 Micron) were incubated by 3 mL stained wastewater solution in a scintillation vial. Scintillation vials were placed in a shaker for 3-24 hrs at 25 ºC. A fluorescent microscope (Eclipse Ti-E, Nikon) was used to take fluorescent images of the membrane surfaces to determine floc size distribution. Membranes were then placed in contact with the hydrogels for 30 min following by gentle detachment.

6.3.4 Hydrogel Preparation

Hydrogels were prepared by a Michael-type addition reaction of photodegradable PEGDA, and PEG-tetrathiol. 5.6 µl solution of photodegradable PEGDA (49 mM) were added to 12 µl of phosphate buffer (pH 8.0). 6.9 µl solution of PEG-tetrathiol (20 mM) then was added to the mixture and thoroughly mixed to prepare the precursor solution. 7 µL of the precursor solution was then pipetted on a perfluoroalkylated glass slides. The thiol functionalized surface will allow for thiol-acrylate coupling to the surface ensuring stable, covalent attachment of hydrogel with the thiolated glass surface. Two tapes (40.0 µm thickness) were placed on the edges of two sides of the thiolated coverslip. Then, perfluoroalkylated glass slides with 7 µL precursor solution were placed upside down on the thiolated coverslip. The reaction time was 22 min. After gelation completed, the top glass slide was peeled off gently to prevent the hydrogel from rupturing.

6.3.5 Hydrogel Functionalization with Bioaffinity Ligands

WGA and poly-l-lysine were functionalized on the hydrogel surfaces to study the effect of affinity molecules on ability of hydrogel to detach cells form the membrane surfaces and cell viability after transfer. Pre-formed hydrogels were incubated with 300 µL solution of Maleimide-PEG-NHS ester in PBS buffer (1.0 mg/mL, pH 6.7) for 2 hrs, following by washing with the same buffer for 5 min. NHS-functionalized hydrogels were then immobilized with 300 µL solutions of WGA in 1XPBS and poly-l-lysine in 1X PBS (0.1 mg/mL, pH 7.4) for another 2 hr. Hydrogel surface finally were washed with 1XPBS for 3 min to remove physiosorbed molecules.

6.3.6 Use of Second Hydrogel for Clean Extraction and Hydrogel Degradation

Membranes were placed in contact with the hydrogels for 30 min following by gentle detachment to prevent the membrane and the hydrogel form rupturing. A 10 g weight was used to apply uniform pressure for conformal contact between membrane and hydrogels. Hydrogels detached from the membranes were analyzed and the sizes of transferred flocs were measured with a BX51 upright microscope and ImageJ software. Some experiments were included placing a second hydrogel layer on the detached hydrogel to trap all not-desired cells and provide a clean extraction protocol. For this, after hydrogel detachment form membrane, a precursor solution was pipetted on a perfluoroalkylated glass slide, then perfluoroalkylated glass slide with precursor solution were placed upside down on the detached hydrogel. The reaction time was 22 min. After gelation of second hydrogel, the top glass slide was peeled off gently to prevent the hydrogels from rupturing. Flocs with specific dimensions were exposed to patterned UV light (365 nm) using the Polygon400 patterning device configured to the upright microscope. The illumination tool can expose light at micron-scale resolution to selected areas on surfaces and enable spatiotemporal control over degradation of the hydrogel with tuning light wavelength, intensity, and irradiation time. Degraded parts of the hydrogel consisting targeted flocs then extracted and stored at -80^{o}C for follow-up sequencing analysis.

6.3.7 Live-Dead Assay

A live/dead assay was used to measure *E.coli* viability after transfer from membrane to the hydrogels following the procedure described in the LIVE/DEAD BacLight Bacterial Viability Kit, L7012[21]. The details have been explained in Section 5.3.8 of this thesis.

6.4 Results and Discussion

6.4.1 Hydrogel Characterization

The first goal of hydrogel characterization studies was to measure cell viability after capture on the hydrogel surfaces. This could reveal information on how different hydrogel chemistries affect the cells after attachment. Here, hydrogels were functionalized with poly-$_L$-lysine and WGA affinity ligands for non-specific binding to bacteria[22] using the coupling procedure described in section 6.3.5. 1 mL of *E. coli* JM 109 solutions (10^6 CFU/mL) were incubated on the hydrogels for 1 hr followed by washing the hydrogels with buffer for 3 min. Fluorescent microscopy and live/dead assay were then used to evaluate the percentage of live cells attached to the hydrogels. Figure 6.2 displays fluorescent images of *E. coli* on the hydrogel and corresponding cell viability data after capture. Live-dead assay revealed that 82 ± 8.1% and 84 ± 9.4% of the attached *E. coli* cells remained alive after contact on the hydrogels (control) and WGA-functionalized hydrogels, respectively. Viability decreased upon contact with the poly lysine-functionalized hydrogels; 69 ± 9.4% of cells were live (Figure 6.2 B), consistent with the fact that poly-$_L$-lysine has known antibacterial properties[23]. Statistical analysis demonstrated no significant change in cell viability after functionalization of hydrogels (P-value > 0.05 for both WGA and poly-$_L$-lysine). These findings confirmed that the hydrogel chemistry is not significantly destructive to cells and majority of them were alive after contact.

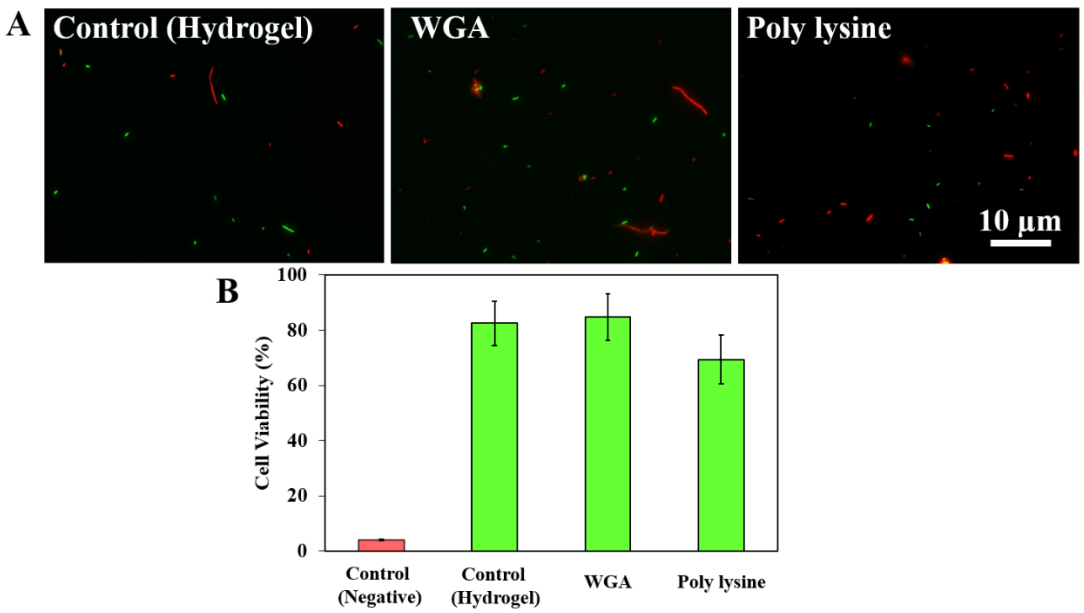

Figure 6.2 (A) Representative fluorescent images and (B) Percentage of live cells in contact with the hydrogel without affinity ligand (control), and functionalized hydrogels with WGA, and poly lysine. Negative control: Attached bacteria were exposed to a 2.5% glutaraldehyde solution and 70% isopropanol solution to verify that dead cells could be detected with the live/dead assay. The values were given as the mean of five different surface locations from three independent surfaces.

The impact of affinity ligands (poly-$_L$-lysine and WGA) on the extraction of *E. coli* cells from membrane to the hydrogels were then studied. Here different concentrations of stained *E. coli* culture (10^6 and 10^7 CFU/mL) were incubated on PVDF membranes for 1.5 hr, then hydrogels functionalized with affinity ligands were placed in contact with the membrane for 30 min. Fluorescent images and image analysis (ImageJ) were then used to measure number of bacteria attached to the hydrogel surfaces. As shown in Figure 6.3, for both bacteria concentrations, WGA-functionalized hydrogels captured significantly more *E. coli* cells compared to the control (P-value < 0.05). Adding poly-$_L$-lysine to the hydrogel could further enhanced number of attached *E. coli* cells (P-value < 0.001). These results clearly confirm that adding affinity ligands to the pre-formed gel matrix can promote microbe extraction from the membrane.

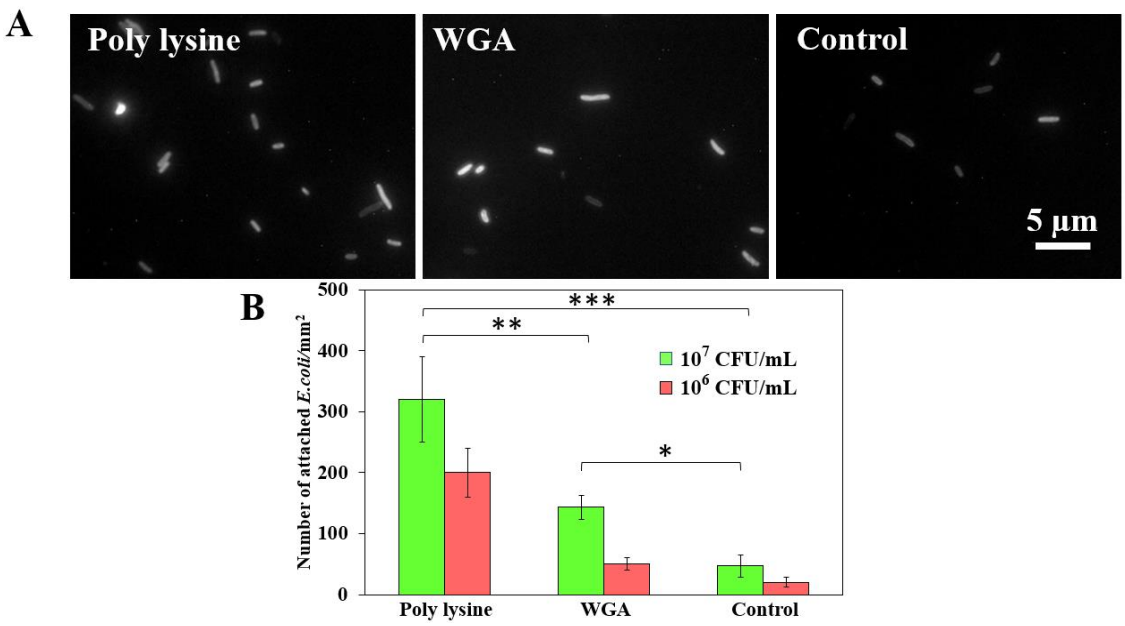

Figure 6.3 (A) Representative fluorescent images of stained-*E. coli* JM 109 transferred from membrane to the hydrogels functionalized with poly-L-lysine and WGA at two different bacteria concentrations. Control: Hydrogel without affinity ligand. (B) Calculated number of transferred *E. coli* JM 109 to the hydrogel surfaces using ImageJ. The values were given as the mean of five different surface locations from three independent surfaces. *** = $P < 0.001$, ** = $P < 0.01$, * = $P < 0.05$. Values are the average ± standard deviation.

Taken together, the combined results in Figures 6.2 and 6.3 highlight the potential trade-offs offered by each affinity ligand. While poly-L-lysine enhanced the number of microbes extracted from the membranes, it decreased the cells viability. For WGA, there was no significant change in cell viability, but number of extracted cells was higher. For applications where only extraction efficiency are important, poly-L-lysine was most beneficial. However, for applications requiring retrieval of live cells for culture-based follow-up analysis, WGA may be more beneficial.

6.4.2 Flocs Size Distribution and Transfer Efficiency

Following hydrogel characterizations, the ability to use these materials to detach wastewater communities from the membrane surface was characterized. To characterize the membrane surfaces, wastewater solutions were incubated over the membranes for various time points (3, 6, 18, and 24 hrs) in an aerobic environment. Solutions were stained with a lipid dye prior to incubation for fluorescent imaging. Incubation times were selected in the range of 3-24 hrs, as the major goal was to extract surfaces after the early-stages of biofouling. After the desired incubation time, membranes were removed from the solutions and washed to remove non-attached cells and placed in contact with pre-formed hydrogels for 30 min. Figure 6.4 (B, D) indicates fluorescent and brightfield images of flocs on the membrane and transferred to the hydrogel surfaces. These images were used to determine the floc size distribution on membrane surface for each incubation time. As Figure 6.4 C shows for 3 and 6 hr incubation times, nearly 60% of all flocs were with of a size less than 1000 μm^2, while this percentage decreased to 45% and 28% for longer incubation times (18 and 24 hr). In addition, considering 3 and 6 hr incubation, larger flocs (> 1000 μm^2) were just attributed to 10% of total flocs, and for some size ranges the percentage was close to zero. In contrast, broad size distribution ranges obtained for 18 and 24 hrs due to the fact that microbes had more time to attach and develop on the surface.

To characterize the transfer of microbes from the membrane to the hydrogels, fluorescent microscopy was again used on membranes fouled after 24 hr incubation. This timepoint was selected as it provided a broad range of flocs sizes, enabling a wider size range for follow-up extraction and sequencing studies. The impact of affinity ligands to floc transfer percentage from membrane to hydrogel was also investigated and reported in Figure 6.4 D. To calculate the transfer percentage, 40 images were taken covering whole surface of membranes before and after contact

with hydrogel. Transfer percentages were then reported for each floc size range from 0 to more than 8000 μm^2. Considering the transfer percentage for each case (control, WGA, and poly-$_L$-lysine) at different size ranges, there was no general trend as floc size increased. However, the average percentages (indicated by dashed lines) across the whole range were 47% ± 7.5, 55% ± 8.5, and 65% ± 7.8 for control, WGA, and poly-$_L$-lysine, respectively, this is also in agreement with the trends noted previously with *E. coli* (Figure 6.3 B). Focusing on WGA, there were ranges that showed increase in flocs transfer percentage compared to control, but just two ranges (0-1000 and 1000-2000 μm^2) with a statistically significant change (P-value < 0.05). This shows that compared to the control, the WGA-functionalized hydrogel was most effective in the transfer, particularly when flocs were smaller than 2000 μm^2. As can be seen, poly-$_L$-lysine impacted the transfer percentage more significantly as there were 5 size ranges with statistically significant increases.

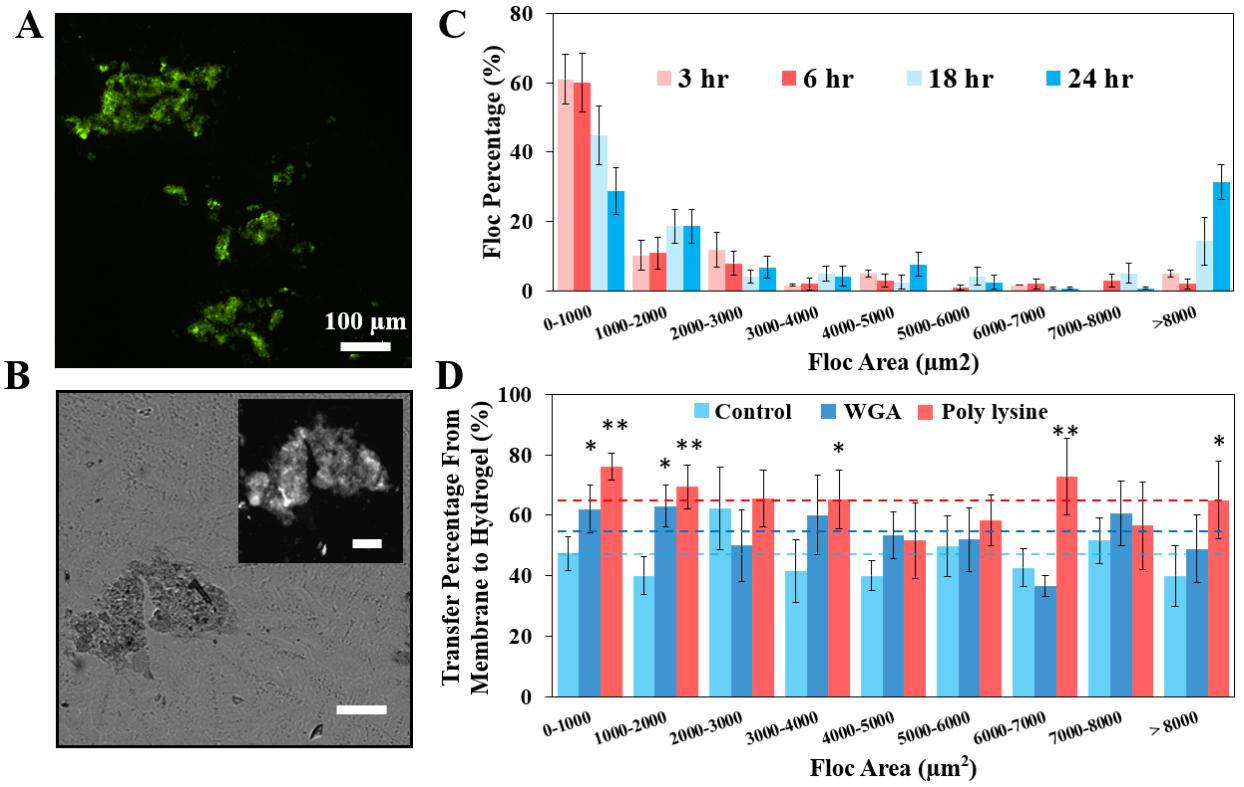

Figure 6.4 Representative (A) fluorescent images of stained-flocs with FM 1-43 lipid dye on the PVDF membrane and (B) upright brightfield and fluorescent images of flocs after transfer to the hydrogel surfaces after 30 min membrane-hydrogel contact. Inset scale bar: 50 µm (C) Flocs size distribution plot on the PVDF membrane surface after 3, 6, 18, and 24 hrs incubation with the wastewater solution. Floc sizes measured by using ImageJ software. (D) Transfer percentage from membrane to affinity-functionalized hydrogels at different floc areas after 24 hrs. Control: Hydrogel without affinity ligand. Dashed lines indicate the average floc transfer percentage for each affinity ligand. The percentage values for each size range were given as the mean of three independent surfaces. Stars demonstrate the statistical analysis of each case compared to control. *** = $P < 0.001$, ** = $P < 0.01$, * = $P < 0.05$. Values are the average ± standard deviation.

6.4.3 Hydrogel Photopatterning, Degradation, and Extraction

The Polygon400 tool allows projecting any patterns on the scale of microns onto the hydrogels, and as a result, biofilm flocs of different morphologies attached to the hydrogel can be released into solution. Here, hydrogels containing microbes detached from the fouled membrane were monitored in real time with brightfield microscopy during patterned exposure. The size of

different flocs transferred from membrane to the hydrogels was first measured, targeted flocs were then identified and exposed to patterned UV light with the 20X objective (0.7-7 mW/mm^2, 20 s). Figure 6.5 demonstrates the photopatterning, degradation, and extraction of flocs from the hydrogel. Here, flocs were observed moving out of the hydrogel over the 20 s exposure period (Figure 6.5 A). Multiple flocs could also be extracted, if desired (Figure 6.5B). After light exposure, media containing the released floc was suctioned using pipette for floc retrieval, aggregates solutions are ready for follow-up molecular characterization. Figure 6.5 C (iii) shows the extracted aggregates placed on the surface of a coverslip. This show the ability of PSD approach to recover targeted flocs. The idea of placing the second hydrogel layer on the hydrogel containing transferred flocs following by light patterning (section 6.3.6) ensure a clean extraction.

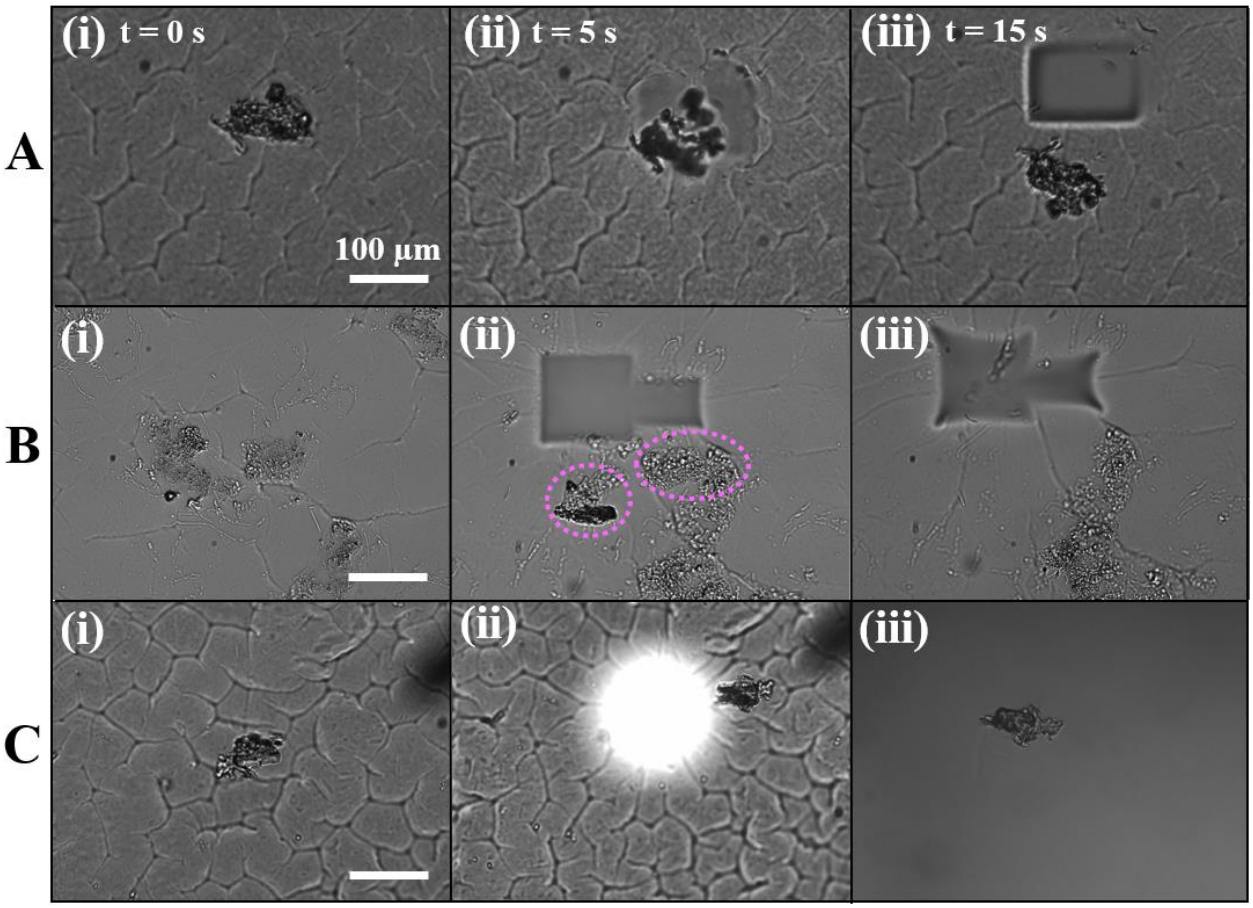

Figure 6.5 Hydrogel photopatterning, degradation and extraction. (A) (i) A targeted single floc after extraction from the PVDF membrane. (ii) Pattern projected on the flocs and release was observed after 5 s (iii) Complete release of the targeted floc from the hydrogel base occurred after 15 s (B) (i) Two flocs targeted for biofilm extraction (ii) Pattern projected on the flocs and release after light exposure. Dashed circles indicate flocs during their release into solution. (iii) Hydrogel after removal of targeted flocs. (C) (i) Floc selected for biofilm extraction. (ii) Pattern projected on the floc and complete release after light exposure. (iii) Recovered floc on a coverslip.

6.4.4 DNA Quantification and Analysis of Quantity of Extracted Samples

Here the major goal was to access the quality and quantity of microbes extracted from the hydrogel after the PSD method was used. This was necessary to access the potential to identify the composition of the extracted cellular aggregates using 16S rRNA amplicon sequencing techniques. Various methods including agarose gel electrophoresis, absorbance measurements, and use of fluorescent DNA-binding dyes can be applied to evaluate the DNA yield. Here a

spectrophotometer was used to measure the absorbance of samples. The absorbance maxima at 280 and 260 nm were determined for proteins and nucleic acids, respectively, and ratio of absorbance (260/280) was used to estimate the purity and quality of the extracted DNA and RNA. An ideal concentration would be at least 10 ng/µL DNA and a quality between 1.8-2[24,25]. However, the sequencing facility can work with lower concentrations (~ 4 ng/µL) and quality (~1.1-1.5) by performing extra quality improving steps. Table 1 demonstrates the minimum requirements, the extracted DNA concentration, and DNA quality measurements of the two floc samples extracted from hydrogel base. The first sample consisted of a floc with the size of 12,500 μm^2. The DNA concentration and quality obtained were 5.7 ng/µL and 1.208, respectively. The second sample combined three extracted flocs of different sizes (3650, 8700, and 1300 μm^2) and quantified the DNA concentration and quality as 8.14 ng/µL and 1.356, respectively. These values show that the developed PSD method can generates DNA quality and quantity sufficient for analysis with 16S sequencing.

Table 6.1 Minimum requirements, the DNA concentration, and DNA quality measurements of the floc samples extracted from hydrogel base.

Sample Information	DNA Concentration (ng/µL)	DNA Quality (260/280)	Aggregate Size(s) (μm^2)
Minimum Requirements	~ 4	1.1-1.5	N/A
Sample 1	5.7	1.208	12500
Sample 2	8.14	1.356	3650 + 8700 + 1300

6.5 Conclusion

This work concentrated on developing the PSD technique to remove and isolate targeted cells and flocs adhered to the PVDF membranes, without destroying the targets or the underlying membrane substrate. A photodegradable PEG-based hydrogel functionalized with affinity ligands for detachment of microbes from a membrane surface was developed to perform the PSD approach. After initial formation of the biofilms, photodegradable hydrogels were placed in contact with the fouled membrane and an illumination tool (Polygon400) projected patterns (on the scale of microns) onto the hydrogels. Targeted biofilm flocs attached to the hydrogel were released from the main hydrogel structure and extracted for follow-up molecular analysis. Poly-$_L$-lysine-functionalized hydrogels demonstrated nearly 15% decrease in cells viability after capture, while WGA did not show significant difference. Use of affinity ligands in hydrogel structure significantly enhanced bacteria capture by a factor of 6.8 and 3 for poly-$_L$-lysine and WGA, respectively (bacteria concentration 10^7 CFU/mL). Bioaffinity functionalization also resulted in ~17% (WGA) and ~38% (poly-$_L$-lysine) increases in average floc transfer percentage from fouled membranes to the hydrogels. Finally, photopatterning and extraction of desired flocs on the hydrogels enabled release of the target from the hydrogel for isolation in preparation of genomic characterization. DNA analysis of the quantity and quality of extracted samples revealed that the PSD approach is able to prepare samples ready for follow-up characterization with 16S rRNA amplicon sequencing. This capability will allow for the precision dissection and isolation of microbes adhered to surfaces. Future work involves using the developed PSD approach to identify early-colonizing microorganisms from wastewater communities, knowledge that will be useful for antifouling strategies that target these sub-communities to mitigate the biofouling process.

6.6 Acknowledgements

This work was supported by National Science Foundation under Grant 1805631.

6.7 References

(1) Jiménez-Benítez, A.; Ferrer, J.; Rogalla, F.; Vázquez, J. R.; Seco, A.; Robles, Á. Energy and Environmental Impact of an Anaerobic Membrane Bioreactor (AnMBR) Demonstration Plant Treating Urban Wastewater. *Curr. Dev. Biotechnol. Bioeng.* **2020**, 289–310. https://doi.org/10.1016/b978-0-12-819854-4.00012-5.

(2) Liao, B.-Q.; Kraemer, J. T.; Bagley, D. M. Anaerobic Membrane Bioreactors: Applications and Research Directions. *Crit. Rev. Environ. Sci. Technol.* **2006**, *36* (6), 489–530. https://doi.org/10.1080/10643380600678146.

(3) Wu, B.; Kim, J. Anaerobic Membrane Bioreactors for Nonpotable Water Reuse and Energy Recovery. *J. Environ. Eng. (United States)* **2020**, *146* (2). https://doi.org/10.1061/(ASCE)EE.1943-7870.0001637.

(4) Chang, S. Anaerobic Membrane Bioreactors (AnMBR) for Wastewater Treatment. *Adv. Chem. Eng. Sci.* **2014**, *04* (01), 56–61. https://doi.org/10.4236/aces.2014.41008.

(5) Maaz, M.; Yasin, M.; Aslam, M.; Kumar, G.; Atabani, A. E.; Idrees, M.; Anjum, F.; Jamil, F.; Ahmad, R.; Khan, A. L.; et al. Anaerobic Membrane Bioreactors for Wastewater Treatment: Novel Configurations, Fouling Control and Energy Considerations. *Bioresour. Technol.* **2019**, *283*, 358–372. https://doi.org/10.1016/j.biortech.2019.03.061.

(6) Mei, X.; Wang, Z.; Miao, Y.; Wu, Z. Recover Energy from Domestic Wastewater Using Anaerobic Membrane Bioreactor: Operating Parameters Optimization and Energy Balance Analysis. *Energy* **2016**, *98*, 146–154. https://doi.org/10.1016/j.energy.2016.01.011.

(7) Herrera-Robledo, M.; Cid-León, D. M.; Morgan-Sagastume, J. M.; Noyola, A. Biofouling in an Anaerobic Membrane Bioreactor Treating Municipal Sewage. *Sep. Purif. Technol.* **2011**, *81* (1), 49–55. https://doi.org/10.1016/j.seppur.2011.06.041.

(8) Xu, M.; Wen, X.; Yu, Z.; Li, Y.; Huang, X. A Hybrid Anaerobic Membrane Bioreactor Coupled with Online Ultrasonic Equipment for Digestion of Waste Activated Sludge. *Bioresour. Technol.* **2011**, *102* (10), 5617–5625. https://doi.org/10.1016/j.biortech.2011.02.038.

(9) Lin, H.; Peng, W.; Zhang, M.; Chen, J.; Hong, H.; Zhang, Y. A Review on Anaerobic Membrane Bioreactors: Applications, Membrane Fouling and Future Perspectives. *Desalination* **2013**, *314*, 169–188. https://doi.org/10.1016/j.desal.2013.01.019.

(10) Meng, F.; Chae, S. R.; Drews, A.; Kraume, M.; Shin, H. S.; Yang, F. Recent Advances in Membrane Bioreactors (MBRs): Membrane Fouling and Membrane Material. *Water Res.* **2009**, *43* (6), 1489–1512. https://doi.org/10.1016/j.watres.2008.12.044.

(11) Gao, D. W.; Zhang, T.; Tang, C. Y. Y.; Wu, W. M.; Wong, C. Y.; Lee, Y. H.; Yeh, D. H.; Criddle, C. S. Membrane Fouling in an Anaerobic Membrane Bioreactor: Differences in Relative Abundance of Bacterial Species in the Membrane Foulant Layer and in Suspension. *J. Memb. Sci.* **2010**, *364* (1–2), 331–338. https://doi.org/10.1016/j.memsci.2010.08.031.

(12) Charfi, A.; Ben Amar, N.; Harmand, J. Analysis of Fouling Mechanisms in Anaerobic Membrane Bioreactors. *Water Res.* **2012**, *46* (8), 2637–2650. https://doi.org/10.1016/j.watres.2012.02.021.

(13) Gao, W.; Liang, H.; Ma, J.; Han, M.; Chen, Z.; Han, Z.; Desalination, G. L.-; 2011, undefined. Membrane Fouling Control in Ultrafiltration Technology for Drinking Water Production: A Review. *Elsevier*.

(14) Dereli, R. K.; Ersahin, M. E.; Ozgun, H.; Ozturk, I.; Jeison, D.; van der Zee, F.; van Lier, J. B. Potentials of Anaerobic Membrane Bioreactors to Overcome Treatment Limitations Induced by Industrial Wastewaters. *Bioresour. Technol.* **2012**, *122*, 160–170. https://doi.org/10.1016/j.biortech.2012.05.139.

(15) Jeison, D.; van Lier, J. B. Cake Formation and Consolidation: Main Factors Governing the Applicable Flux in Anaerobic Submerged Membrane Bioreactors (AnSMBR) Treating Acidified Wastewaters. *Sep. Purif. Technol.* **2007**, *56* (1), 71–78. https://doi.org/10.1016/j.seppur.2007.01.022.

(16) Hwang, B. K.; Lee, W. N.; Yeon, K. M.; Park, P. K.; Lee, C. H.; Chang, I. S.; Drews, A.; Kraume, M. Correlating TMP Increases with Microbial Characteristics in the Bio-Cake on the Membrane Surface in a Membrane Bioreactor. *Environ. Sci. Technol.* **2008**, *42* (11), 3963–3968. https://doi.org/10.1021/es7029784.

(17) Meng, F.; Chae, S. R.; Drews, A.; Kraume, M.; Shin, H. S.; Yang, F. Recent Advances in Membrane Bioreactors (MBRs): Membrane Fouling and Membrane Material. *Water Res.* **2009**, *43* (6), 1489–1512. https://doi.org/10.1016/j.watres.2008.12.044.

(18) Nguyen, T.; Roddick, F. A.; Fan, L. Biofouling of Water Treatment Membranes: A Review of the Underlying Causes, Monitoring Techniques and Control Measures. *Membranes (Basel).* **2012**, *2* (4), 804–840. https://doi.org/10.3390/membranes2040804.

(19) Darton, T.; Annunziata, U.; del Vigo Pisano, F.; Gallego, S. Membrane Autopsy Helps to Provide Solutions to Operational Problems. *Desalination* **2004**, *167* (1–3), 239–245. https://doi.org/10.1016/j.desal.2004.06.133.

(20) Pontié, M.; Thekkedath, A.; Kecili, K.; Habarou, H.; Suty, H.; Croué, J. P. Membrane Autopsy as a Sustainable Management of Fouling Phenomena Occurring in MF, UF and NF Processes. *Desalination* **2007**, *204* (1-3 SPEC. ISS.), 155–169. https://doi.org/10.1016/j.desal.2006.03.538.

(21) LIVE/DEAD™ *Bac*Light™ Bacterial Viability Kit, for microscopy & quantitative assays https://www.thermofisher.com/order/catalog/product/L7012#/L7012 (accessed Mar 3, 2020).

(22) Arnfinnsdottir, N. B.; Ottesen, V.; Lale, R.; Sletmoen, M. The Design of Simple Bacterial Microarrays: Development towards Immobilizing Single Living Bacteria on Predefined Micro-Sized Spots on Patterned Surfaces. *PLoS One* **2015**, *10* (6), e0128162. https://doi.org/10.1371/journal.pone.0128162.

(23) Alkekhia, D.; Shukla, A. Influence of Poly-l-Lysine Molecular Weight on Antibacterial Efficacy in Polymer Multilayer Films. *J. Biomed. Mater. Res. - Part A* **2019**, *107* (6), 1324–1339. https://doi.org/10.1002/jbm.a.36645.

(24) Lite, N. T123-TECHNICAL BULLETIN Interpretation of Nucleic Acid 260/280 Ratios www.thermoscientific.com/nanodrop (accessed Apr 17, 2020).

(25) Matlock, B. Assessment of Nucleic Acid Purity www.thermoscientific.com (accessed Apr 17, 2020).

Chapter 7 - Conclusions and Recommendations

7.1 Design of patterned polymer interfaces to tailor the surface reactivity towards biomolecules

Strategies for making polymer-functionalized biointerfaces include self-assembled monolayers, polymer coating and printing techniques followed by their combination with bioreceptors. Strong motivation in polymer patterning originated from the diversity of synthetic polymers and the ability of them to be post-functionalized with different biological ligands. Polymer functionalized three-dimensional micro and nanostructures that are engineered to combine bioreceptors with physical structures may show significant enhancement in sensing performance. In this work, they have provided a significant enhancement in capture of bacterial pathogens. In addition, they can be used to mimic features of natural host surfaces or to design antifouling surfaces. When functionalized with different bioreceptors, these patterned interfaces motivate capture within pre-determined areas on the surface while show strong resistance to capture in surrounding regions. This allows spatial control and the capability of allocate bacteria in designated working areas separate from other capture sites. Spatially patterned surfaces are often desirable for synthetic biological interfaces, specifically for applications in sensing, biological/chemical capture, and cell culture. For example, patterning functional polymers is useful for controlling the amount of material captured or for controlling cell proliferation.

Azlactone-based polymers offer; (1) high reactivity, (2) no by-product after ring-opening reaction with nucleophiles, and (3) ability to be functionalized with broad range of biomolecules under aqueous solutions without significance hydrolysis. While azlactone-based polymers have been explored in many different applications, most publications do not use spatial patterning.

Patterning these polymers in biologically or chemically inert backgrounds is not trivial, many traditional co-patterning approaches can compromise azlactone functionality during processing steps or generate non-uniform films.

The first portion of this thesis addressed this limitation through developing methods of fabricating micro/nano-structured patterns of the novel block co-polymer, $PGMA_{56}$-*b*-$PVDMA_{175}$ onto the silicon slides. Bottom-up and top-down chemical co-patterning methods, including microcontact printing, parylene lift-off, and interface directed assembly were investigated for formation of reproducible, brush-like and crosslinked polymers on the substrates. Parylene lift-off and interface-directed assembly methods generated microscale patterns of the block copolymer in chemically or biologically inert backgrounds. The functionality of azlactone groups was preserved during fabrication, and patterned films appeared as uniform, 80–120 nm brushlike films. A top-down patterning approach was developed as well, with a novel microcontact stamping method to generate cross-linked, three-dimensional structures of the azlactone-based polymer with controllable, microscale thicknesses (3-9 μm). The methods in this work were novel because they presented techniques for achieving well-controlled, functional films with controlled thicknesses in inert backgrounds.

7.1.1 Ideas for Future Investigation

Future investigations can exploit the high reactivity and multi-functionality of azlactone polymers to generate surfaces functionalized with more than one type of biomolecule or chemical group. These multifunctional materials have potential to broaden the use of engineered interfaces in biological, environmental, and medical applications. Introducing new surface physical topographies and chemical functionalities can also result in functional interfaces for potential use

in drug delivery, tissue engineering, and for improved capture and separation of biological analytes from complex mixtures for monitoring and diagnostic applications.

Polymer-patterned interfaces still have unmet challenges that require more future. The fabrication procedures should be performed in a manner that can generate high-resolution patterns on the surfaces while being inexpensive, highly scalable across large areas, and defect-free. The big challenge here is achieving a reasonable balance between fabrication cost, sample throughput and speed, and resolution. For example, as mentioned in Chapters 3 and 4, μCP showed great advantages in straightforward low-cost patterning of PGMA-*b*-PVDMA polymers as 3-D crosslinked structures, however, enhanced patterning resolution of this method is compromised by the increased cost of manufacturing high resolution masters to be used for soft lithography and stamp fabrication. One current technique to fabricate required masters for μCP is photolithography which is normally applied for high-resolution patterning of substrates; however, lithography needs cleanroom facilities and expensive fabrication tools. Instrumentation such as e-beam lithography are required when a pattern resolution in nanometer scales is desired. Further investigation on the combination of different patterning methods will be critical to design fabrication procedures that are low-cost, scalable, and that offer high performance and resolution.

A primary challenge in the μCP protocols usually comes from the use of volatile solvents such as chloroform and toluene to prepare the polymer inking solution. Rapid solvent evaporation across the stamp can cause non-uniform polymer inking, compromising pattern reproducibility. Many research works have reported an unequal distribution of polymer inking solution on the stamp during the μCP process. The suggestion here is using a ratio of high and low-boiling point solvents. This ratio is needed to be optimized by considering the characteristics of the polymer wishes to print. There is a growing need to study surface chemistry and wetting behavior of

printing stamp and targeted substrate. Optimizing the surface chemistry of both the stamp and the substrate is essential to maintaining efficient polymer transfer while maintaining high pattern integrity. Many μCP protocols use PDMS for soft lithography and fabrication of stamps. Treating the stamp with chemical groups such as a silane can decrease the surface free energy of the stamp and facilitate the polymer transfer. This could be accompanied with treating substrates before printing to provide reactive surface groups for coupling to functional groups present in polymer. Stamp deformation is another challenge leading to non-uniform patterns which can be solved by changing the ratio of PDMS base/curing agent in soft lithography step to generate stiffer stamps. There is also an opportunity to use the high reactivity of azlactone-based surface polymers with broad range of other nucleophiles in other environmental, biomedical and engineering applications such as (1) CO_2 capture and release and removal of toxic chemicals, and (2) clustering peptides, proteins, antibodies and other biomolecules to improve binding.

7.2 Bio-functionalization of surface polymers with lectin molecules for bacteria capture

The second part of the thesis focused on developing a physico-chemically-optimized lectin interface with enhanced cell capture properties. The key interface and experimental parameters that influence lectin densities over the designer azlactone-based block copolymer $PGMA_{56}$-b-$PVDMA_{175}$ first identified. Using the optimized experimental parameters including polymer chain surface density, lectin molecular weight and lectin coupling buffer, the impact of physical structure and topography of the surfaces on bacterial capture efficiency, detection sensitivity, and cell viability were also explored. Silicon surfaces consisting of the nanopillar arrays were first coated with the polymer and then immobilized with lectin. The microbe detection sensitivity and

bactericidal impact of the nanopillar arrays were then measured and compared to the polymer-coated flat silicon surfaces.

Compared to lectin surfaces functionalized with control chemistry (carbodiimide coupling, (EDC/NHS)), the PVDMA flat surface exhibited lower detection limit (LOD) by roughly one order of magnitude (~10^3 CFU/mL) because the polymer generates higher levels of lectin surface density. PVDMA-coated nanopillar arrays (~ 300 nm tall) improved the sensitivity by an additional order of magnitude (~10^2 CFU/mL) due the three-dimensional surface structure that provided enhanced contact area with the bacterial cells. The range of achieved detection limits allows these optimized interfaces to be used in various medical and environmental applications with desired LOD ranges from urinary tract infection diagnosis (LOD ~ 10^3 CFU/mL), detection of bacteria pathogens in water and wastewater (LOD ~ 10^3-10^5 CFU/mL), to applications in need of higher sensitivity such as human sepsis (LOD 1-100 CFU/mL). The bactericidal activity demonstrated a significant decrease in cells viability after attachment to the nano-structured surfaces compared to flat surface. Bacteria were stretched over a number of pillars, and appeared deformed and ruptured. Finally, the competing effects on capture due lectin surface density and due to exopolysaccharide expression levels on the bacteria cell surface were compared.

7.2.1 Ideas for Future Investigations

Lectin-carbohydrate recognition is useful for capture and detection of microbes from contaminated solutions. The major question that still needs to be addressed is if lectin-carbohydrate interactions are stable enough to be considered as an alternative to the antibodies or nucleic acid-based capture approaches. The main challenges of applying these interactions for bacteria capture studies come from the fact that (1) compared to antibody-antigen interactions, lectins provide

weaker affinity interactions with cell carbohydrates, (2) lectins demonstrate random orientation and heterogeneous coverage on the surface, and (3) lectins denature on surfaces, particularly when they are dehydrated. The ideas for future studies are divided into two main approaches. The first approach focuses on implementing surface chemistry and fabrication techniques to develop physico-chemically optimized interfaces as the underlying template for lectin immobilization. These interfaces are be able to tune the lectin density and orientation. The second pathway is to apply the state of art of lectin engineering by a multidisciplinary collaboration between bioengineers, glycoscientists, and synthetic glycobiologists to enhance the lectin properties including specificity, stability and affinity toward analytical targets in capture and detection approaches.

The limiting factors emphasize the critical importance of the future studies to develop synthetic interfaces that generate high lectin densities, tailored physical surface features, controlled orientation of lectins on the surface, and high stability of lectins. Use of His-tagged lectin proteins is one promising approach for controlling orientation, novel biofunctional polymers such as dendrimers have also been shown to have excellent potential for modulation of lectin density and orientation on the surfaces. Control of the lectins orientation during the immobilization can also be achieved by developing functional glycan derivatives consisting -NH_2 for covalent amine coupling. To promote surface stability, coupling lectins with stabilizing molecules such as monosaccharides or within hydrogels layers has shown potential. These advancements will progress these biofunctional interfaces for capture and isolation of bacteria cells from broad range of contaminated solutions, from water to blood, or to develop lectin structures as receptor elements in biosensors. Taking these facts together, optimizing surface-related parameters is critically important to design interfaces able to tune spatial arrangement and orientation, and to prevent

denaturation of lectins. Another idea for future investigation could be combining lectins with other binding interactions (hydrophobic or secondary carbohydrate-mediated interactions) to enhance the binding avidity in bacteria capture approaches. This could provide affinity strength comparable to antibody-antigen interactions and ultimately improve the capture efficiency and detection sensitivity of interfaces.

In addition to surface optimization, strategies to perform lectin engineering including protein engineering, nucleic acid engineering, and chemical engineering by using boronate to enhance the lectin affinity, stability and physico-chemical characteristics. This will also provide new binding preferences and enhance the sensitivity and practical efficiency of engineered lectins as biomarker/bioreceptor in capture and detection approaches. For example, mixing biotinylated lectin with streptavidin could provide a tetrameric lectin which improves the poor sugar-binding functionality. New lectin properties could be achieved by dimerization, multimerization and functionalization with boronic acids derivatives. Recombinant DNA technology (as part of lectin engineering approaches) could also provide superior knowledge to identify and characterize the specific amino acids responsible for recognition of a particular carbohydrate, and synthesize modified lectins with adjusted specificity and/or affinity.

The majority of the research performed in the literature reported the application of lectin-functional interfaces for bacteria capture from simple, idealized solutions such as buffers. There is a critical need for future studies to evaluate the sensitivity and capture efficiency of the lectin-functionalized surfaces in more complex, real samples such as blood, food matrices, or water. It is anticipated that the interference of the biochemical ingredients will likely compromise the sensitivity and capture efficiency. For example, the presence of sodium chloride, sucrose, and lysine in food matrices causes interference to lectins functionality, which ultimately reduces the

sensitivity of the interface. Finally, it is anticipated that development of lectin-based interfaces could provide applications beyond cell capture, including discovery and implementation of new disease markers based on aberrant glycosylation patterns, relevant to cancer diagnostics.

7.3 Bio-functional, photodegradable hydrogels for dissection of microbes from surfaces during early-stage biofouling events

The last portion of this thesis investigated the use of photoresponsive biofunctional polymers to isolate organisms involved in early-stage biofouling on membranes used in wastewater treatment systems. Considering the limitations associated with the traditional methods such as laser capture microdissection (LCM) and membrane autopsy techniques for investigation and mitigation of biofouling, here the primary motivation was to develop a technique to remove microbes from the membrane surface in a manner that was not detrimental to microorganisms or membrane substrates. The novel polymer surface dissection (PSD) approach was performed to achieve these goals. PSD uses polyethylene glycol (PEG)-based photo-responsive hydrogel altered with *o*-NB chromophores for non-destructive removal and detachment of microbes from membrane surfaces. It was shown that functionalization of polymeric hydrogels with bioaffinity ligands such as poly-$_{L}$-lysine and WGA enhance the flocs transfer percentage from membrane to the hydrogels while hydrogel chemistry had no significant impact on cell viability. Photopatterning, extraction, and release of desired flocs from the hydrogel surfaces were conducted with a light patterning tool connected to an optical microscope. The extracted flocs were released and retrieved for further downstream characterization.

The PSD approach has excellent potential to be applied for fundamental fouling investigation in other systems hindered by biofouling, including industrial systems (ex. pipelines

and heat exchangers) and medical devices and implant surfaces. This non-destructive approach enables researchers to investigate the microbe-surface interactions and the spatiotemporal characteristics of fouling communities instead of just bulk analysis, as it provides tools to isolate aggregates from specific sites on the surface where fouling is initiated. Information obtained by molecular characterization of extracted aggregates will be accompanied with the characterization of underlying surfaces. These detailed insights ultimately provide a fundamental understanding of early-stage biofouling processes, adhesion mechanisms, and microbial community dynamics, knowledge useful for designing materials and processes that prevent biofilm formation.